

**Development of ionic liquid-based materials in gas chromatographic separations  
and microextraction techniques**

by

**Cheng Zhang**

A dissertation submitted to the graduate faculty  
in partial fulfillment of the requirements for the degree of

DOCTOR OF PHILOSOPHY

Major: Analytical Chemistry

Program of Study Committee:  
Jared L. Anderson, Major Professor  
R. Samuel Houk  
Emily A. Smith  
Anja Verena Mudring  
Surya Mallapragada

Iowa State University

Ames, Iowa

2016

Copyright © Cheng Zhang, 2016. All rights reserved.

## TABLE OF CONTENTS

	Page
<b>ACKNOWLEDGEMENTS</b> .....	v
<b>ABSTRACT</b> .....	vi
<b>CHAPTER 1 INTRODUCTION</b>	
1.1 A brief overview of comprehensive two-dimensional gas chromatography .....	1
1.2 A brief overview of microextraction technique .....	2
1.3 Unique physiochemical properties of ionic liquids (ILs) and polymeric ionic liquids (PILs) .....	5
1.4 Applications of ILs and PILs as stationary phases in comprehensive two-dimensional gas chromatography .....	8
1.5 Applications of ILs and PILs in microextraction techniques ...	9
1.6 Organization of the dissertation .....	11
References .....	13
<b>CHAPTER 2 IDENTIFYING IMPORTANT STRUCTURAL FEATURES OF IONIC LIQUID STATIONARY PHASES FOR THE SELECTIVE SEPARATION OF NONPOLAR ANALYTES BY COMPREHENSIVE TWO-DIMENSIONAL GAS CHROMATOGRAPHY</b>	
Abstract .....	15
2.1 Introduction .....	16
2.2 Experimental .....	18
2.3 Results and Discussion .....	22
2.4 Conclusion .....	35

Acknowledgements .....	36
References .....	36
 <b>CHAPTER 3    CROSSLINKED STRUCTURALLY-TUNED POLYMERIC IONIC LIQUIDS AS STATIONARY PHASES FOR THE ANALYSIS OF HYDROCARBONS IN KEROSENE AND DIESEL FUELS BY COMPREHENSIVE TWO- DIMENSIONAL GAS CHROMATOGRAPHY</b>	
Abstract .....	39
3.1 Introduction .....	41
3.2 Experimental .....	42
3.3 Results and Discussion .....	48
3.4 Conclusion .....	64
Acknowledgements .....	65
References .....	65
 <b>CHAPTER 4    POLYMERIC IONIC LIQUID BUCKY GELS AS SORBENT COATINGS FOR SOLID-PHASE MICROEXTRACTION</b>	
Abstract .....	67
4.1 Introduction .....	68
4.2 Experimental .....	70
4.3 Results and Discussion .....	76
4.4 Conclusion .....	87
Acknowledgements .....	88
References .....	88

<b>CHAPTER 5</b>	<b>RAPID AND SENSITIVE ANALYSIS OF POLYCHLORINATED BIPHENYLS AND ACRYLAMIDE IN FOOD SAMPLES USING IONIC LIQUID-BASED IN SITU DISPERSIVE LIQUID-LIQUID MICROEXTRACTION COUPLED TO HEADSPACE GAS CHROMATOGRAPHY</b>	
	Abstract .....	90
0	5.1 Introduction .....	91
	5.2 Experimental .....	94
	5.3 Results and Discussion .....	99
	5.4 Conclusion .....	117
	Acknowledgements .....	118
	References .....	118
<b>CHAPTER 6</b>	<b>GENERAL CONCLUSIONS</b> .....	122
<b>APPENDIX A</b>	<b>SUPPLEMENTAL INFORMATION ACCOMPANYING CHAPTER 2</b> .....	124
<b>APPENDIX B</b>	<b>SUPPLEMENTAL INFORMATION ACCOMPANYING CHAPTER 3</b> .....	131
<b>APPENDIX C</b>	<b>SUPPLEMENTAL INFORMATION ACCOMPANYING CHAPTER 4</b> .....	135
<b>APPENDIX D</b>	<b>SUPPLEMENTAL INFORMATION ACCOMPANYING CHAPTER 5</b> .....	138

## ACKNOWLEDGMENTS

I would like to express my deep appreciation and gratitude to my advisor, Dr. Jared Anderson. His great enthusiasm and broad knowledge in science have always been a positive mentoring effect on me. I want to also thank him for all his contributions of time, guidance, and funding to make my PhD experience productive and stimulating. It is my great fortune to be one of his students. I would like to acknowledge my committee members, Dr. Houk, Dr. Smith, Dr. Mudring, and Dr. Mallapragada for their guidance and support in my research.

I would like to thank my current group members: Omprakash, Kevin, He, Jiwoo, Stephen, and Jeffrey for their collaboration and assistance. Additionally, I also extend my gratitude towards my previous lab mates: Manishkumar, Tianhao, Tien, Honglian, Ali, Rodney, Isaiah, Melissa, Pamela, and Will for their help and advice, and being good friends. I would also like to express my thanks to our visiting student from Brazil, Leandro, for working together with me in several projects.

I would like to express my sincerest gratitude towards my family, especially my wife (Xian), daughter (Ivy), and parents for their love, support and encouragement.

Last but not least, I would like to thank my friends, colleagues, the department faculty and staff at Iowa State University and University of Toledo.

## ABSTRACT

Ionic liquids (ILs) are organic salts with melting points below 100 °C. These compounds exhibit a number of unique characteristics including high thermal stability, negligible vapor pressures, wide liquid range, and tunable viscosities. More importantly, they can be functionalized to process a broad range of solvation interactions and exhibit unique selectivities toward different classes of analytes. The research work presented in this dissertation is focused on the development of novel ILs and PILs in chromatographic separations (i.e., stationary phases for gas chromatography) and microextraction techniques (i.e., extraction phases for solid-phase microextraction and dispersive liquid-liquid microextraction).

A series of dicationic ILs containing different structural features were employed as secondary columns in comprehensive two-dimensional gas chromatography (GC×GC) for the separation of aliphatic hydrocarbons from kerosene. The solvation parameter model was applied to establish a quantitative structure-retention relationship to understand the role that the structural features of the IL play on the selectivity in GC separations. It was observed that long alkyl side chain substituents and long linkage chains between the two imidazolium cations are the most important structural features for the resolution of aliphatic hydrocarbons. However, it was also observed that the dicationic ILs did not exhibit good thermal stability at high operating temperatures (i.e., >250 °C). In order to address this issue, crosslinked PIL-based stationary phases were prepared using imidazolium-based IL monomers and crosslinkers possess similar structural features (i.e., alkyl side chain substituents and long linkage chains) via in-column free radical polymerization. The crosslinked PIL-based stationary phase containing 50% (w/w) of crosslinker exhibited excellent selectivity for the GC×GC separation of aliphatic hydrocarbons and showed a maximum allowable operating temperature of 325 °C, which is significantly higher than

commercial available polar phases. Finally, the crosslinked PIL-based stationary phases were compared with SUPELCOWAX 10 and DB-17 columns for the separation of aliphatic hydrocarbons in diesel fuel. Better resolution of aliphatic hydrocarbons was obtained when employing the crosslinked PIL-based stationary phase as the second-dimension column.

Crosslinked PIL-based sorbent coatings were prepared and coupled to GC-FID/MS for the analysis of polycyclic aromatic hydrocarbons (PAHs) from aqueous samples. In this study, novel cross-linked polymeric ionic liquid (PIL) bucky gels were formed by free-radical polymerization of IL monomer gelled with multi-walled carbon nanotubes (MWCNT). The incorporation of MWCNTs to the PIL phases significantly enhanced the  $\pi$ - $\pi$  interaction between the sorbent coatings and target analytes (i.e., PAHs). A partitioning extraction mechanism was observed for PIL bucky gel sorbent coatings, which allows the further determination of the analyte-to-coating partition coefficients ( $\log K_{fs}$ ). Recovery studies were also performed in different environmental water samples to validate the applicability of the PIL bucky sorbent coatings.

ILs were also employed as extraction solvents in *in situ* DLLME coupled to HS-GC-ECD/or MS for the analysis of polychlorinated biphenyl (PCBs) and acrylamide from complex food samples at trace levels. Five halide-based ILs containing varied functional groups were prepared to evaluate the effect of different structural features on the extraction efficiency of the target analytes. Extraction parameters including molar ratio of IL to metathesis reagent and IL mass were optimized. The effects of HS oven temperature and the HS volume of the sample vial on the analyte response were also evaluated. The matrix-compatibility of the developed method was proven by quantifying acrylamide in brewed coffee samples. This method is much simpler and provides higher sample throughput compared to the previously reported SPME GC-MS method and can be applied for the routine analysis of contaminants present in complex food samples.

## CHAPTER 1

### INTRODUCTION

#### 1.1 A brief overview of comprehensive two-dimensional gas chromatography

The separation and identification of volatile and semi-volatile organic compounds in complex mixtures (i.e., petroleum samples, fragrances, and organic pollutants) is a very challenging task. These samples typically contain hundreds to thousands of components which possess a wide range of properties often present at varied concentration levels. It is very difficult to separate these samples using conventional one-dimensional GC because the separation capacity provided by a single GC column is insufficient for hundreds of compounds. Moreover, the GC stationary phase may not possess selectivity required to achieve resolution of the analytes with very similar physical and chemical properties. In order to solve these issues, comprehensive two-dimensional gas chromatography (GC×GC) was first introduced by Phillips and Liu in 1991 [1] and has been widely used for the separation, identification, and quantification of complex samples [2-5]. A typical GC×GC separation is achieved by employing two gas chromatographic separations in a continuous and sequential fashion (see Figure 1), which can result in increased peak capacity and selectivity. In order to achieve maximum resolving power, the two stationary phases should possess complementary selectivities (i.e., distinct solvating capabilities). Polysiloxane and polyethylene glycol (PEG)-derived stationary phases are most commonly employed columns for GC×GC separations. By applying these stationary phases in nonpolar × polar or polar × nonpolar column sets, a broad spectrum of analytes, including hydrocarbons, fatty acid methyl esters, flavors and fragrance have been successfully separated [6-9]. However, the selectivity provided by commercial



columns is still limited and may be insufficient for more complicated samples. Therefore, the development of new stationary phases possessing alternative selectivities and high thermal stability is needed to fully exploit the separation power of  $GC \times GC$ .

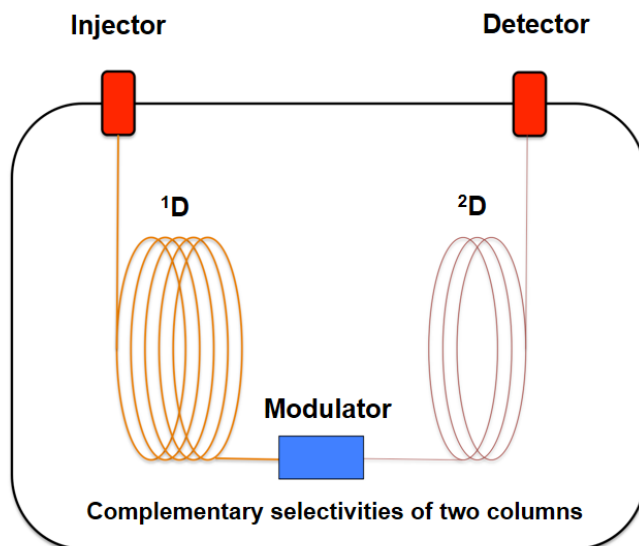


**Figure 1.** Schematic of comprehensive two-dimensional gas chromatography ( $GC \times GC$ )

## 1.2 A brief overview of microextraction techniques

Sampling and sample preparation plays a vital role in analyzing target analytes from complex sample matrices. It includes the isolation and/or pre-concentration of target analytes from sample matrices as well as making the analytes more suitable for separation and detection. Moreover, since more than 80% of the analysis time is spent on sampling and sample preparation (e.g., purification, extraction, preconcentration), choosing the appropriate sample preparation method greatly influences the sample throughput. Many conventional sample preparation methods, such as liquid-liquid extraction (LLE) and solid phase extraction (SPE), have been widely applied for routine analysis. However, these techniques are time-consuming and require large quantities of organic solvent and/or other consumables. Additionally, the

demand for high sensitivity and selectivity has begun to rapidly eclipse the capabilities of traditional extraction techniques. To address these issues, high throughput, selective, and cost-effective microextraction alternatives, are becoming increasingly desirable.

SPME is a sampling and sample preparation technique developed by Pawliszyn and co-workers in the early 1990s [10]. This technique is based on the adsorption or partitioning of analytes to a thin sorbent coating. Depending on the properties of the analytes and the sample matrices, SPME can be performed using two different extraction modes, namely, headspace and direct immersion (see Figure 2). In headspace extraction mode, the SPME fiber is exposed into the headspace above the sample matrix. This sampling approach prevents the direct contact of the fiber with the sample matrix and therefore eliminates fiber contamination. However, this sampling mode is only suitable for the extraction of high

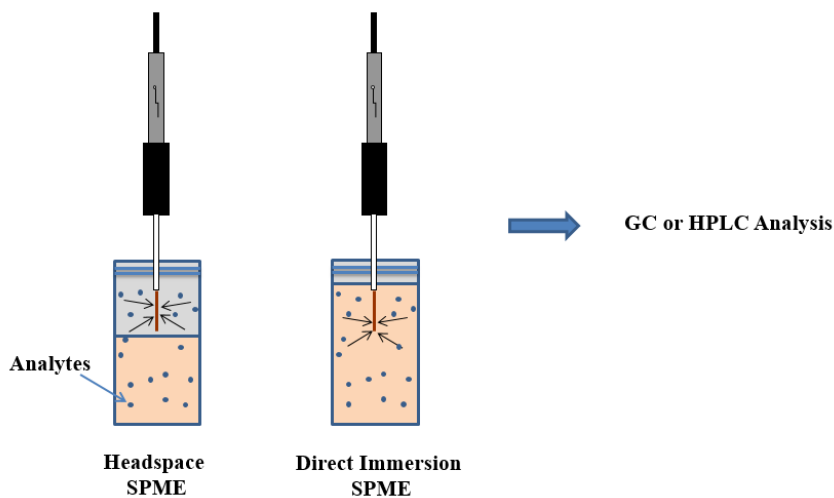


**Figure 2.** Schematic of extraction modes in SPME

volatility analytes as nonvolatile or low volatility compounds are difficult to be transferred to the headspace. In direct immersion mode, the SPME fiber is directly immersed into the liquid sample and the analytes are directly extracted from the sample matrix to the fiber coating. This extraction mode can improve the capture of nonvolatile or low volatility compounds (i.e.,

polycyclic aromatic hydrocarbons) but the interference from the sample matrix can be challenging. After the extraction step, the analytes are rapidly desorbed for chromatographic analysis using high temperature in GC or organic solvents in high performance liquid chromatography (HPLC).

Currently, there are a number of commercial available SPME sorbent coatings including polydimethylsyloxane (PDMS), polyacrylate (PA), PDMS-divinylbenzene (PDMS-DVB) and Carboxen-PDMS. However, these coatings still lack the selectivity needed for extracting specific classes of analytes, especially in the presence of complex sample matrices. As a result, the addition of novel SPME sorbent coatings that can provide better sensitivity and selectivity can be highly beneficial for the expansion of SPME in sample analyses.

Dispersive liquid-liquid microextraction (DLLME) is another powerful microextraction technique developed by Rezaee and coworkers in 2006 [11]. It is a solvent extraction technique that preconcentrates analytes from an aqueous sample to a water-immiscible extraction phase in the presence of a disperser solvent. A traditional DLLME procedure is shown in Figure 3. Microliter volumes of a hydrophobic extraction solvent is added to an aqueous sample solution and dispersed into fine microdroplets

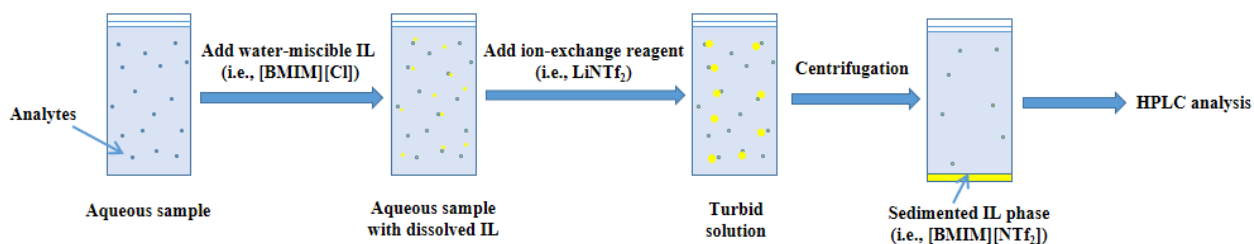


**Figure 3.** Schematic of DLLME procedure

with the assistance of a disperser solvent (i.e., an organic modifier that is miscible with the aqueous sample and the extraction solvent). The formation of the microdroplets can

significantly increase the contact area between the fine droplets of the extraction phase and the analytes, leading to an enhancement in analyte extraction efficiency. After the extraction step, the extraction phase can be recovered from the aqueous sample solution via centrifugation or with the aid of controlled temperature and subjected to chromatographic analysis. Compared to traditional LLE, DLLME requires lower solvent consumption and exhibits higher sample throughput and excellent extraction efficiency. One major limitation of this technique is the selectivity provided by the organic extraction solvents (i.e., carbon tetrachloride, chloroform, toluene, benzene, 1-octanol, 1-undecanol and n-hexane) may not be sufficient for analyzing compounds possess a wide range of properties at trace-levels.

### 1.3 Unique physiochemical properties of ionic liquids (ILs) and polymeric ionic liquids (PILs)

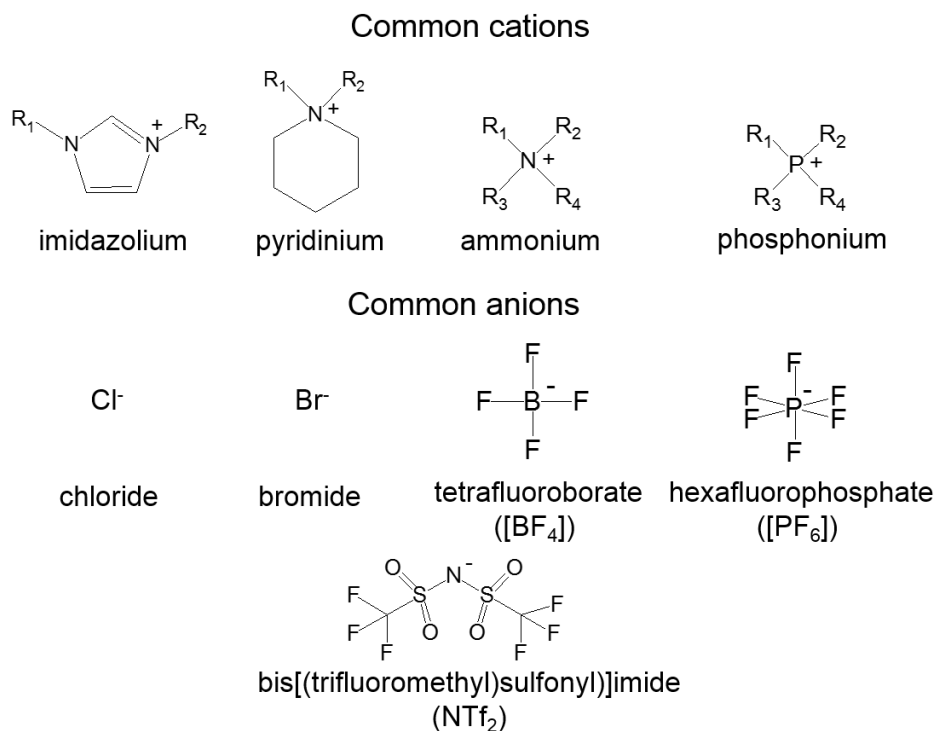


**Figure 4.** Structures of common IL cations and anions

The thermal stability of ILs and PILs is an important characteristic that governs the operating temperature and long-term stability (i.e., life time) when they are employed as GC stationary phases [15]. Under high operating temperatures, the volatilization and/or decomposition of the stationary phase can cause high column bleed, which can cause the shifting of analyte retention times and is also not ideal for trace-level analysis or GC/MS analyses. In serious cases, the stationary phase will be destroyed and the column efficiency will be diminished. The thermal stability is also critical for applying ILs/PILs as sorbent coatings for SPME. The SPME sorbent coating should be sufficiently stable to withstand the high desorption temperature of the GC injector. If the desorption temperature exceeds the maximum thermally stable temperatures of the ILs/PILs, volatilization/decomposition of the ILs/PILs can lead to the contamination of the GC inlet and/or column. Moreover, the loss of the sorbent coatings can result in poor extraction-to-extraction reproducibility.

It is well known that the thermal stability of the ILs depends on both the cationic and anionic moieties that comprise the ILs [16, 17]. Ammonium-based ILs exhibit the lowest thermal stability due to the higher propensity of alkyl ammonium salts to undergo elimination reactions at high temperatures. ILs containing imidazolium cations tend to be more thermally stable than ammonium-based ILs. Many applications have been reported using this type of ILs as stationary phases in GC as well as sorbent coatings in SPME [14, 18, 19]. Phosphonium-based ILs with long alkyl chains were also developed as GC stationary phases and could be operated at temperatures up to 405 °C [20]. On the other hand, the nature of the anion plays a more prominent role in the overall thermal stability of the ILs. ILs with halide anions usually have the lowest thermal stability due to the nucleophilic nature of these anions since it is possible for them to undergo  $S_N1$  or  $S_N2$  nucleophilic reactions [15]. On the contrary, ILs with

less nucleophilic or coordinating anions (i.e., NTf<sub>2</sub><sup>-</sup>) usually exhibit higher thermal stability. Based on previously reported result, the thermal stability of imidazolium based ILs increases as follows: Cl<sup>-</sup>, Br<sup>-</sup>, I<sup>-</sup> < BF<sub>4</sub><sup>-</sup> < CF<sub>3</sub>SO<sub>3</sub><sup>-</sup> < NTf<sub>2</sub><sup>-</sup> < PF<sub>6</sub><sup>-</sup>. In addition, for the ILs with similar cation/anion combinations, dicationic ILs and polymeric ionic liquids (PILs) possess higher thermal stability compared to monocationic ILs [21, 22].

The viscosity of the ILs/PILs is another factor that influences their applications in GC separations and sample preparation (e.g., extraction phase for SPME and DLLME) [14, 18]. When applied as GC stationary phases, ILs/PILs possessing low viscosity may have tendency to flow at elevated GC temperatures and high flow rate, which can result in film thickness inconsistencies throughout the column and low column efficiency. A relatively high viscosity is also required when applying ILs/PILs as sorbent coatings for SPME because it can minimize the loss of the SPME sorbent coatings during the thermal desorption. On the contrary, when they are employed as extraction phases in DLLME, ILs with low viscosity can facilitate the mass transfer of the analytes into the extraction phase and result in enhanced extraction efficiency. The viscosity of ILs are largely governed by hydrogen bonding, van der Waals forces, and electrostatic interactions. For imidazolium-based ILs, increasing the length of the alkyl chain substituents can increase their viscosity [23]. ILs with strongly coordinating anions (i.e., Cl<sup>-</sup>, Br<sup>-</sup>, I<sup>-</sup>) usually exhibit high viscosity due to the strong hydrogen bonding interactions between the halide anion and the cation. Larger anions, such as NTf<sub>2</sub><sup>-</sup> and TfO<sup>-</sup> in which the charge is more diffuse yield ILs with lower viscosity. As a result, choosing an IL/PIL with suitable viscosity is imperative for optimal separation or extraction performance.

One of the most attractive features for ILs/PILs is they can be functionalized to process a broad range of solvation interactions and unique selectivities toward different classes of

analytes. For example, by altering the anion of the IL from  $\text{NTf}_2^-$  to  $\text{Cl}^-$ , the interaction between the IL and the hydrogen-bond acidic solutes such as alcohols can be significantly increased. Moreover, it has been previously reported that incorporating aromatic moieties to the IL can significantly increase the  $\pi$ - $\pi$  interactions between the IL phase and the aromatic compounds, including polycyclic aromatic hydrocarbons, polychlorinated biphenyls, and aromatic sulfoxides [14].

#### **1.4 Applications of ILs and PILs as stationary phases in comprehensive two-dimensional gas chromatography**

The increasing interest in IL and PIL-based stationary phases has resulted in the commercialization of IL-based GC columns. Currently, there are a number of commercially available GC phases prepared by imidazolium-based and phosphonium-based ILs, namely, SLB-IL 59, 60, 61, 76, 82, 100, and 111 [24]. The column codes assigned by the manufacturer are based on the polarity number of each IL, which is determined by the normalized sum of the Kovats retention indices, with respect to the polarity number of IL 100 (i.e., poly[1,9-di(3-vinylimidazolium)nonane] [ $\text{NTf}_2$ ]) [25]. Due to their unique selectivities and solvation properties, these columns have been employed as 1D or 2D columns in the GC $\times$ GC separation of complex samples. For example, SLB-IL59 was employed as 2D column for the separation of 196 polychlorinated biphenyl congeners by GC $\times$ GC-MS [26]. An SLB-IL111  $\times$  IL 59 column set was employed for the separation of fatty acid methyl esters (FAMES) from safflower oil. The two IL-based column sets provided excellent separation of FAMES compared to PEG-based phases [27]. The retention behavior of polycyclic aromatic sulfur heterocycles (PASH) and their alkylated homologues on commercial IL-based stationary

phases were compared with the GC×GC-MS result obtained using polydimethylsiloxane-based columns. It was observed that IL-based columns provided increased separation for polar analytes [28]. However, for specific groups of analytes, the solvation power provided by commercial IL-based columns are still limited. It was observed in our previous study that nonpolar analytes, such as aliphatic hydrocarbons could not be resolved using IL-based columns [29]. Moreover, the maximum allowable operating temperature (MAOT) for commercial IL-based columns is around 300 °C (i.e., SLB-IL 59 and 60), which is insufficient for the separation of analytes with high boiling points. This result indicates that less polar ILs with high thermal stability may be interesting alternatives for the separation of nonpolar analytes with a broad range of boiling points, such as those found in the field of fuel and petrochemical analysis.

### **1.5 Applications of ILs and PILs in SPME and DLLME**

ILs were first introduced by Liu and coworkers in 2005 as SPME sorbent coatings for the headspace sampling of benzene, toluene, ethylbenzene, and xylene (BTEX) from paints [30]. Due to the fact that the IL was physically coated on a stainless steel wire, the sorbent coating was disposable for each extraction, which can potentially increase the cost of the analysis. In order to enhance the robustness and reusability of the sorbent coating, PIL-based sorbent coating was firstly introduced by Zhao and coworkers [31]. Imidazolium-based PILs were prepared through free radical polymerization using 2,2'-Azobis(2-methylpropionitrile) (AIBN) and were applied as sorbent coatings in the headspace sampling of FAMES and esters in wine samples. The application of PILs can significantly increase the viscosity of the sorbent coatings at high temperatures and prevent the flowing of the coatings during the thermal desorption. As



a result, high thermal stability and longer fiber lifetimes (i.e., over 150 extraction circles) could be obtained.

Various approaches have been previously employed to prepare PIL-based sorbent coatings. Physical dip coating is the most quick and straightforward strategy for loading the PIL onto a SPME support. This method was applied for the preparation of PIL-based sorbent coatings composed of different functional groups and cation/anion combinations for the headspace analysis of genotoxic impurities (i.e., alkyl halides and aromatics) in water [32]. However, the physically coated PILs still lacks the mechanical strength needed for extractions in harsh conditions. For example, halide-based linear PILs are not suitable for direct immersion SPME as they have a tendency to solubilize in water. To overcome this drawback, various chemical bonding techniques were developed to immobilize PIL phase to a silica or a treated metal support. Including electrochemical deposition, in situ surface radical chain-transfer polymerization, and sol-gel technique [18, 33].

The tunable chemical structures and unique solvation capabilities make ILs/PILs attractive sorbent coatings for SPME. The tunable selectivity of the ILs/PILs towards a wide variety of target analytes has been demonstrated in many studies. In a work reported by Meng and coworkers, imidazolium-based PILs containing aromatic moieties were applied for the extraction of polycyclic aromatic hydrocarbons (PAHs) from aqueous samples [34]. Due to the enhanced  $\pi$ - $\pi$  interactions between the PIL-based sorbent coating and aromatic compounds (i.e., PAHs), the extraction efficiency for PAHs was significantly increased when compared to analogous PILs containing no aromatic substituents. A similar trend was also observed when applying crosslinked PIL containing aromatic moieties for the extraction of polychlorinated biphenyls (PCBs) from ocean water and bovine milk samples [35].

ILs have also been widely applied as extraction solvents in DLLME since 2009 [36]. Compared to conventional extraction solvents employed for DLLME (i.e., chlorobenzene, chloroform, and carbon tetrachloride), ILs exhibit many unique characteristics including lower toxicity, negligible vapor pressures, tunable viscosity and varied solvation interactions. Depending on the purpose of the analysis and the physical chemical property of the ILs, various sampling techniques including conventional IL-based DLLME, temperature-assisted IL-based DLLME, and IL-based *in situ* DLLME has been reported [37]. IL-based *in situ* DLLME was demonstrated by Baghdadi and our group in 2009 [38, 39]. In this approach, a hydrophilic IL-based extraction solvent is dissolved in an aqueous sample solution. An anion exchange reagent (e.g., lithium bis[(trifluoromethyl)sulfonyl]imide, LiNTf<sub>2</sub>) is then added to the solution to form fine droplets of the hydrophobic IL phase that can be easily separated from the aqueous solution. This technique is simple, rapid, and has been applied for the determination of organics (i.e., aromatic compounds, insecticides, and medicinal products) and metal ions in various samples [37].

## 1.6 Organization of the dissertation

**Chapter 2** describes the preparation and application of dicationic IL-based stationary phases as secondary columns for the separation of aliphatic hydrocarbons from kerosene using GC×GC. The solvation parameter model was used to probe the solvation properties of the IL-based stationary phases. It was observed that long free alkyl side chain substituents and long linker chains between the two cations are important structural features for the resolution of nonpolar aliphatic hydrocarbons.

**Chapter 3** expands the development of PIL-based stationary phases for the GC×GC separation of aliphatic hydrocarbons. A series of PIL-based stationary phases containing long alkyl side chains and linkage chains were prepared. The optimal resolution of aliphatic hydrocarbons was achieved when 50% (w/w) of crosslinker was incorporated into the PIL-based stationary phase. The resulting stationary phase exhibited superior selectivity for aliphatic hydrocarbons from kerosene and diesel samples and can be operated at higher oven temperature (i.e., 325 °C) compared to commercial PEG-based columns.

**Chapter 4** describes the preparation of novel cross-linked PIL bucky gels by free-radical polymerization of IL monomer gelled with multi-walled carbon nanotubes. The PIL bucky gel was applied as SPME sorbent coating for the extraction of PAHs and exhibited excellent extraction efficiency, high precision, and good recovery.

**Chapter 5** describes the development of IL-based extraction phases in *in situ* DLLME coupled to HS-GC-ECD/or MS for the analysis of PCBs and acrylamide at trace levels from milk and coffee samples. The optimized *in situ* DLLME method exhibited good analytical precision, good linearity, and provided detection limits down to the low ppt level for PCBs and low ppb level for acrylamide. The matrix-compatibility of the developed method was also proven by quantifying acrylamide in brewed coffee samples. This method exhibited much higher sample throughput compared to the previously reported SPME GC-MS method.

**Chapter 6** provides the summary of the completed research projects.

## References

- [1] Z. Liu, J.B. Phillips, *J. Chromatogr. Sci.* 29 (1991) 227
- [2] P. Marriott, R. Shellie, *TrAC, Trends Anal. Chem.* 21 (2002) 573
- [3] J. Dallüge, J. Beens, A. Udo, *J. Chromatogr. A* 1000 (2003) 69
- [4] M. Adahchour, J. Beens, R. Vreuls, U.T. Brinkman, *TrAC, Trends Anal. Chem.* 25 (2006) 438
- [5] J.V. Seeley, S.K. Seeley, *Anal. Chem.* 85 (2012) 557
- [6] C. Vendeuvre, F. Bertoncini, L. Duval, J.-L. Duplan, D. Thiébaud, M.-C. Hennion, *J. Chromatogr. A* 1056 (2004) 155
- [7] L. Mondello, A. Casilli, P.Q. Tranchida, P. Dugo, G. Dugo, *J. Chromatogr. A* 1019 (2003) 187
- [8] H.-J. de Geus, I. Aidos, J. de Boer, J.B. Luten, A.T. Udo, *J. Chromatogr. A* 910 (2001) 95
- [9] L. Mondello, A. Casilli, P.Q. Tranchida, G. Dugo, P. Dugo, *J. Chromatogr. A* 1067 (2005) 235
- [10] C.L. Arthur, J. Pawliszyn, *Anal. Chem.* 62 (1990) 2145
- [11] M. Rezaee, Y. Assadi, M.-R. Milani Hosseini, E. Aghaee, F. Ahmadi, S. Berijani, *J. Chromatogr. A* 1116 (2006) 1
- [12] J.L. Anderson, D.W. Armstrong, G.-T. Wei, *Anal. Chem.* 78 (2006) 2892
- [13] T.D. Ho, C. Zhang, L.W. Hantao, J.L. Anderson, *Anal. Chem.* 86 (2014) 262
- [14] C. Yao, J.L. Anderson, *J. Chromatogr. A* 1216 (2009) 1658
- [15] C. Maton, N. De Vos, C.V. Stevens, *Chem. Soc. Rev.* 42 (2013) 5963
- [16] H.L. Ngo, K. LeCompte, L. Hargens, A.B. McEwen, *Thermochim Acta* 357–358 (2000) 97
- [17] W.H. Awad, J.W. Gilman, M. Nyden, R.H. Harris Jr, T.E. Sutto, J. Callahan, P.C. Trulove, H.C. DeLong, D.M. Fox, *Thermochim Acta* 409 (2004) 3
- [18] T.D. Ho, A.J. Canestraro, J.L. Anderson, *Anal. Chim. Acta* 695 (2011) 18
- [19] C.F. Poole, S.K. Poole, *J. Sep. Sci.* 34 (2011) 888
- [20] Z.S. Breitbach, D.W. Armstrong, *Anal. Bioanal. Chem.* 390 (2008) 1605

- [21] J.L. Anderson, R. Ding, A. Ellern, D.W. Armstrong, *J. Am. Chem. Soc.* 127 (2005) 593-604.
- [22] J.L. Anderson, D.W. Armstrong, *Anal. Chem.* 77 (2005) 6453
- [23] A.A. Fannin, D.A. Floreani, L.A. King, J.S. Landers, B.J. Piersma, D.J. Stech, R.L. Vaughn, J.S. Wilkes, J.L. Williams, *J. Phys. Chem.* 88 (1984) 2614
- [24] C.F. Poole, N. Lenca, *J. Chromatogr. A*, 1357 (2014) 87
- [25] C. Ragonese, D. Sciarrone, P.Q. Tranchida, P. Dugo, G. Dugo, L. Mondello, *Anal. Chem.* 83 (2011) 7947
- [26] M. Zapadlo, J. Krupčík, T. Kovalczuk, P. Májek, I. Špánik, D.W. Armstrong, P. Sandra, *J. Chromatogr. A*, 1218 (2011) 746
- [27] A. Nosheen, B. Mitrevski, A. Bano, P.J. Marriott, *J. Chromatogr. A*, 1312 (2013) 118
- [28] P. Antle, C. Zeigler, A. Robbat, *J. Chromatogr. A*, 1361 (2014) 255
- [29] L. Hantao, A. Najafi, C. Zhang, F. Augusto, J.L. Anderson, *Anal. Chem.* 86 (2014) 3717
- [30] J.-f. Liu, N. Li, G.-b. Jiang, J.-m. Liu, J.Å. Jönsson, M.-j. Wen, *J. Chromatogr. A*, 1066 (2005) 27
- [31] F. Zhao, Y. Meng, J.L. Anderson, *J. Chromatogr. A*, 1208 (2008) 1
- [32] T.D. Ho, M.D. Joshi, M.A. Silver, J.L. Anderson, *J. Chromatogr. A*, 1240 (2012) 29
- [33] J. Feng, H. Qiu, X. Liu, S. Jiang, J. Feng, *TrAC, Trends Anal. Chem.* 46 (2013) 44
- [34] Y. Meng, J.L. Anderson, *J. Chromatogr. A*, 1217 (2010) 6143
- [35] M.D. Joshi, T.D. Ho, W.T. Cole, J.L. Anderson, *Talanta*, 118 (2014) 172
- [36] Y. Liu, E. Zhao, W. Zhu, H. Gao, Z. Zhou, *J. Chromatogr. A*, 1216 (2009) 885
- [37] M.J. Trujillo-Rodríguez, P. Rocío-Bautista, V. Pino, A.M. Afonso, *TrAC, Trends Anal. Chem.* 51 (2013) 87
- [38] M. Baghdadi, F. Shemirani, *Anal. Chim. Acta* 634 (2009) 186
- [39] C. Yao, J.L. Anderson, *Anal. Bioanal. Chem.* 395 (2009) 1491

**CHAPTER 2****IDENTIFYING IMPORTANT STRUCTURAL FEATURES OF IONIC LIQUID STATIONARY PHASES FOR THE SELECTIVE SEPARATION OF NONPOLAR ANALYTES BY COMPREHENSIVE TWO-DIMENSIONAL GAS CHROMATOGRAPHY**

Reprinted with permission from *Journal of Chromatography A* **2015**, 1386, 89-97

Copyright © 2015, Elsevier

Cheng Zhang, Isaiah C. Ingram, Leandro W. Hantao, Jared L. Anderson

**Abstract**

A series of dicationic ionic liquid (IL)-based stationary phases were evaluated as secondary columns in comprehensive two-dimensional gas chromatography (GC×GC) for the separation of aliphatic hydrocarbons from kerosene. In order to understand the role that structural features of ILs play on the selectivity of nonpolar analytes, the solvation parameter model was used to probe the solvation properties of the IL-based stationary phases. It was observed that room temperature ILs containing long free alkyl side chain substituents and long linker chains between the two cations possess less cohesive forces and exhibited the highest resolution of aliphatic hydrocarbons. The anion component of the IL did not contribute significantly to the overall separation, as similar selectivities toward aliphatic hydrocarbons were observed when examining ILs with identical cations and different anions. In an attempt to further examine the separation capabilities of the IL-based GC stationary phases, columns of the best performing stationary phases were prepared with higher film thickness and resulted in enhanced selectivity of aliphatic hydrocarbons.

## 2.1 Introduction

Comprehensive two-dimensional gas chromatography (GC×GC) is a valuable tool for the separation and identification of volatile and semi-volatile constituents in many complex samples [1-7]. A typical GC×GC separation is generally achieved through the use of a modulation device situated between a long first column and a short secondary column, which results in increased peak capacities. In order to achieve a significant improvement in the resolving power, the stationary phases employed should possess complementary selectivities (i.e., distinct solvating capabilities). The most commonly employed columns in GC×GC separations are poly(siloxane)- or poly(ethylene glycol)-derived stationary phases in both nonpolar × polar and polar × nonpolar column configurations [8]. However, the solvation capabilities provided by these stationary phases are still limited and may not provide complete separation of complex samples.

Ionic liquids (ILs) are organic salts with melting points below 100 °C. These compounds exhibit a number of unique characteristics such as high thermal stability, negligible vapor pressures, wide liquid ranges, and tunable viscosities [9]. More importantly, ILs can often be functionalized by the addition of substituents to the cations to provide a broad range of solvation interactions and unique selectivities toward different classes of analytes [10-12]. Many of these properties have made ILs an interesting new class of stationary phases in GC [13,14]. Currently, there are a number of commercial IL-based GC stationary phases available including SLB-IL 59, SLB-IL 60, SLB-IL 61, SLB-IL 76, SLB-IL 82, SLB-IL 100 and SLB-IL 111 [15]. These GC columns were successfully employed for the separation of mid- to high-polarity analytes, such as fatty acid methyl esters [16-18], polychlorinated dibenzo-p-dioxins and dibenzofurans [19], flavor and fragrance compounds [20], alkyl phosphates [21],

benzothiazoles and benzotriazoles [22], and aromatic hydrocarbons [23] by conventional gas chromatography (1D-GC) and GC×GC [23-29]. However, it has been observed that due to the high polarity and cohesive forces of the commercial IL-based columns, nonpolar analytes such as aliphatic hydrocarbons are not resolved very well [20,23,29,30]. As a result, there is increasing interest in developing new IL-based stationary phases that are capable of exhibiting better separation performance compared to commercial IL-based columns.

Recently, a series of ILs were evaluated by our group as second-dimension columns for the separation of aliphatic hydrocarbons in GC×GC [30]. The solvation parameter model was used to probe the solvation properties of the stationary phases to understand their role in providing the unique selectivity required to resolve nonpolar analytes. It was observed that ILs capable of strong dispersive interactions exhibited better separation of aliphatic hydrocarbons compared to the commercial SUPELCOWAX 10 column. However, the solvation properties of the ILs can be varied by combining different types of cations (e.g., imidazolium-based or phosphonium-based) and anions (e.g., bis[(trifluoromethyl)sulfonyl]imide ([NTf<sub>2</sub>)<sup>-</sup>] or tetrachloroferrate ([FeCl<sub>4</sub>)<sup>-</sup>]). Moreover, even with the same cation, slight modification of the functional groups (e.g., alkane or aromatic groups) appended to the cation can significantly vary their solvation properties [14].

Geminal dicationic ILs have been explored as commercial GC stationary phases due to their superior thermal stability [15]. In addition, their side chains and linker chains can be functionalized to impart different solvation properties to the resulting ILs [10]. Commercial IL-based columns such as SLB-IL 82 and SLB-IL 111 contain short alkyl side chains and possess high cohesive forces, which is not conducive for producing high separation of nonpolar analytes such as aliphatic hydrocarbons [8,31]. Recently, our work revealed that imparting



longer alkyl substituents into the cationic moiety can significantly decrease the cohesive forces of the IL and thus enhance the resolution of aliphatic hydrocarbons in GC×GC separations [30]. In order to further understand the role that structural features of ILs play on the enhanced selectivity of nonpolar analytes, a more comprehensive study is needed to evaluate functionalized ILs with varied cation/anion composition. In this study, a total of twelve imidazolium-based dicationic ILs containing homoanions and heteroanions were examined as second-dimension stationary phases in GC×GC separations. In order to better understand the physical properties of ILs, GC×GC was also applied to evaluate the lowest operation temperature of IL-based stationary phases. The solvation parameter model was employed to evaluate the solvation properties of the IL-based stationary phases. The best performing IL-based stationary phases were used to prepare highly selective GC columns for the separation of kerosene by GC×GC.

## 2.2 Experimental procedure

### 2.2.1 Materials

The reagents imidazole (99%), 1-methylimidazole (99%), acrylonitrile (99%), 1,4-dibromobutane (99%), 1,10-dibromodecane (97%), 1,12-dibromododecane (98%), 1-chlorodecane (98%), 1-bromodecane (98%), 1-bromohexadecane (97%) and iron (III) chloride hexahydrate ( $\text{FeCl}_3 \cdot 6\text{H}_2\text{O}$ ) (97%) were purchased from Sigma-Aldrich (St. Louis, MO, USA). Lithium bis[(trifluoromethyl)sulfonyl]imide was purchased from SynQuest Labs (Alachua, FL, USA). Chloroform, methylene chloride, methanol, isopropanol, ethyl acetate, and hexane (HPLC grade) were purchased from Fisher Scientific (Fair Lawn, NJ, USA). Untreated fused silica capillary tubing (0.25-mm I.D.) was obtained from Supelco (Bellefonte, PA, USA).

Kerosene was purchased from a local distributor. The forty-six probe molecules selected for the characterization of the IL stationary phases using the solvation parameter model have been described previously by our group [30]. A complete list of all probe molecules and their corresponding solute descriptors is shown in Table A1 (Appendix A).

### 2.2.2 Instrumental analysis

The melting points of the ILs were determined using a Perkin Elmer Pyris 1 Differential Scanning Calorimeter. All gas chromatography measurements used to characterize the IL-based stationary phases were performed on an Agilent 6850 gas chromatograph employing a flame ionization detector (GC-FID). Two-dimensional separations were performed on a GC×GC-FID system using an Agilent 6890 GC-FID equipped with a two-stage cryogenic loop modulator. A full description and illustration of the home built system has been previously reported [30].

### 2.2.3 Synthesis of dicationic ionic liquids

The structures and abbreviations for all ILs examined in this work are shown in Figure 1. IL **1** was synthesized following a previously reported procedure [10]. The halide counteranion was then exchanged to  $[\text{FeCl}_3\text{Br}]^-$  using equimolar amounts of iron(III) chloride hexahydrate in methanol to obtain IL **1**.

ILs **2**, **4-10** were synthesized following previously reported procedures [33]. The synthetic route for the dication platform is shown in Figure A1 (Appendix A). Briefly, 0.10 mol of imidazole and 0.13 mol of acrylonitrile were added to 10 mL of methanol. The mixture was heated at 45 °C for 5 h under nitrogen. Methanol and excess acrylonitrile were subsequently

removed under vacuum. This product was dissolved in 30 mL of chloroform followed by the addition of 0.05 mol of the appropriate dibromoalkane. The resulting solution was refluxed overnight and 40 mL of 15% (w/w) NaOH aqueous solution was

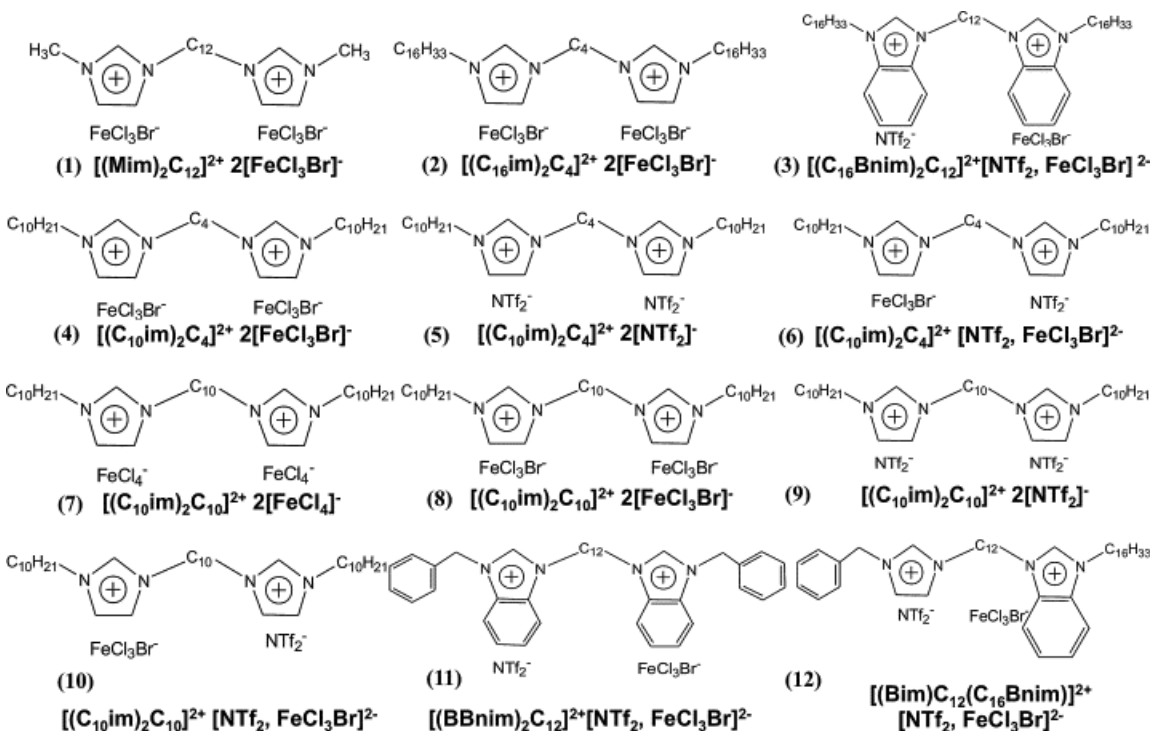


**Figure 1.** Structure and abbreviations of ILs examined in this study.

added. The mixture was stirred overnight at room temperature. The chloroform layer was then washed five times with water. The product was re-dissolved in isopropanol and reacted with two molar equivalents of the bromoalkane/chloroalkane. The halide counteranion was then exchanged to  $[\text{NTf}_2]^-$  and  $[\text{FeCl}_3\text{Br}]^-/[\text{FeCl}_4]^-$  to yield ILs **2**, **4**, **5**, **7**, **8** and **9**. Equimolar amounts of the  $[\text{NTf}_2]^-$ -based IL and  $[\text{FeCl}_3\text{Br}]^-$ -based IL were mixed in methanol at room temperature for 24 h to obtain ILs **6** and **10**. The  $^1\text{H}$  NMR and ESI-MS spectra are shown in Figures A2-A6 (Appendix A). The synthesis of ILs **3**, **11** and **12** was described in a previously reported procedure [33].

#### 2.2.4 GC column preparation

Prior to coating the IL-based columns, all ILs were placed under vacuum at 75 °C overnight to remove any traces of water. A 0.25% (w/v) or 0.45% (w/v) coating solution was prepared by dissolving the neat IL in dry methylene chloride. Five-meter segments of untreated capillary column were coated by the static method at 40 °C. All coated columns were conditioned from 30 °C to 100 °C at 1 °C min<sup>-1</sup> and held isothermally at 100 °C for 3 h. Helium was used as carrier gas at a constant flow of 1 mL min<sup>-1</sup>. Column efficiency was determined using naphthalene at 100 °C. All coated columns possessed efficiencies of at least 1800 plates per meter.

#### 2.2.5 Chromatographic analysis by GC×GC-FID

When evaluating the selectivities of the IL-based columns by GC×GC-FID analysis, the primary column consisted of a Rtx-5 capillary column (30 m × 250 μm,  $d_f$  = 0.25 μm, Restek, Bellefonte, PA, USA) connected to a second-dimension IL-coated capillary column (1.2 m × 250 μm,  $d_f$  = 0.15 or 0.28 μm). In all experiments, 1 μL of the kerosene sample was injected using a 300:1 split ratio at 250 °C. The chromatographic oven was programmed from 40 °C to 120 °C at 2 °C min<sup>-1</sup>, followed by a secondary ramp from 120 °C to 200 °C at 20 °C min<sup>-1</sup>. Hydrogen was employed as carrier gas at a constant flow of 1.2 mL min<sup>-1</sup>. The peak widths in the first dimension were estimated to be in the range of 10-14 s. The modulation period was 7 s for all separations except for the evaluation of IL **3** as <sup>2</sup>D columns with 0.28 μm film thickness where a 9 s modulation cycle was used, which yield the modulation ratios in the range of 1.2 to 2. All separations were performed in duplicate.

## 2.3 Results and Discussion

### 2.3.3 Physical properties of IL-based stationary phases examined in this study

In order for ILs to be successfully employed as GC stationary phases, a number of their physical and chemical properties need to be evaluated. Among these properties, the melting point is critical as it determines the liquid range of the stationary phase and influences the retention mechanism by which the analytes are retained during GC analysis [13]. Typically, analytes are retained by stationary phases through either partition or adsorption. If the melting point of the IL is higher than the operating oven temperature, then retention of analytes is likely governed by adsorption and can result in decreased column efficiency due to poor mass transfer [13,14].

In this study, all the ILs examined were liquids at room temperature except for IL **2** (melting point: 77 °C) and IL **4** (melting point: 50 °C). These melting points are in agreement with previously reported data, since dicationic ILs with short linker chains possess higher melting points [10]. On the other hand, an increase in the IL linker chain results in decreased melting points, as observed for IL **8**, which is a room temperature IL.

To illustrate the undesired separations produced by gas-solid chromatography, visual inspection of the GC×GC chromatogram representing the separation of kerosene in Figure 2A indicates that when IL **2** is employed as the second-dimension column, aliphatic hydrocarbons are not resolved. In addition, poor chromatographic efficiency is observed. This lack of <sup>2</sup>D selectivity is attributed to the fact that adsorption is the governing mechanism of analyte retention. Poole and co-workers described a method to evaluate the lowest operation temperature of IL-based stationary phases [13]. By repetitive injection of the analyte at a series of chromatographic runs with increasing temperature, the minimum temperature limit is

measured at the oven temperature where acceptable peak shape and chromatographic efficiency are obtained. In the current study, it was observed that GC $\times$ GC is a feasible alternative to determine the practical minimum operating temperature of the stationary phase. In the Rtx-5  $\times$  IL column set, the temperature programmed analysis of a homologous series of analytes, such as those found in kerosene, emulates Poole's method in a single run. During

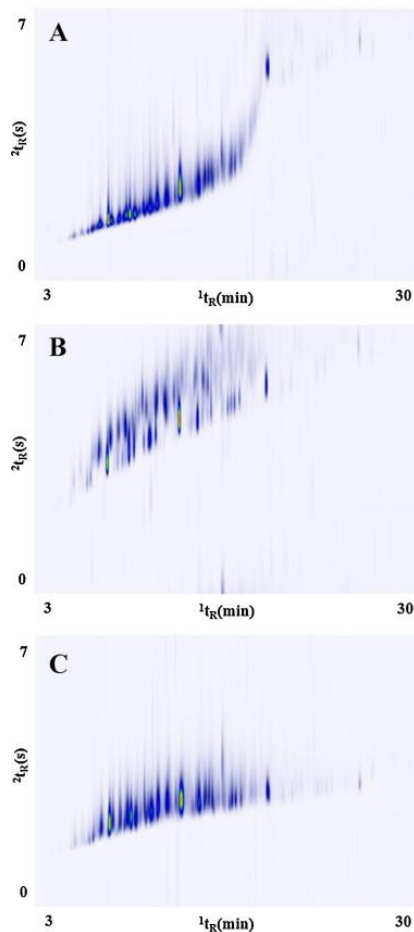


**Figure 2.** GC $\times$ GC chromatograms of kerosene employing ILs capable of undergoing different extents of dispersive-type interactions as  $^2$ D columns: (A) Rtx-5  $\times$  IL **2**, (B) Rtx-5  $\times$  IL **3**, and (C) Rtx-5  $\times$  IL **1**.

GC $\times$ GC analysis, there are a series of continuous and periodic transfers of analytes to the  $^2$ D column. As the analysis of the homologous series proceeds, there is also a steady increase in the oven temperature. Consequently, when the peaks in the chromatogram begin exhibiting

improved  $^2D$  peak shapes and acceptable efficiencies (see Figure 2A near 18 min), that moment determines the lower operating temperature of the stationary phase. From this experiment, the practical minimum operating temperature for IL **2** was found to be 76 °C, which is identical to its melting point.

### 2.3.2 Solvation Parameter Model

Previous studies have shown that the Abraham solvation parameter model is a powerful tool to accurately and comprehensively evaluate the solvation properties of ILs. This model, as described by Equation 1, also allows separation scientists to establish quantitative structure-retention relationships to understand the role that IL structural features play on the selectivity in 1D-GC and GC×GC separations [30,31,35].

$$\text{Log } k = c + eE + sS + aA + bB + lL \quad (1)$$

where  $k$  is the retention factor of each probe molecule on the liquid stationary phase at a specific temperature. The solute descriptors ( $E$ ,  $S$ ,  $A$ ,  $B$  and  $L$ ) have been previously determined and are shown in Table A1 (Appendix A) [34]. The solute descriptors are defined as:  $E$ , the excess molar refraction calculated from the solute's refractive index;  $S$ , the solute dipolarity/polarizability;  $A$ , the solute hydrogen bond acidity;  $B$ , the solute hydrogen bond basicity; and  $L$ , the solute gas hexadecane partition coefficient determined at 298 K. The system constants ( $e$ ,  $s$ ,  $a$ ,  $b$ , and  $l$ ) are used to characterize the strength of each solvation interaction and are defined as:  $e$ , the ability of the stationary phase to interact with analytes by electron lone pair interactions;  $s$ , a measure of the dipolarity/polarizability of the stationary phase;  $a$  and  $b$ , the IL hydrogen bond basicity and acidity of the stationary phase, respectively; and  $l$  describes the dispersion forces/cavity formation of the IL.

The system constants of ten IL-based GC columns evaluated in this study are shown in Table 1. The calculated system constants are generally statistically sound as represented by the moderate value of the Fisher coefficients, which shows high statistical significance of components in the model. In addition, the system constants exhibit a temperature dependence as the strength of the individual solvation interactions decrease with increasing temperature, as expected for gas-liquid chromatography [8]. It can be readily observed that these stationary phases exhibit unique system constants when compared to contemporary “polar” stationary phases [8,13,31].

### 2.3.3 Effect of IL cation/anion on system constants

IL **1** and IL **8**, as shown in Figure 1, contain similar alkyl linker chains and are paired with the  $[\text{FeCl}_3\text{Br}]^-$  anion. However, they are distinguished from each other by the length of the free alkyl side chain substituent (e.g., methyl versus decyl). As shown in Table 1, similar system constants were observed for the two ILs except for the  $e$  and  $l$  terms, which represents electron lone pair interactions and dispersion forces. It has been previously reported that imparting long alkyl chain substituents to the cationic moiety can generate less cohesive ILs [36]. The same trend was observed in this study where IL **8** exhibited a  $l$  term of 0.74 at 50 °C compared to the significantly lower  $l$  term of IL **1** ( $l = 0.61$ ). Analogously, this trend was observed when examining ILs **2** and **4**. Due to its high melting point, the system constants of IL **2** could not be measured at 50 °C. When comparing the system constants at 80 °C, IL **2** ( $l = 0.75$ ) exhibited the highest  $l$  term for all ten ILs examined in this study.

A comparison of IL **4** ( $l = 0.69$ ) and IL **8** ( $l = 0.74$ ) at 50 °C reveals that the longer alkyl linker between the imidazolium cations results in a slight increase in dispersion forces. This is



in agreement with a previously reported study [10]. The same trend was also observed for ILs that possess similar structures. As seen in Table 1, a comparison of two ILs with the  $[\text{NTf}_2]^-$  anion shows that IL **9** possessing a decane linker chain between the cations exhibited a higher  $l$  term ( $l = 0.77$ ) than IL **5** in which a butyl chain links the two cations ( $l = 0.70$ ).

The dipolarity and hydrogen bond basicity of the ILs are largely determined by the nature of the counter anion [14]. In this study, several ILs based on the  $[(\text{C}_{10}\text{im})_2\text{C}_{10}]^{2+}$  cation were paired with different counter anions, including  $[\text{FeCl}_4]^-$ ,  $[\text{FeCl}_3\text{Br}]^-$ , and  $[\text{NTf}_2]^-$  to produce ILs **7**, **8**, **9**, and **10**. At 50 °C, it was observed that the  $s$  and  $a$  terms of these ILs ranged from 1.78-1.97 and 1.98-2.24, respectively. Considering the standard deviations of the system constants shown in Table 1, the dipolarity and hydrogen bond basicity remained largely unchanged in this group of ILs. Analogously, the same trend was observed for ILs with identical cationic components (*i.e.*, ILs **4**, **5**, and **6**).

**Table 1.** System constants of the IL-based stationary phases examined in this study.

IL No.	Temperature (°C)	System constant									
		<i>c</i>	<i>e</i>	<i>s</i>	<i>a</i>	<i>b</i>	<i>l</i>	n	R <sup>2</sup>	F	
1	[(Mim) <sub>2</sub> C <sub>12</sub> ] <sup>2+</sup> 2[FeCl <sub>3</sub> Br] <sup>-</sup>										
	50	-3.35	0.42	1.83	1.93	0.92	0.61	34	0.99	488	
		(0.10) <sup>a</sup>	(0.10)	(0.12)	(0.15)	(0.15)	(0.02)				
	80	-3.35	0.39	1.72	1.79	0.75	0.50	33	0.99	470	
		(0.10)	(0.08)	(0.11)	(0.13)	(0.13)	(0.02)				
	110	-3.42	0.29	1.63	1.73	0.61	0.42	32	0.99	430	
(0.09)		(0.07)	(0.09)	(0.11)	(0.12)	(0.02)					
2	[(C <sub>16</sub> im) <sub>2</sub> C <sub>4</sub> ] <sup>2+</sup> 2[FeCl <sub>3</sub> Br] <sup>-</sup> <sub>-<sup>b</sup></sub>										
	50										
	80	-3.98	0	1.51	1.75	0.58	0.75	32	0.99	368	
		(0.11)		(0.13)	(0.16)	(0.17)	(0.02)				
	110	-3.32	0.11	1.21	1.32	0.45	0.55	32	0.99	431	
		(0.08)	(0.07)	(0.09)	(0.10)	(0.11)	(0.02)				
3	[(C <sub>16</sub> BnIM) <sub>2</sub> C <sub>12</sub> ] <sup>2+</sup> [NTf <sub>2</sub> , FeCl <sub>3</sub> Br] <sup>2-</sup>										
	50	-3.25	-0.15	1.59	1.89	0.42	0.75	39	0.99	603	
		(0.10)	(0.08)	(0.11)	(0.11)	(0.13)	(0.02)				
	80	-3.35	-0.08	1.44	1.52	0.51	0.66	36	0.99	551	
		(0.10)	(0.07)	(0.09)	(0.11)	(0.12)	(0.02)				
	110	-3.37	-0.06	1.35	1.27	0.40	0.56	34	0.99	478	
(0.09)		(0.06)	(0.08)	(0.10)	(0.10)	(0.02)					
4	[(C <sub>10</sub> im) <sub>2</sub> C <sub>4</sub> ] <sup>2+</sup> 2[FeCl <sub>3</sub> Br] <sup>-</sup>										
	50	-3.32	0.26	1.48	1.74	0.78	0.69	30	0.99	475	
		(0.10)	(0.10)	(0.12)	(0.15)	(0.18)	(.02)				

**Table 1.** (continued)

<b>5</b>	80	-3.31 (0.07)	0.15 (0.05)	1.55 (0.07)	1.56 (0.09)	0.51 (0.10)	0.58 (0.02)	31	0.99	798
	110	-3.27 (0.05)	0.18 (0.04)	1.32 (0.05)	1.49 (0.07)	0.59 (0.07)	0.48 (0.01)	31	0.99	978
	[(C <sub>10</sub> im) <sub>2</sub> C <sub>4</sub> ] <sup>2+</sup> 2[NTf <sub>2</sub> ] <sup>-</sup>									
	50	-3.29 (0.08)	-0.14 (0.08)	1.81 (0.09)	2.04 (0.08)	0.28 (0.11)	0.70 (0.02)	39	0.99	730
	80	-3.30 (0.07)	0.02 (0.06)	1.55 (0.07)	1.60 (0.06)	0.45 (0.09)	0.58 (0.01)	37	0.99	718
	110	-3.38 (0.06)	0.03 (0.05)	1.50 (0.06)	1.42 (0.05)	0.33 (0.08)	0.50 (0.01)	37	0.99	822
	[(C <sub>10</sub> im) <sub>2</sub> C <sub>4</sub> ] <sup>2+</sup> [NTf <sub>2</sub> , FeCl <sub>3</sub> Br] <sup>2-</sup>									
	50	-3.28 (0.09)	0.09 (0.08)	1.76 (0.11)	2.00 (0.14)	0.44 (0.15)	0.68 (0.02)	38	0.99	491
	80	-3.43 (0.08)	0.10 (0.06)	1.53 (0.08)	1.73 (0.08)	0.57 (0.10)	0.60 (0.02)	35	0.99	636
	110	-3.45 (0.07)	0.04 (0.05)	1.51 (0.07)	1.67 (0.07)	0.32 (0.08)	0.51 (0.01)	34	0.99	615
	[(C <sub>10</sub> im) <sub>2</sub> C <sub>10</sub> ] <sup>2+</sup> 2[FeCl <sub>4</sub> ] <sup>-</sup>									
	50	-3.78 (0.09)	0	1.78 (0.08)	2.07 (0.08)	0.73 (0.12)	0.77 (0.02)	35	0.99	811
<b>7</b>	80	-4.02 (0.11)	0	1.78 (0.11)	2.32 (0.13)	0.50 (0.15)	0.72 (0.02)	35	0.99	398
	110	-3.40 (0.09)	0	1.50 (0.08)	1.68 (0.08)	0.34 (0.11)	0.52 (0.02)	33	0.99	414
	[(C <sub>10</sub> im) <sub>2</sub> C <sub>10</sub> ] <sup>2+</sup> 2[FeCl <sub>3</sub> Br] <sup>-</sup>									

**Table 1.** (continued)

<b>8</b>	50	-3.60 (0.10)	0.07 (0.09)	1.85 (0.12)	1.98 (0.15)	0.72 (0.15)	0.74 (0.02)	38	0.99	579
	80	-3.54 (0.09)	0.06 (0.08)	1.68 (0.10)	1.85 (0.13)	0.55 (0.13)	0.62 (0.02)	35	0.99	488
	110	-3.43 (0.08)	0.16 (0.06)	1.39 (0.08)	1.62 (0.10)	0.56 (0.10)	0.51 (0.02)	31	0.99	534
$[(C_{10}im)_2C_{10}]^{2+}2[NTf_2]^-$										
<b>9</b>	50	-3.31 (0.09)	-0.11 (0.08)	1.85 (0.09)	2.24 (0.08)	0.22 (0.17)	0.77 (0.02)	41	0.99	619
	80	-3.27 (0.08)	-0.06 (0.06)	1.67 (0.08)	1.84 (0.07)	0.17 (0.10)	0.59 (0.02)	40	0.99	600
	110	-3.19 (0.07)	-0.02 (0.05)	1.50 (0.07)	1.50 (0.05)	0.12 (0.08)	0.49 (0.01)	40	0.99	633
$[(C_{10}im)_2C_{10}]^{2+} [NTf_2, FeCl_3Br]^{2-}$										
<b>10</b>	50	-3.67 (0.10)	-0.07 (0.10)	1.97 (0.12)	2.11 (0.16)	0.62 (0.16)	0.74 (0.03)	38	0.99	490
	80	-3.60 (0.08)	-0.03 (0.07)	1.80 (0.10)	1.87 (0.12)	0.45 (0.13)	0.62 (0.02)	38	0.99	569
	110	-3.55 (0.09)	0.01 (0.07)	1.61 (0.09)	1.58 (0.11)	0.42 (0.11)	0.52 (0.02)	33	0.99	484

<sup>a</sup>: The values in brackets are standard deviations.

<sup>b</sup>: Due to the high melting point of IL **2**, the system constants could not be measured at 50 °C.

n: number of probe analytes subjected to multiple linear regression

R<sup>2</sup>: correlation coefficient.

F: Fisher coefficients.

### 2.3.4 GC×GC analysis of kerosene

Kerosene was selected as the model complex sample in this study because it contains numerous aliphatic hydrocarbons and its group-type separation by GC×GC has been previously described [30, 37-39]. A total of ten IL-based stationary phases were evaluated as the second-dimension column in GC×GC separations. The chosen column arrangement was the nonpolar × polar combination, as it facilitates assessment of the <sup>2</sup>D selectivity by simple visual inspection. Before GC×GC analysis, the temperature program was optimized by applying different heating rates (i.e., 2 °C min<sup>-1</sup>, 4 °C min<sup>-1</sup>, and 6.4 °C min<sup>-1</sup>). As shown in Figure A7 (Appendix A), 2 °C min<sup>-1</sup> shows the best separation for kerosene sample and was chosen for all subsequent GC×GC analysis.

Previous work by our group showed that less cohesive IL-based stationary phases are capable of resolving aliphatic hydrocarbons within kerosene [30]. In order to validate this hypothesis and establish a qualitative structure-retention relationship of IL stationary phases and nonpolar solutes, this study began by examining the less cohesive room temperature ionic liquid (IL **3**) as the <sup>2</sup>D stationary phase. As shown in Figure 2B, IL **3** provided good separation of the aliphatic hydrocarbons. For comparison, a more cohesive IL (IL **1**) was examined and resulted in significantly lower analyte retention in the second-dimension, as shown in Figure 2C.

Imparting longer alkyl linker chains between the imidazolium cations can also produce slightly less cohesive RTILs which is favorable for the separation of nonpolar analytes. To explore this structural feature, two groups of ILs were evaluated using the Rtx-5 × IL column set. The first group of ILs (ILs **4**, **5** and **6**) consisted of the [(C<sub>10</sub>im)<sub>2</sub>C<sub>4</sub>]<sup>2+</sup> cation with a butane linker chain paired with different anions (Figure 3), while the second group of ILs (ILs **7**, **8**, **9** and **10**) was comprised of the [(C<sub>10</sub>im)<sub>2</sub>C<sub>10</sub>]<sup>2+</sup> cation employing a decane linker chain and paired with different anions (Figure 4). It can be observed in Figure 3 that

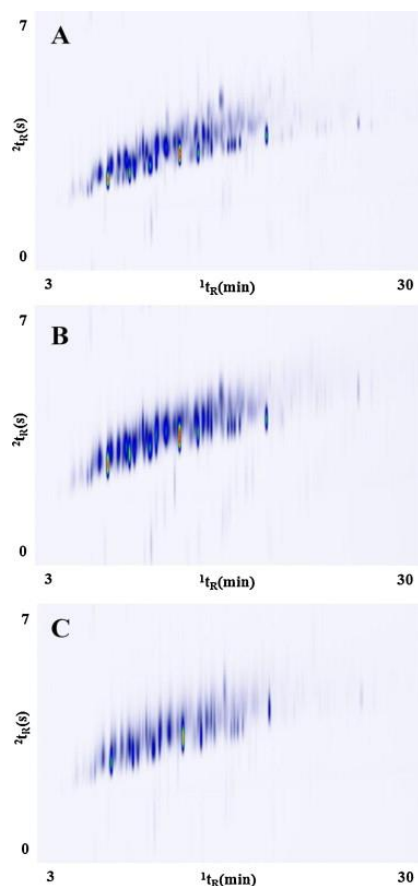


**Figure 3.** GC×GC chromatograms showing the effect of employing ILs based on the  $[(C_{10}im)_2C_4]^{2+}$  cation paired with different counter anions as  $^2D$  columns in the separation of kerosene: (A) Rtx-5  $\times$  IL 4 ( $2[FeCl_3Br]^-$ ), (B) Rtx-5  $\times$  IL 5 ( $2[NTf_2]^-$ ), and (C) Rtx-5  $\times$  IL 6 ( $[NTf_2, FeCl_3Br]^{2-}$ ).

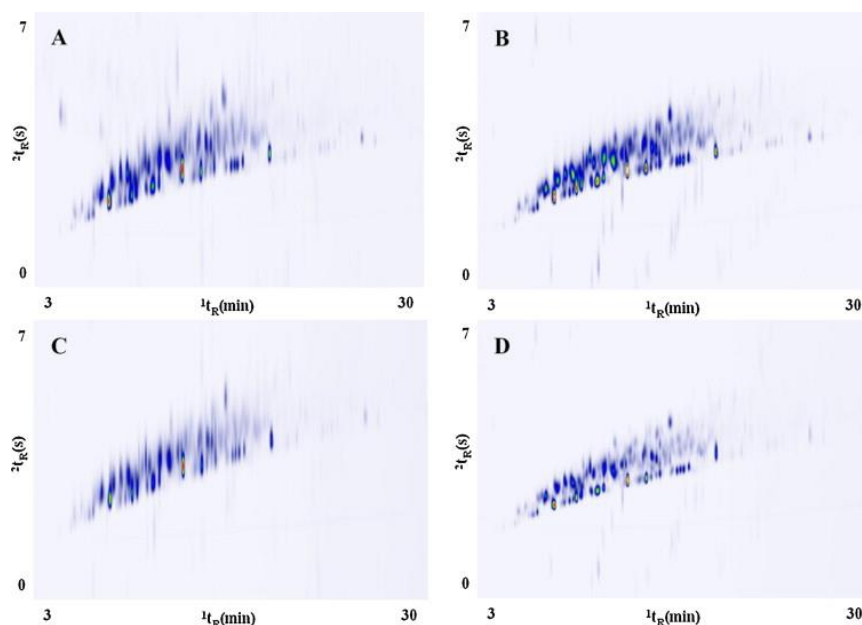


**Figure 4.** GC×GC chromatograms of kerosene employing ILs based on the  $[(C_{10}im)_2C_{10}]^{2+}$  cation paired with different counter anions as  $^2D$  column: (A) Rtx-5  $\times$  IL 7 ( $[FeCl_4]^-$ ), (B) Rtx-5  $\times$  IL 9 ( $2[NTf_2]^-$ ), (C) Rtx-5  $\times$  IL 8 ( $2[FeCl_3Br]^-$ ), and (D) Rtx-5  $\times$  IL 10 ( $[NTf_2, FeCl_3Br]^{2-}$ ).

the counteranion does not strongly influence the overall GC×GC separation. Similar selectivities toward the aliphatic hydrocarbons were attained, which is in accordance with the similar  $l$  values ( $l = 0.69$ - $0.70$ ). However, a comparison of contour plots for ILs **7**, **8**, **9**, and **10**, which possess larger differences in  $l$  terms (from  $0.74$ - $0.77$ ) shows that the less cohesive IL (e.g., IL **7**) exhibits a larger elution window compared to the other more cohesive ILs (see Figure 4). Broader peaks were observed in some chromatograms, such as Figure 4C, which is likely due to the slightly lower column efficiency of the second-dimension column compared to the other column sets. By comparing the chromatograms in Figure 3 and 4, it can be observed that less cohesive ILs, such as IL **7**, exhibited the best distribution of aliphatic hydrocarbons in the retention plane. A side-by-side comparison of the expanded regions of the GC×GC chromatograms of kerosene employing different column sets is shown in Figures A8 and A9 (Appendix A). It can be clearly observed, as highlighted by the selected regions, that many peaks that overlap in Figure A8 are resolved in A9. In light of this result, long free alkyl side chain substituents and long linker chains between the two cations of the ILs are two important structural features that give rise to the highly selective separation of aliphatic hydrocarbons.

As mentioned previously in Section 2.3.2, analytes can interact with the stationary phase through a multitude of different interactions. In order to study this effect while still retaining the high thermal stability of the IL, benzyl moieties were incorporated within the cation structure to evaluate the effect of  $\pi$ - $\pi$  interactions on the selectivity of the <sup>2</sup>D column. These two ILs, ILs **11** and **12**, were evaluated using the Rtx-5 × IL column set. System constants of monocationic ILs with similar structures to ILs **11** and **12** were reported in a previous study [11]. It was demonstrated that replacing the free alkyl side chain of the imidazolium-based IL with an aromatic group increases the  $e$  term while decreasing the  $l$  term. From the structure of IL **11**, it can be expected that analytes may interact via  $\pi$  and

nonbonding electrons as well as dispersive-type interactions. For IL **12**, one cation is identical to IL **3** while another cation is functionalized with the benzyl moiety, which can engage in strong dispersive interactions as well as moderate  $\pi$ - $\pi$  interactions with analytes. Examination of the two ILs as the  $^2D$  stationary phase indicates that IL **11** (Figure 5A) exhibits poor selectivity in the resolution of the aliphatic hydrocarbons. However, IL **12** (Figure 5B) exhibited a significant enhancement in the selectivity of nonpolar analytes compared to IL **11**. A comparison of the chromatograms of IL **11** and IL **3** in Figure 5B and

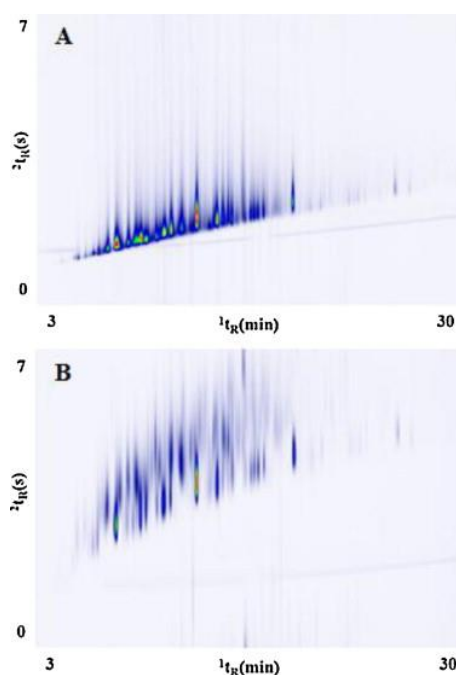


**Figure 5.** GC $\times$ GC chromatograms showing the effect of aromatic moieties within the IL structure when used as  $^2D$  columns in the separation of kerosene: (A) Rtx-5  $\times$  IL **11**, and (B) Rtx-5  $\times$  IL **12**.

Figure 2B, respectively, reveals a similar distribution of the analytes in the retention plane. Although only the benzimidazolium cation within this unsymmetrical dicationic IL possesses the long alkyl substituent, this structural feature was sufficient to provide the selectivity required for improved resolution of the aliphatic hydrocarbons. This observation further proves that long alkyl side chain substituents are important structural features for dicationic ILs in the separation of nonpolar analytes.



### 2.3.5 Effect of stationary phase film thickness on GC×GC separations

It is well known that larger film thickness of the  $^2\text{D}$  stationary phase can reduce  $^2\text{D}$  column over loading and offers better retention and selectivity [40-42]. However, thicker films can produce chromatographic band broadening and cause wrap-around due to excessive retention. Therefore, these parameters must be carefully optimized to preserve the separation of each individual stage while maximizing the overall peak capacity.

As shown in the previous section, IL-based stationary phases with 0.15  $\mu\text{m}$  film thickness provided good selectivity in resolving aliphatic hydrocarbons from kerosene. In an attempt to further enhance the separation capacity of the IL-based GC columns, the best performing ILs (i.e., IL **3**, **7**, **8**, and **10**) were used to prepare columns with a 0.28  $\mu\text{m}$  film thickness. The GC×GC chromatograms of kerosene obtained using these column sets are shown in Figure 6. It is evident that the higher stationary phase loading in the  $^2\text{D}$  column offered more retention and better selectivity although some band broadening was observed. No significant wrap-around was observed, except for IL **3**. In an effort to eliminate wrap-around, a modulation period of 9 s was examined. A side-by-side comparison between Figures 4 and 6 reveals a wider distribution of the analytes within the retention plane when employing  $^2\text{D}$  columns with 0.28  $\mu\text{m}$  film thickness, especially for ILs **3** and **7**. This observation was further validated by visual inspection the expanded regions of the GC×GC chromatograms of kerosene. As shown in Figures A10 (Appendix A), many peaks that overlap in Figure A9 can be resolved in A10. It can be concluded that in cases where high modulation ratio is required for trace analysis, a column containing a 0.15  $\mu\text{m}$  film thickness would likely be the best choice. However, when analyzing more complex samples where better  $^2\text{D}$  resolution is required, columns with 0.28  $\mu\text{m}$  film thickness produce better results. In addition, columns with larger film thickness also lower the chances of overloading in the  $^2\text{D}$  column.

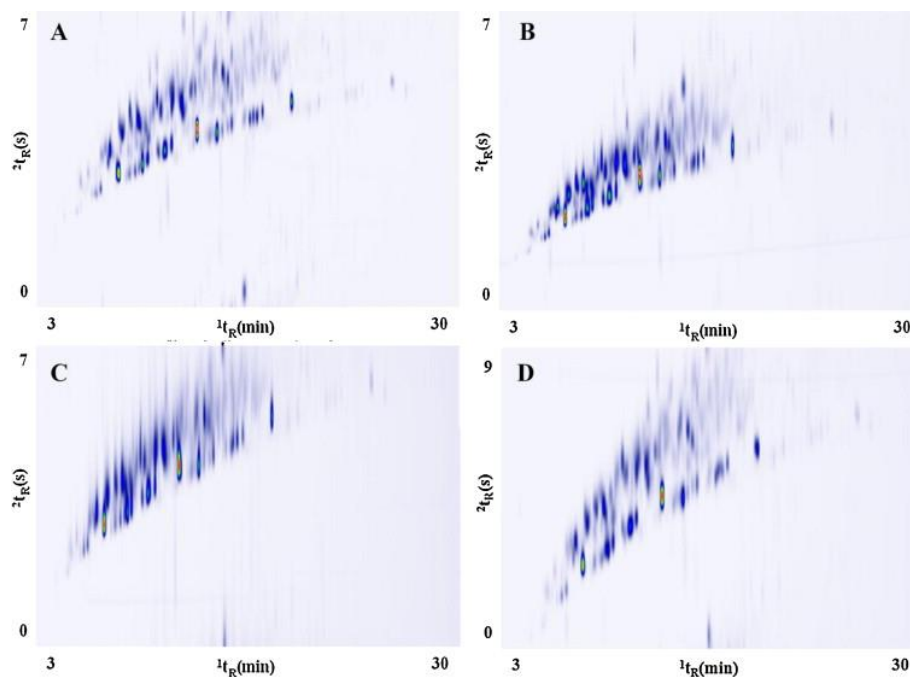


**Figure 6.** GC×GC chromatograms of kerosene employing select IL-based stationary phases with 0.28  $\mu\text{m}$  film thickness as  $^2\text{D}$  columns: (A) Rtx-5  $\times$  IL **7**, (B) Rtx-5  $\times$  IL **9**, (C) Rtx-5  $\times$  IL **8**, and (D) Rtx-5  $\times$  IL **3**.

## 2.4 Conclusions

A total of twelve dicationic IL-based stationary phases were examined in this study as second-dimension columns for the separation of aliphatic hydrocarbons within kerosene using GC×GC. The structural tuning of dicationic ILs was guided by examining the solvation properties of ILs using the solvation parameter model as well as evaluating the separation results from GC×GC separations. ILs containing long side alkyl chain substituents and long linker chains between the cations can engage in strong dispersive interactions and offer the best selectivity for aliphatic hydrocarbons. The best performing ILs were selected to prepare stationary phases with 0.28  $\mu\text{m}$  film thickness and provided enhanced selectivity. These results show that dispersive interactions play a key role in the resolution of nonpolar aliphatic hydrocarbons by IL-based stationary phases. Ultimately, this knowledge will guide the structural design of new high thermal stable IL-based stationary phases that provide strong dispersive interactions for the separation of nonpolar

analytes within complex samples, particularly those within the petrochemical industry. Moreover, this approach can also be applied for the development of new IL-based stationary phases that possess other types of solvation properties (e.g.,  $\pi$ - $\pi$  interactions, hydrogen bonding, etc.) for the GC $\times$ GC separation of complex samples of interest to the flavors and fragrance and pharmaceutical industries.

### Acknowledgements

The authors acknowledge funding from Chemical Measurement and Imaging Program at the National Science Foundation (Grant number CHE-1413199).

### References

- [1] J. Dallüge, J. Beens, U.A.T. Brinkman, *J. Chromatogr. A* 1000 (2003) 69
- [2] P. Marriott, R. Shellie, *Trends Anal. Chem.* 21 (2002) 573
- [3] M. Adahchour, J. Beens, R.J.J. Vreuls, U.A.T. Brinkman, *Trends Anal. Chem.* 25 (2006) 438
- [4] M. Adahchour, J. Beens, U.A.T. Brinkman, *J. Chromatogr. A* 1186 (2008) 67
- [5] J.V. Seeley, S.K. Seeley, *Anal. Chem.* 85 (2012) 557
- [6] P.J. Marriott, S.-T. Chin, B. Maikhunthod, H.-G. Schmarr, S. Bieri, *Trends Anal. Chem.* 34 (2012) 1
- [7] L. Mondello, P.Q. Tranchida, P. Dugo, G. Dugo, *Mass Spectrom. Rev.* 27 (2008) 101
- [8] C.F. Poole, S.K. Poole, *J. Chromatogr. A* 1184 (2008) 254
- [9] T.D. Ho, C. Zhang, L.W. Hantao, J.L. Anderson, *Anal. Chem.* 86 (2013) 262
- [10] J.L. Anderson, R.F. Ding, A. Ellern, D.W. Armstrong, *J. Am. Chem. Soc.* 127 (2004) 593
- [11] J.L. Anderson, D.W. Armstrong, *Anal. Chem.* 75 (2003) 4851
- [12] J.L. Anderson, J. Ding, T. Welton, D.W. Armstrong, *J. Am. Chem. Soc.* 124 (2002) 14247
- [13] C.F. Poole, N. Lenca, *J. Chromatogr. A* 1357 (2014) 87

- [14] C. Yao, J.L. Anderson, *J. Chromatogr. A* 1216 (2009) 1658
- [15] Ionic liquid capillary GC columns, <http://www.sigmaaldrich.com/il-gc>, Accessed Oct 31, 2014
- [16] C. Ragonese, D. Sciarrone, P.Q. Tranchida, P. Dugo, L. Mondello, *J. Chromatogr. A* 1255 (2012) 130
- [17] P. Delmonte, A.-R. Fardin Kia, J.K.G. Kramer, M.M. Mossoba, L. Sidisky, J.I. Rader, *J. Chromatogr. A* 1218 (2011) 545
- [18] C. Ragonese, P.Q. Tranchida, P. Dugo, G. Dugo, L.M. Sidisky, M.V. Robillard, L. Mondello, *Anal. Chem.* 81 (2009) 5561
- [19] L. Do, P. Liljelind, J. Zhang, P. Haglund, *J. Chromatogr. A* 1311 (2013) 157
- [20] C. Cagliero, C. Bicchi, C. Cordero, E. Liberto, B. Sgorbini, P. Rubiolo, *J. Chromatogr. A* 1268 (2012) 130
- [21] B.M. Weber, J.J. Harynuk, *J. Chromatogr. A* 1271 (2013) 170
- [22] C. Domínguez, C. Reyes-Contreras, J.M. Bayona, *J. Chromatogr. A* 1230 (2012) 117
- [23] J. Krupčík, R. Gorovenko, I. Špánik, I. Bočková, P. Sandra, D.W. Armstrong, *J. Chromatogr. A* 1301 (2013) 225
- [24] A. Nosheen, B. Mitrevski, A. Bano, P.J. Marriott, *J. Chromatogr. A* 1312 (2013) 118
- [25] P. Antle, C. Zeigler, A. Robbat Jr, *J. Chromatogr. A* 1361 (2014) 255
- [26] Q. Gu, F. David, F. Lynen, P. Vanormelingen, W. Vyverman, K. Rumpel, G. Xu, P. Sandra, *J. Chromatogr. A* 1218 (2011) 3056
- [27] G. Purcaro, P.Q. Tranchida, C. Ragonese, L. Conte, P. Dugo, G. Dugo, L. Mondello, *Anal. Chem.* 82 (2010) 8583
- [28] M. Zapadlo, J. Krupčík, P. Májek, D.W. Armstrong, P. Sandra, *J. Chromatogr. A* 1217 (2010) 5859
- [29] W.C. Siegler, J.A. Crank, D.W. Armstrong, R.E. Synovec, *J. Chromatogr. A* 1217 (2010) 3144
- [30] L.W. Hantao, A. Najafi, C. Zhang, F. Augusto, J.L. Anderson, *Anal. Chem.* 86 (2014) 3717
- [31] C.F. Poole, S.K. Poole, *J. Sep. Sci.* 34 (2011) 888
- [32] Q.Q. Baltazar, J. Chandawalla, K. Sawyer, J.L. Anderson, *Colloids Surf., A* 302 (2007) 150
- [33] O. Nacham, K. D. Clark, H. L. Yu, J.L. Anderson, *Chem. Mater.* (under review)
- [34] M.H. Abraham, *Chem. Soc. Rev.* 22 (1993) 73

- [35] P. Twu, Q.C. Zhao, W.R. Pitner, W.E. Acree Jr, G.A. Baker, J.L. Anderson, J. Chromatogr. A 1218 (2011) 5311
- [36] Q.C. Zhao, J. Eichhorn, W. Pitner, J.L. Anderson, Anal. Bioanal. Chem. 395 (2009) 225
- [37] M.P. Pedroso, L.A.F. de Godoy, E.C. Ferreira, R.J. Poppi, F. Augusto, J. Chromatogr. A 1201 (2008) 176
- [38] R. Gorovenko, J. Krupčík, I. Špánik, I. Bočková, P. Sandra, D.W. Armstrong, J. Chromatogr. A 1330 (2014) 51
- [39] B. Kehimkar, J.C. Hoggard, L.C. Marney, M.C. Billingsley, C.G. Fraga, T.J. Bruno, R.E. Synovec, J. Chromatogr. A 1327 (2014) 132
- [40] Z.Y. Zhu, J. Harynuk, T. Górecki, J. Chromatogr. A 1105 (2006) 17
- [41] J. Harynuk, T. Górecki, J.d. Zeeuw, J. Chromatogr. A 1071 (2005) 21
- [42] C. Cordero, C. Bicchi, M. Galli, S. Galli, P. Rubiolo, J. Sep. Sci. 31 (2008) 3437

**CHAPTER 3****CROSSLINKED STRUCTURALLY-TUNED POLYMERIC IONIC LIQUIDS AS STATIONARY PHASES FOR THE ANALYSIS OF HYDROCARBONS IN KEROSENE AND DIESEL FUELS BY COMPREHENSIVE TWO-DIMENSIONAL GAS CHROMATOGRAPHY**

Reprinted with permission from *Journal of Chromatography A* **2016**, 1440, 160-171

Copyright © 2016, Elsevier

Cheng Zhang, Rodney A. Park, Jared L. Anderson

**Abstract**

Structurally tuned ionic liquids (ILs) have been previously applied as the second-dimension column in comprehensive two-dimensional gas chromatography (GC×GC) and have demonstrated high selectivity in the separation of individual aliphatic hydrocarbons from other aliphatic hydrocarbons. However, the maximum operating temperatures of these stationary phases limit the separation of analytes with high boiling points. In order to address this issue, a series of polymeric ionic liquid (PIL)-based stationary phases were prepared in this study using imidazolium-based IL monomers via in-column free radical polymerization. The IL monomers were functionalized with long alkyl chain substituents to provide the needed selectivity for the separation of aliphatic hydrocarbons. Columns were prepared with different film thicknesses to identify the best performing stationary phase for the separation of kerosene. The bis[(trifluoromethyl)sulfonyl]imide ([NTf<sub>2</sub>])-based PIL stationary phase with larger film thickness (0.28 μm) exhibited higher selectivity for aliphatic hydrocarbons and showed a maximum allowable operating temperature of 300 °C. PIL-based stationary phases containing varied amount of IL -based crosslinker were

prepared to study the effect of the crosslinker on the selectivity and thermal stability of the resulting stationary phase. The optimal resolution of aliphatic hydrocarbons was achieved when 50% (w/w) of crosslinker was incorporated into the PIL-based stationary phase. The resulting stationary phase exhibited good selectivity of different groups of aliphatic hydrocarbons even after being conditioned at 325 °C. Finally, the crosslinked PIL-based stationary phase was compared with SUPELCOWAX 10 and DB-17 columns for the separation of aliphatic hydrocarbons in diesel fuel. Better resolution of aliphatic hydrocarbons was obtained when employing the crosslinked PIL-based stationary phase as the second-dimension column.

### 3.1 Introduction

The trace level separation and analysis of complex mixtures such as petroleum products, fragrances, and organic pollutants can be very challenging. These samples typically contain hundreds to thousands of components which possess a wide range of properties often present at varied concentration levels [1]. Comprehensive two-dimensional gas chromatography (GC×GC) is a powerful and versatile tool for the separation, identification, and quantification of volatile and semi-volatile analytes in complex samples [2-8]. By employing two gas chromatographic separations in a continuous and sequential fashion, the peak capacity of the separation system can be significantly increased. In order to achieve a significant improvement in the resolving power, the two employed stationary phases should possess distinct solvation properties. Polysiloxane and polyethylene glycol (PEG)-derived stationary phases are commonly employed in GC × GC separations. By applying these stationary phases in nonpolar × polar or polar × nonpolar column sets, a broad spectrum of analytes, including hydrocarbons [9,10], fatty acid methyl esters [11,12], flavors and fragrance [13,14] have been successfully separated. However, the main

limitation of polyethylene glycol-derived stationary phases is their limited operation at high temperature, which can significantly limit the applications of GC×GC for high temperature analysis.

Ionic liquids (ILs) are class of organic salts with low melting points (usually defined as below 100 °C) and have been applied as stationary phases in gas chromatography [15-17]. These compounds exhibit unique characteristics such as high thermal stability, negligible vapor pressures, wide liquid ranges, and tunable selectivity. A number of IL stationary phases have been commercialized and their thermal stabilities reported [18]. For example, SLB-IL 59 and SLB-IL 60 stationary phases have a maximum allowable operating temperature (MAOT) of 300 °C, which is significantly higher than the polar PEG columns. The increased thermal stability of IL-based stationary phases has expanded the analysis of complex samples with high boiling points, such as coal tar [19] and heavy petroleum fractions [20,21]. However, the resolving power offered by commercial IL-based columns is still limited. For example, aliphatic hydrocarbons cannot be resolved on commercial IL-based stationary phases in GC×GC separations [22].

Our group has reported that dicationic ILs containing long free alkyl side chain substituents and lengthy linkage chains between the two cations exhibit high selectivity in the separation of different groups of aliphatic hydrocarbons when used as second-dimension stationary phases in GC×GC [23]. The thermal stability of the dicationic IL-based stationary phases was slightly lower than the PEG column, which may not be sufficient for high temperature GC×GC separations. One approach to improve the thermal stability is to explore polymeric analogs of ILs that possess the necessary structural features to provide high separation selectivity for target analytes. Compared to monocationic or dicationic ILs with similar structural features, PIL-based stationary phases offer similar



solvation properties but often exhibit higher thermal stability [24]. The thermal stability of the stationary phases can be further enhanced by creating crosslinked PIL stationary phases.

In this study, a total of 15 PIL-based stationary phases were prepared using imidazolium-based IL monomers via in-column free radical polymerization. To overcome the aforementioned challenges while retaining the unique solvation characteristics of the ILs, all PIL-based stationary phases were functionalized with long alkyl chain substituents to provide the selectivity required for the separation of individual aliphatic hydrocarbons from other aliphatic hydrocarbons in kerosene. The effect of the IL anion, film thickness of the stationary phase, and the chain length/amount of the IL-based crosslinker were evaluated and carefully optimized to prepare a highly selective stationary phase for the separation of aliphatic hydrocarbons under high separation temperatures. The inner surface of the capillary wall was modified with vinyltrimethoxysilane (VTMS) to produce a highly immobilized stationary phase. The best performing crosslinked PIL-based stationary phase was used for the GC×GC separation of diesel samples. Compared to the commercial PEG and DB-17 columns, crosslinked PIL-based stationary phases exhibited better separation performance in terms of selectivity and thermal stability.

## 3.2 Experimental

### 3.2.1 Materials

1-vinylimidazole (99%), 1-bromohexadecane (97%), 1,4 dibromobutane (99%), 1,8 dibromooctane (98%), 1,12-dibromododecane (98%), 2,2'-azobis (2-methylpropionitrile) (98%) (AIBN), vinyltrimethoxysilane (98%) (VTMS), and iron (III) chloride hexahydrate ( $\text{FeCl}_3 \cdot 6\text{H}_2\text{O}$ ) (97%) were purchased from Sigma-Aldrich (St. Louis, MO, USA). Lithium bis[(trifluoromethyl)sulfonyl]imide was purchased from SynQuest Labs (Alachua, FL, USA). Methylene chloride, methanol, isopropanol, ethyl acetate, and hexane (HPLC grade)

were purchased from Fisher Scientific (Fair Lawn, NJ, USA). Untreated fused silica capillary (0.25-mm I.D.) and SUPELCOWAX 10 column (30 m  $\times$  200  $\mu$ m,  $d_f$  = 0.20  $\mu$ m) were purchased from Supelco (Bellefonte, PA, USA). CP-Wax 52 CB (30 m  $\times$  200  $\mu$ m,  $d_f$  = 0.20  $\mu$ m), DB-WAX (30 m  $\times$  200  $\mu$ m,  $d_f$  = 0.20  $\mu$ m), HP-INNOWax (30 m  $\times$  200  $\mu$ m,  $d_f$  = 0.20  $\mu$ m), and DB-17 (20 m  $\times$  180  $\mu$ m,  $d_f$  = 0.18  $\mu$ m) columns were purchased from Agilent (Santa Clara, CA, USA). Kerosene and diesel fuels were purchased from a local distributor.

### 3.2.2 Chromatographic instrumentation

All gas chromatography measurements used to characterize the IL-based columns were performed on an Agilent 6850 gas chromatograph employing a flame ionization detector (GC-FID). Two-dimensional separations were performed on a GC $\times$ GC-FID system using an Agilent 6890 GC-FID equipped with a two-stage cryogenic loop modulator. A full description and illustration of the home built system has been previously reported [22].

### 3.2.3 Synthesis of ionic liquid monomer and cross-linkers

Chemical structures of the IL monomers and IL-based cross-linkers used in this work are shown in Figure 1. Synthesis of the IL monomer and cross-linkers was performed according to previously reported procedures [25-27]. Briefly, 0.05 mol of 1-vinylimidazole and 0.075 mol of 1-bromohexadecane were mixed in 15 mL of isopropanol at 70 °C for 24 h. The product was then dissolved in 10 mL of water and washed with three 10 mL aliquots of ethyl acetate. The water layer containing the IL monomer was recovered and dried under vacuum at 80 °C for 24 h to yield [VHDIM] [Br]. The halide counteranion was then exchanged to [NTf<sub>2</sub>] or [FeCl<sub>3</sub>Br] by metathesis reaction using one equivalent of lithium bis[(trifluoromethyl)sulfonyl]imide or FeCl<sub>3</sub>•6H<sub>2</sub>O. The mixture was then stirred overnight

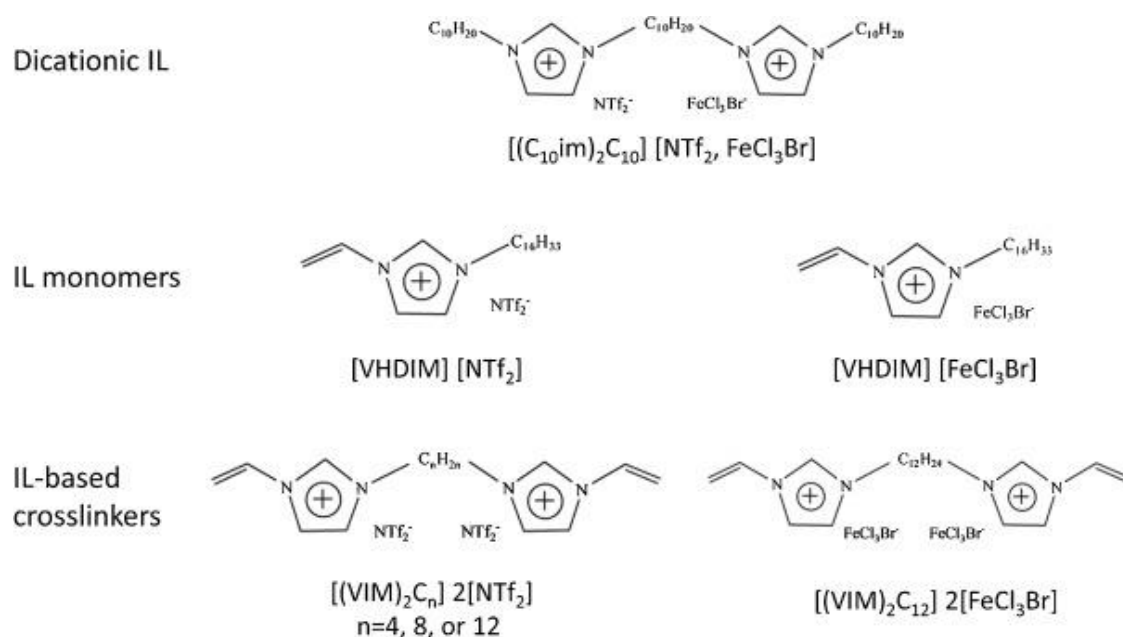


**Figure 1.** Chemical structures and abbreviations of the dicationic IL, IL monomers, and IL-based crosslinkers examined in this study.

at room temperature and washed with water to yield [VHDIM] [NTf<sub>2</sub>] and [VHDIM] [FeCl<sub>3</sub>Br]. The IL-based crosslinker was synthesized by reacting 0.1 mol of 1-vinylimidazole with 0.05 mol of 1,4 dibromobutane in 15 mL of isopropanol at 70 °C for 24 h. The dicationic IL was then dissolved in 10 mL of water and washed with three 10 mL aliquots of ethyl acetate, and dried under vacuum at 80 °C for 24 h. Crosslinkers with octyl or dodecyl linkage chains separating the two cations were synthesized using a similar approach [27]. The halide counteranion was then exchanged to [NTf<sub>2</sub>] or [FeCl<sub>3</sub>Br] by metathesis reaction using one molar equivalent of lithium bis[(trifluoromethyl)sulfonyl]imide or FeCl<sub>3</sub>•6H<sub>2</sub>O to yield [(VIM)<sub>2</sub>C<sub>4</sub>] 2[NTf<sub>2</sub>], [(VIM)<sub>2</sub>C<sub>8</sub>] 2[NTf<sub>2</sub>], [(VIM)<sub>2</sub>C<sub>12</sub>] 2[NTf<sub>2</sub>], and [(VIM)<sub>2</sub>C<sub>12</sub>] 2[FeCl<sub>3</sub>Br]. The NMR spectra for all IL monomers and IL-based crosslinkers are shown in Figure B1-B6 (Appendix B).

### 3.2.4 GC column preparation

Surface modification of the capillary was performed using two methods prior to coating. In the first method, the capillary was filled with VTMS. Both ends of the capillary were then sealed and the capillary placed in a GC oven at 85 °C for 2 h to chemically bond the organosilane to the silanol groups on the inner capillary surface. The capillary was then purged with nitrogen and conditioned at 150 °C for 10 min. In the second method, the capillary was filled with VTMS vapor at 150 °C for 30 min. The capillary was then purged with nitrogen and conditioned at 150 °C for 10 min.

Prior to coating the IL-based columns, all IL monomers and crosslinkers were placed under vacuum at 75 °C overnight to remove any traces of solvent. A 0.25% (w/v) or 0.45% (w/v) coating solution was prepared by dissolving the mixture of IL monomer, IL cross-linker and AIBN (3.5% w/w) in dry methylene chloride. Five-meter segments of capillary column were coated by the static method at 40 °C. After coating, the two ends of the GC capillary were sealed and the capillary was placed in a GC oven and heated from 40 °C to 80 °C at 2 °C min<sup>-1</sup>. The capillary was then held isothermally at 80 °C for 5 h to ensure complete polymerization. The prepared columns were conditioned from 30 °C to 100 °C at 2 °C min<sup>-1</sup> and held isothermally at 100 °C for 3 h. Hydrogen was used as a carrier gas at a constant flow of 1 mL min<sup>-1</sup>. Column efficiency was determined using naphthalene at 100 °C. All coated columns possessed efficiencies of at least 1875 plates per meter. The composition and efficiency of all PIL-based columns prepared and evaluated in this study are shown in Table 1.

**Table 1.** PIL-based stationary phases examined in this study

Column No.	IL monomers and crosslinkers used for preparing PIL-based GC stationary phases	Film thickness	Retention factor (k) <sup>a</sup>	Efficiency (Plates/meter)	Resolution of selected analytes <sup>b</sup>		
					1 and 2	3 and 4	5 and 6
1	Neat [VHDIM] [NTf <sub>2</sub> ]	0.15 µm	10.79	2276	1.11	0.65	2.07
2	Neat [VHDIM] [NTf <sub>2</sub> ]	0.28 µm	13.20	2811	1.52	0.82	4.55
3	Neat [VHDIM][FeCl <sub>3</sub> Br]	0.15 µm	11.26	1986	1.21	0.86	3.36
4	[VHDIM] [NTf <sub>2</sub> ] + 25% [(VIM) <sub>2</sub> C <sub>4</sub> ] 2[NTf <sub>2</sub> ]	0.28 µm	7.63	1974	1.25	0.73	1.88
5	[VHDIM] [NTf <sub>2</sub> ] + 50% [(VIM) <sub>2</sub> C <sub>4</sub> ] 2[NTf <sub>2</sub> ]	0.28 µm	8.02	1875	- <sup>c</sup>	- <sup>c</sup>	1.71
6	[VHDIM] [NTf <sub>2</sub> ] + 50% [(VIM) <sub>2</sub> C <sub>8</sub> ] 2[NTf <sub>2</sub> ]	0.28 µm	10.62	2335	1.01	1.25	2.18
7	[VHDIM] [NTf <sub>2</sub> ] + 50% [(VIM) <sub>2</sub> C <sub>12</sub> ] 2[NTf <sub>2</sub> ]	0.28 µm	11.73	2575	2.16	1.75	5.36
8	[VHDIM] [NTf <sub>2</sub> ] + 25% [(VIM) <sub>2</sub> C <sub>12</sub> ] 2[NTf <sub>2</sub> ]	0.28 µm	12.53	2457	1.73	1.20	4.15
9	[VHDIM] [NTf <sub>2</sub> ] + 75% [(VIM) <sub>2</sub> C <sub>12</sub> ] 2[NTf <sub>2</sub> ]	0.28 µm	8.71	1994	1.60	0.74	3.59

**Table 1.** (continued)

<b>10</b>	[VHDIM] [NTf <sub>2</sub> ] + 100% [(VIM) <sub>2</sub> C <sub>12</sub> ] 2[NTf <sub>2</sub> ]	0.28 μm	7.82	2316	0.96	0.48	2.50
<b>11</b>	Neat [(VIM) <sub>2</sub> C <sub>12</sub> ] 2[NTf <sub>2</sub> ]	0.28 μm	5.54	1897	- <sup>c</sup>	- <sup>c</sup>	- <sup>c</sup>
<b>12</b>	[VHDIM] [FeCl <sub>3</sub> Br] + 50% [(VIM) <sub>2</sub> C <sub>12</sub> ] 2[FeCl <sub>3</sub> Br]	0.15 μm	11.58	2625	1.54	0.80	4.87
<b>13</b>	Neat [VHDIM] [NTf <sub>2</sub> ] on VTMS treated column	0.28 μm	10.17	2148	1.37	0.94	3.82
<b>14</b>	[VHDIM] [NTf <sub>2</sub> ] + 50% [(VIM) <sub>2</sub> C <sub>12</sub> ] 2[NTf <sub>2</sub> ] on VTMS treated column	0.28 μm	10.09	3842	1.44	0.97	3.73
<b>15</b>	[VHDIM] [NTf <sub>2</sub> ] + 50% [(VIM) <sub>2</sub> C <sub>12</sub> ] 2[NTf <sub>2</sub> ] on VTMS gas treated column	0.28 μm	7.79	1948	1.28	0.71	2.63

<sup>a</sup>: Measured isothermally for naphthalene at 100 °C, flow rate 1 mL min<sup>-1</sup>.

<sup>b</sup>: Selected pairs of analytes are shown within the representative contour plot in Figure 2.

<sup>c</sup>: Due to the poor separation, the resolution of selected analytes could not be measured.

### 3.2.5 Chromatographic analysis by GC×GC-FID

When evaluating the selectivity of the PIL-based columns by GC×GC-FID analysis, the primary column consisted of a Rtx-5 capillary column (30 m × 250  $\mu$ m,  $d_f$  = 0.25  $\mu$ m, Restek, Bellefonte, PA, USA) connected to a second-dimension PIL-coated capillary column (1.2 m × 250  $\mu$ m,  $d_f$  = 0.15 or 0.28  $\mu$ m). In all experiments, 0.5  $\mu$ L of the kerosene or diesel sample was injected using a 300:1 split ratio at 250 °C. The GC oven for the separation of kerosene was programmed from 40 °C to 120 °C at 2 °C min<sup>-1</sup>, followed by a secondary ramp from 120 °C to 200 °C at 20 °C min<sup>-1</sup>. The temperature program for the separation of diesel was set from 50 °C to 240 °C at 5 °C min<sup>-1</sup> and held for 5 min. Hydrogen was employed as a carrier gas at a constant flow of 1.2 mL min<sup>-1</sup>. The modulation period was 7 s for all separations. All separations were performed in duplicate.

The thermal stability of the PIL-based stationary phases was evaluated by programming the GC oven after GC×GC separations from 40 °C to a specific temperature (i.e., 250, 275, 300, and 325 °C) at a ramp of 10 °C min<sup>-1</sup> and then held at that temperature for 30 min. After the thermal conditioning step, the GC×GC separation was performed and the resolution of selected analytes from kerosene was compared with those obtained prior to high temperature conditioning. The MAOT was determined to be the highest separation temperature achieved before a significant decrease in resolution was observed.

## 3.3 Results and Discussion

### 3.3.1 Thermal stability of dicationic ILs for GC×GC separation

It was recently reported that dicationic ILs containing long free alkyl side chain substituents and long linkage chains between the two cations exhibit high selectivity for the separation of different groups of aliphatic hydrocarbons in kerosene when used as second-dimension stationary phases in GC×GC [23]. This feature is important for the separation of

nonpolar analytes within complex samples. However, the MAOT of the stationary phase also needs to be considered because the IL-based stationary phases should possess high thermal stability to permit high temperature separation. In order to test the robustness of the dicationic IL-based stationary phase, a quantitative measurement was carried out by calculating the resolution of selected pairs of analytes within the GC×GC contour plot. As shown in Figure 2, of the column was tested by evaluating the resolving power of these three pairs of analytes from kerosene after high temperature conditioning. This approach is

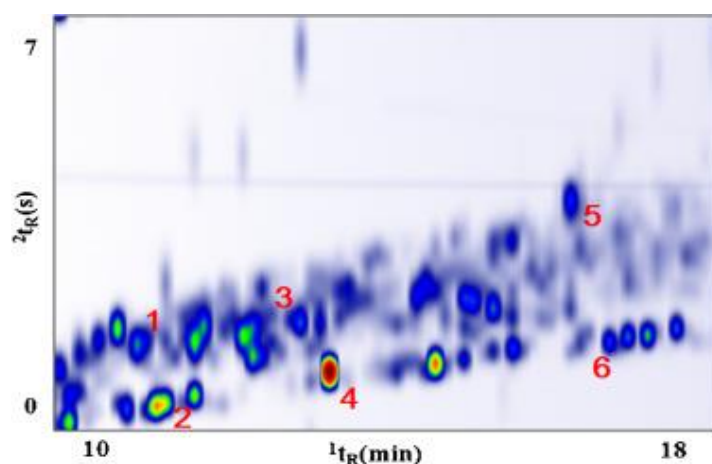


**Figure 2.** Expanded GC×GC contour plot showing the analytes selected for determining the resolving power of the stationary phase.

capable of detecting any viscosity and/or morphology change of the stationary phases at elevated temperature that may result in a change to the efficiency and resolving power of the stationary phases. The best performing IL from a previous study [23],  $[(C_{10}im)_2C_{10}][NTf_2, FeCl_3Br]$  (see Figure 1), was tested using this approach. As shown in Table 2, a significant decrease in resolution was obtained when this IL was conditioned at 250 °C. The stationary phase was thermally stable in the temperature range between 250 °C to 275 °C, as the resolution values of the analytes did not change appreciably when the column was conditioned up to 275 °C. After the stationary phase was conditioned to 300 °C, the stationary phase exhibited very poor column efficiency and the resolution between analytes 3 and 4 could not be measured (see Table 2). The MAOT of the dicationic IL-based



stationary phase was determined to be approximately 275 °C, which is insufficient for high temperature GC×GC separations.

### 3.3.2 Non-crosslinked linear PILs as stationary phases for GC×GC separations

PILs have been demonstrated as alternative materials to improve the thermal stability of monocationic and dicationic IL-based stationary phases. Monocationic IL monomers and IL-based crosslinkers can be polymerized within the column to form PIL-based stationary phases, which have been shown to exhibit MAOTs higher than 300 °C [24]. The structures for all IL monomers applied in this study are shown in Figure 1. Both IL monomers possess hexadecyl side chain substituents to enhance their selectivity towards nonpolar analytes. IL monomers containing NTf<sub>2</sub><sup>-</sup> or FeCl<sub>3</sub>Br<sup>-</sup> counteranions were synthesized to examine their effects on the selectivity and thermal stability of the resulting PILs. Due to the fact that the film thickness of the stationary phase can play an important role in GC×GC separations, stationary phases with film thicknesses of 0.15 μm and 0.28 μm were prepared using the neat [VHDIM] [NTf<sub>2</sub>] IL monomer. As shown in Figures 3A and 3B, a wider distribution of the analytes within the separation window was observed when employing the PIL-based stationary phase with a 0.28 μm film thickness as the second-dimension column. To better evaluate the selectivity of the second-dimension column, the resolution between selected pairs of analytes within the kerosene sample was calculated and is shown in Table 1. The column with 0.28 μm film thickness (column **2**) exhibited significantly higher resolving power for the selected analytes compared to the column with 0.15 μm film thickness (column **1**). By comparing PILs possessing different anions, it can be observed that the PIL containing the FeCl<sub>3</sub>Br<sup>-</sup> anion (column **3**) exhibited higher resolution than the NTf<sub>2</sub><sup>-</sup>-based PIL stationary phase (column **1**). This is in good agreement with previously reported results for dicationic ILs (non-polymerized) possessing similar structural features [23].

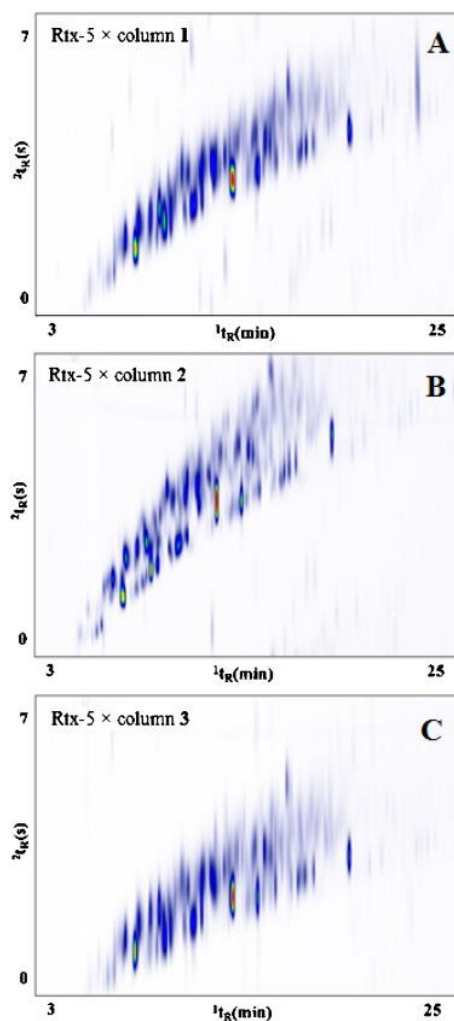


**Figure 3.** GC×GC separations of kerosene employing linear (non-crosslinked) PIL-based stationary phases as second-dimension columns: (A) Rtx-5 × column 1, (B) Rtx-5 × column 2, and (C) Rtx-5 × column 3. See Table 1 for a description of each column designation and composition.

In order to further test the thermal stability of the non-crosslinked linear PIL-based column, the better performing PIL (column 2) was examined by evaluating the resolving power towards selected pairs of analytes within kerosene after being conditioned at high oven temperatures. As indicated in Table 2, no significant loss of resolution was observed after the column was conditioned to 250 °C. However, after conditioning at 325 °C, an approximate 50% loss of resolution for the selected pairs of analytes was observed compared to the resolution of the column conditioned at 250 °C. Although the linear PIL stationary phase exhibited significantly higher selectivity than the non-polymerized

dicationic ILs after being conditioned at high temperature, the thermal stability was still not sufficient for high temperature separations. To produce more robust stationary phases that are able to endure higher temperatures, crosslinked PIL-based stationary phases were subsequently examined.

### 3.3.3 Effect of IL-based crosslinker linkage chain on GC×GC separation

In order to better understand the effects of different crosslinkers on the efficiency, selectivity, and thermal stability of the PIL-based stationary phases, PILs with varying amounts of dicationic IL-based crosslinker (i.e., 25 and 50% w/w), and crosslinkers possessing different lengths of linkage chains between the two cations (i.e., [(VIM)<sub>2</sub>C<sub>4</sub>] 2[NTf<sub>2</sub>], [(VIM)<sub>2</sub>C<sub>8</sub>] 2[NTf<sub>2</sub>] and [(VIM)<sub>2</sub>C<sub>12</sub>] 2[NTf<sub>2</sub>]) were compared. The structures of all studied crosslinkers are shown in Figure 1. The column composition and efficiencies are shown in Table 1 and the accompanying contour plots demonstrating the separations of kerosene using these stationary phases are shown in Figure 4.

With regard to the PIL-based stationary phases containing different crosslinkers, a few trends can be observed by comparing columns **5**, **6**, and **7** in Table 1. Column **7** containing the crosslinker with a dodecyl linkage chain exhibited higher column efficiency than column **5** and **6**, which possessed crosslinkers with shorter linkage chains (octyl and butyl chain). One possible explanation may be that the crosslinker with a shorter linkage chain produces a more rigid polymer matrix, resulting in slower mass transfer between the analytes and stationary phase. In order to test this assumption, the rigidity of the PIL stationary phase was varied by decreasing the amount of the [(VIM)<sub>2</sub>C<sub>4</sub>] 2[NTf<sub>2</sub>] crosslinker from 50% (w/w) to 25% (w/w). A slightly higher column efficiency was obtained for column **4** (efficiency = 1974 plates/m) compared to column **5** (efficiency = 1875 plates/m). Moreover, a wider distribution of the analytes and narrower peak widths

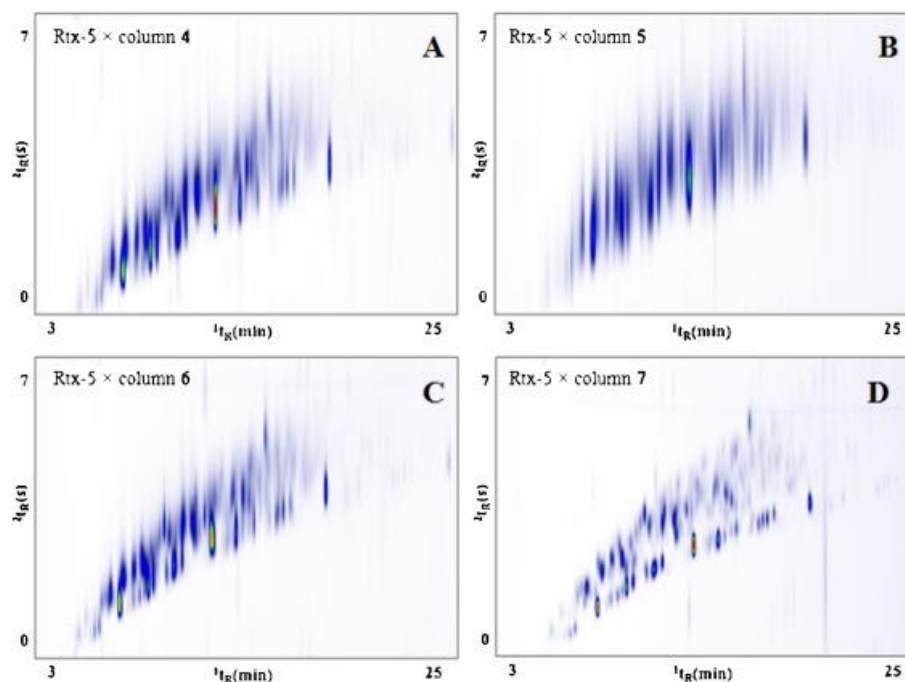


**Figure 4.** GC×GC chromatograms showing the effect of linkage chain length of IL-based crosslinker on the separation of kerosene: (A) Rtx-5 × column 4, (B) Rtx-5 × column 5, (C) Rtx-5 × column 6, and (D) Rtx-5 × column 7.

were observed for column 4, as shown in Figure 4A. By comparing the contour plots for columns 5, 6, and 7 in Figure 4, it is evident that the stationary phases comprised of the [(VIM)<sub>2</sub>C<sub>12</sub>] 2[NTf<sub>2</sub>] crosslinker (Figure 4D) exhibited the best separation of kerosene. This is in good agreement with previous work using structurally tuned ILs for GC×GC separations and further demonstrates that longer linkage chain between the two imidazolium cations is an important structural feature for the separation of aliphatic hydrocarbons [23]. This result also indicates that the necessary structural features for separation of aliphatic hydrocarbons can be imparted into IL-based crosslinkers to produce crosslinked PIL-based stationary phases and that the selectivity is preserved.

The resolution for selected analytes using the crosslinked PILs as second-dimension columns is shown in Table 1. The highest resolution for selected analytes was obtained using column 7 as the second-dimension column, which contains 50% (w/w) of the [(VIM)<sub>2</sub>C<sub>12</sub>] 2[NTf<sub>2</sub>] crosslinker. The result was compared with column 2, comprised of a

non-crosslinked PIL stationary phase prepared by the polymerization of the neat [VHDIM][NTf<sub>2</sub>] IL monomer. A significant increase in resolution was obtained when the stationary phase was partially crosslinked using the IL-based crosslinker. The retention times of the analytes on the two contour plots were very similar, as shown in Figure 3B and 4D. However, the peak widths produced by column **7** are much smaller, yielding higher resolution compared to column **2** (see Table 1).

### 3.3.4 GC×GC separation of kerosene using PIL-based stationary phases with varied amount of crosslinkers

It has been previously reported that PIL-based stationary phases containing low to moderate amount of crosslinker exhibited modest column efficiency and are stable up to 285 °C [24]. By increasing the ratio of the crosslinker, the thermal stability of the PIL-based stationary phases can be increased to 380 °C, but the efficiency may be sacrificed. In order to evaluate the effect of the amount of crosslinker on the selectivity and thermal stability of the stationary phases, PIL-based stationary phases with varied amount of the [(VIM)<sub>2</sub>C<sub>12</sub>] 2[NTf<sub>2</sub>] crosslinker (i.e., 25, 50, 75, and 100% w/w and neat crosslinker) were prepared and compared. The GC×GC separation of kerosene using these column sets are shown in Figures 4 and 5. For comparison purposes, the resolution for selected analytes in kerosene was also calculated and is shown in Table 1. It can be observed that the selectivity for low boiling analytes can be increased by adding small amounts of crosslinker to the PIL-based stationary phases. This is highlighted in the example of column **8** which exhibited better resolution for analytes 1 and 2 compared to column **2**. The same trend can be observed when the amount of crosslinker was increased from 25% (w/w) to 50% (w/w). Column **7** exhibited the highest resolution for all three pairs of analytes. However, when 75% (w/w) of the crosslinker was incorporated into the stationary phase, a significant drop in the

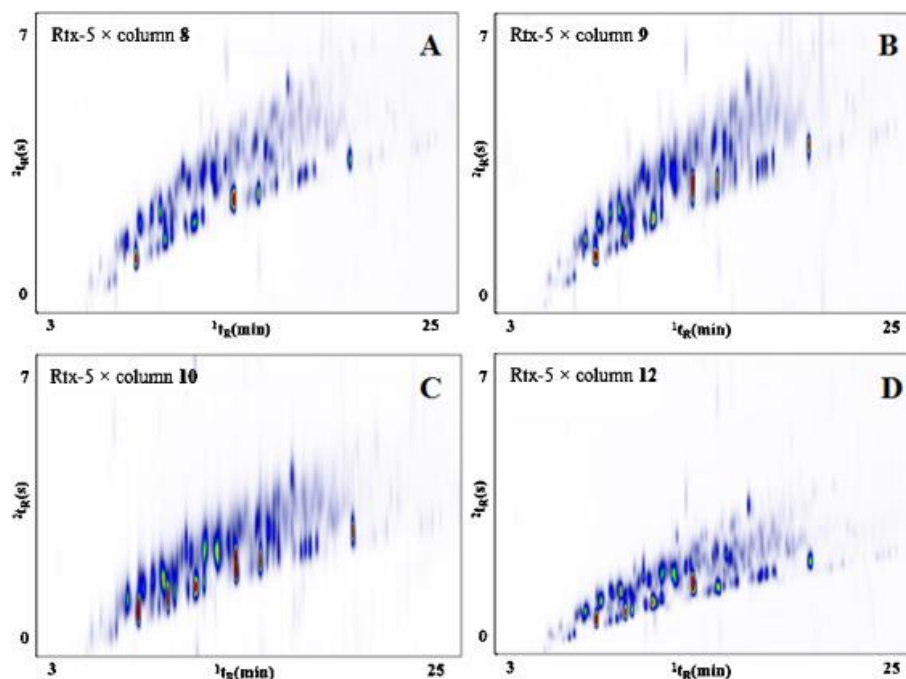


**Figure 5.** GC×GC contour plots of kerosene employing PIL-based stationary phases as the second-dimension columns containing with varied amounts of crosslinker: (A) Rtx-5 × column 8, (B) Rtx-5 × column 9, (C) Rtx-5 × column 10, and (D) Rtx-5 × column 12.

overall resolving power was observed (see Table 1). As shown in Figure 5B, an increased amount of the crosslinker can apparently increase the rigidity of the PIL-based stationary phase and subsequently increase the peak width within the second-dimension column. This trend was also observed for column 10 which contains 100% (w/w) of crosslinker (see Figure 5C). The retention times for all analytes separated by column 10 decreased significantly and broader peaks were observed. In order to further examine the performance of the highly crosslinked PIL-based stationary phase, a stationary phase consisting of neat polymerized [(VIM)<sub>2</sub>C<sub>12</sub>] 2[NTf<sub>2</sub>] crosslinker (column 11) was prepared. Although acceptable column efficiency (1897 plates/m) was obtained, very poor GC×GC separation of kerosene was observed for the highly crosslinked PIL-based stationary phase (see Figure B7, Appendix B).

As mentioned earlier, the FeCl<sub>3</sub>Br<sup>-</sup>-based PIL stationary phase (column 3) exhibited good selectivity for different groups of aliphatic hydrocarbons in the GC×GC separation of

kerosene. In order to further improve the separation performance of the  $\text{FeCl}_3\text{Br}^-$ -based PIL stationary phase at high oven temperatures, a column containing the [VHDIM]  $[\text{FeCl}_3\text{Br}^-]$  IL monomer and 50% (w/w) of  $[(\text{VIM})_2\text{C}_{12}]$   $2[\text{FeCl}_3\text{Br}^-]$  crosslinked stationary phase was prepared. It can be observed in Table 2 that the partially crosslinked  $\text{FeCl}_3\text{Br}^-$ -based PIL (column **12**) provided better resolution for selected analytes compared to the non-crosslinked linear  $\text{FeCl}_3\text{Br}^-$ -based PIL (column **3**). It was also observed that although the  $\text{FeCl}_3\text{Br}^-$ -based stationary phase possesses smaller film thickness (0.15  $\mu\text{m}$ ) than the  $\text{NTf}_2^-$ -based stationary phase (0.28  $\mu\text{m}$ ), it exhibited very similar resolution for the selected analytes compared to column **7** (see Table 1).

The three best performing crosslinked PIL stationary phases, namely, columns **7**, **8** and **12** were selected for evaluation of their thermal stability. The two  $\text{NTf}_2^-$ -based stationary phases (column **7** and **8**) exhibited a small but steady decrease in resolution after being conditioned at 250, 275, and 300  $^\circ\text{C}$ , respectively, as shown Table 2. After being conditioned at 325  $^\circ\text{C}$ , the PIL-based stationary phase containing 25% (w/w) of crosslinker exhibited a significant decrease in resolution. However, better thermal stability was obtained for the PIL-based stationary phase with 50% (w/w) of crosslinker. Even after being conditioned at 325  $^\circ\text{C}$ , column **7** still exhibited good retention and selectivity for the target analytes. However, as shown in Table 2, the  $\text{FeCl}_3\text{Br}^-$ -based stationary phase (column **12**) did not exhibit good thermal stability and very poor resolution was observed after the column was conditioned at 275  $^\circ\text{C}$ . In spite of its high selectivity for aliphatic hydrocarbons, the low MAOT of the  $\text{FeCl}_3\text{Br}^-$ -based PIL stationary phases makes it undesirable for high temperature separations.

### 3.3.5 Immobilized PIL-based stationary phases using vinyltrimethoxysilane (VTMS) treated columns

Modification of the silica surface using vinyl alkoxysilane is a well-known strategy in polymer science [28,29]. After modification, the surface can be polymerized using monomers and crosslinkers to form a crosslinked network, which can significantly increase the mechanical strength and thermal stability of the polymer matrix [30]. Two modification procedures that have been previously reported include liquid phase reaction and vapor phase reaction [29]. Liquid phase reaction utilizes an alkoxysilane solution for modification and is typically easier to operate. This approach has been used previously by our group to immobilize crosslinked PILs as the outer sorbent coating on a fused silica support for solid-phase microextraction analysis [27], thereby hindering the sloughing of the PIL sorbent at high temperatures. It has also been reported that passing alkoxysilane vapor through the silica substrate allows better control of reaction conditions and can lead to a more reproducible monolayer modification [31]. In order to identify the best approach for surface modification, PIL-based stationary phases were prepared on capillary treated using liquid phase reaction and vapor phase reaction. Following VTMS surface modification, two PIL-based stationary phases that exhibited the highest resolving power for kerosene, namely, neat [VHDIM] [NTf<sub>2</sub>] and [VHDIM] [NTf<sub>2</sub>] with 50% (w/w) of the [(VIM)<sub>2</sub>C<sub>12</sub>] 2[NTf<sub>2</sub>] crosslinker, were coated on these capillary columns. As shown in Table 1, moderate to very high column efficiencies were obtained for the neat [VHDIM] [NTf<sub>2</sub>] stationary phase (column **13**) and crosslinked stationary phase (column **14**) prepared using the liquid phase treated capillary. However, in the case of column **15** prepared by the VTMS vapor treated column, somewhat lower column efficiency was obtained. One possible explanation may be due to the higher reactivity of the VTMS vapor at higher temperature [29].



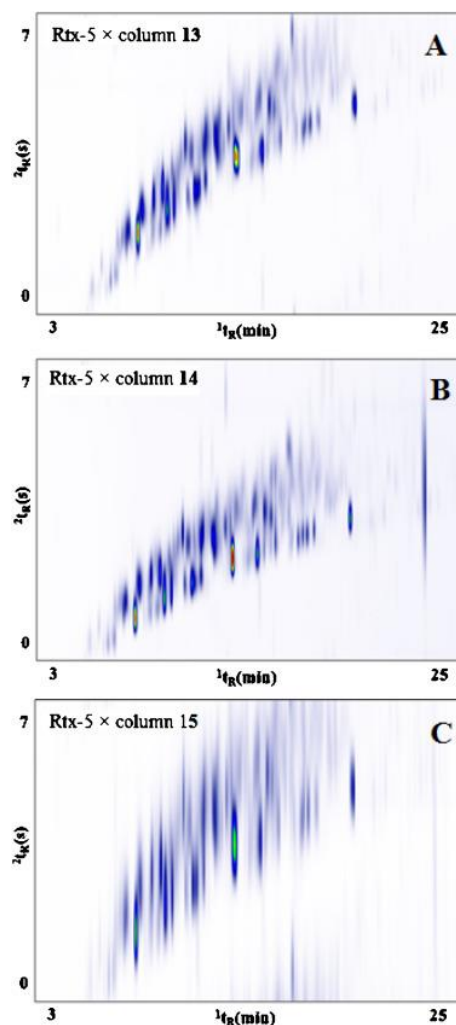


**Figure 6.** GC×GC chromatograms of kerosene employing PIL-based stationary phases coated on vinyltrimethoxysilane (VTMS) treated columns: (A) Rtx-5 × column **13**, (B) Rtx-5 × column **14**, (C) Rtx-5 × column **15**.

Columns **13**, **14**, and **15** were employed for the GC×GC separation of kerosene and the results are shown in Figure 6 and Table 1. A few interesting trends can be observed by comparing the PIL-based stationary phases prepared on the untreated capillary (column **1**) and VTMS treated capillary (column **13**). Due to the crosslinked network apparently formed by grafting of the PIL stationary phase onto the silica capillary, column **13** exhibited higher resolution for selected analytes than column **1**. This is in good agreement with the results obtained in Section 3.4 since the partially crosslinked PIL (column **4**) exhibited higher resolution compared to the non-crosslinked PIL (column **1**). However, when comparing the observed resolution between column **7** and column **14**, a decrease in

resolution was observed after the crosslinked PIL stationary phase was immobilized onto the capillary. As the degree of crosslinking was increased by grafting the PIL stationary phase to the capillary surface, the resolving power towards selected pairs of analytes of the best performing PIL-based stationary phase was decreased. When the amount of crosslinker was increased from 50 % (w/w) to 75 % (w/w), column **9** exhibited a decreased resolution for the selected analyte pairs compared to column **7** (see Table 1). As shown in Figure 6, the VTMS vapor treated column (column **15**) exhibited poor resolving power for kerosene in the GC×GC separation and very broad peaks were observed. The resolution for selected analytes on column **15** (Figure 6C) was much lower than column **14** (Figure 6B), indicating that the liquid phase reaction is a better approach for surface modification.

The thermal stability of column **13** was tested as it exhibited the best selectivity for different groups of aliphatic hydrocarbons in kerosene. Compared to column **2**, which has the same stationary phase composition and is coated on untreated capillary column, column **13** exhibited almost no loss of resolution after being conditioned at 275 °C. After conditioning to 325 °C, the column still exhibited good retention and selectivity for the target analytes. The results indicate that the MAOT of the neat [VHDIM][NTf<sub>2</sub>] stationary phase can be significantly enhanced by exploiting a VTMS treated capillary column. However, comparing the resolving power of column **13** and column **7** (the best performing PIL-based stationary phase in Section 3.4), column **7** produced superior selectivity for aliphatic hydrocarbons.

### 3.3.6 Selectivity and thermal stability comparison for PIL-based and commercial PEG stationary phases

Due to its polar nature, PEG stationary phases have been widely applied as second-dimension columns for the separation of hydrocarbons in GC×GC [9,10]. However, it is

also well-known that PEG columns have lower MAOTs (250-260 °C) and exhibit high column bleed and surface activity at higher temperatures resulting in shifting of the retention time. In order to better evaluate the analytical performance of the crosslinked PIL stationary phases, four commercial PEG-based columns, namely, SUPELCOWAX 10, DB-WAX, CP-Wax 52 CB, and HP-INNOWax were evaluated as reference stationary phases for the separation of aliphatic hydrocarbons at high temperature. The GC×GC separations of kerosene using the four commercial PEG-based columns are shown in Figure 7. A similar distribution of the analytes within the separation window can be observed for all columns

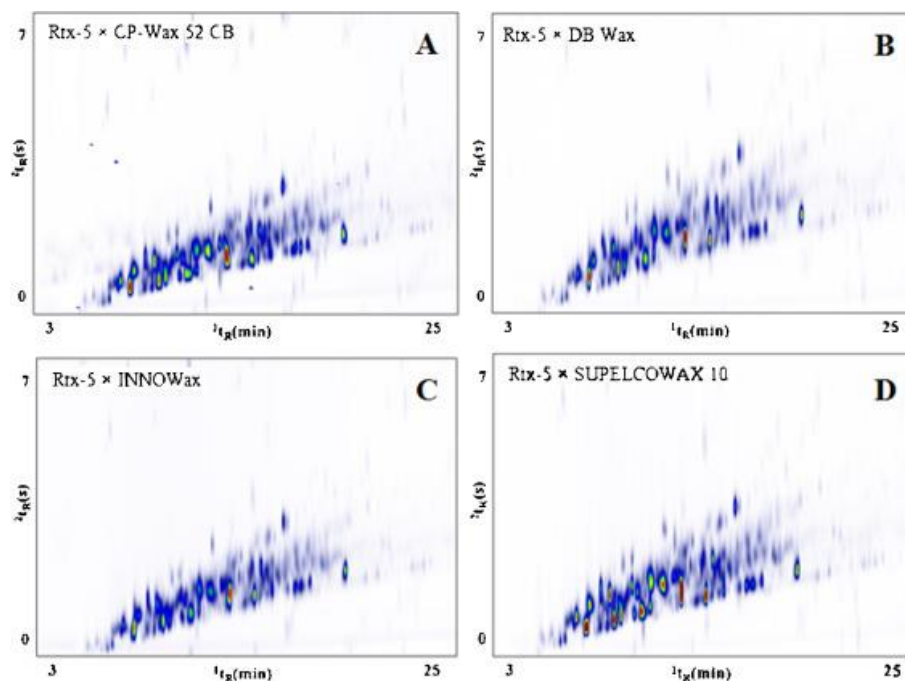


**Figure 7.** GC×GC separations of kerosene employing various commercial PEG-based stationary phases as second-dimension columns: (A) Rtx-5 × CP-Wax 52 CB, (B) Rtx-5 × DB Wax, (C) Rtx-5 × INNOWax, and (D) Rtx-5 ×SUPELCOWAX 10.

indicative of their similar composition. The resolving power for selected analytes is shown in Table 2. To conduct a fair comparison, the resolution of select analytes from column 7 after conditioning at 275 °C was determined, as this temperature is higher than the MAOTs of most commercial PEG phases. Column 7 provided higher resolution compared to the PEG columns, especially for analytes with lower boiling points (i.e., analytes 1 and 2, 3

**Table 2.** Resolution of selected analytes on tested columns after being conditioned at high oven temperature:-

Condition Temperature (°C)	Resolution of analyte pairs					
	1 and 2	3 and 4	5 and 6	1 and 2	3 and 4	5 and 6
	[(C <sub>10</sub> im) <sub>2</sub> C <sub>10</sub> ] [NTf <sub>2</sub> , FeCl <sub>3</sub> Br]			Neat [VHDIM] [NTf <sub>2</sub> ] (Column 2)		
100	0.90	0.48	3.25	1.52	0.82	4.55
250	0.61	0.26	2.57	1.35	0.76	3.13
275	0.55	0.25	2.42	1.44	0.66	3.35
300	0.48	- <sup>a</sup>	1.86	1.60	0.40	1.48
325	- <sup>a</sup>	- <sup>a</sup>	- <sup>a</sup>	0.84	0.45	1.65
	[VHDIM] [NTf <sub>2</sub> ] + 25% [(VIM) <sub>2</sub> C <sub>12</sub> ] 2[NTf <sub>2</sub> ] (Column 8)			[VHDIM] [NTf <sub>2</sub> ] + 50% [(VIM) <sub>2</sub> C <sub>12</sub> ] 2[NTf <sub>2</sub> ] (Column 7)		
100	1.73	1.20	4.15	2.16	1.75	5.36
250	1.47	0.95	3.98	1.69	1.24	4.09
275	1.32	0.81	3.41	1.59	1.33	3.83
300	1.03	0.68	2.92	1.29	1.05	3.29
325	0.71	0.41	1.88	1.02	0.81	2.85
	[VHDIM] [FeCl <sub>3</sub> Br] + 50% [(VIM) <sub>2</sub> C <sub>12</sub> ] 2[FeCl <sub>3</sub> Br] (Column 12)			Neat [VHDIM] [NTf <sub>2</sub> ] on VTMS treated column (Column 13)		
100	1.54	0.80	4.87	1.37	0.94	3.82
250	1.48	0.77	4.06	1.29	0.84	3.82
275	- <sup>a</sup>	0.10	0.92	1.15	0.80	3.50
300	- <sup>a</sup>	- <sup>a</sup>	- <sup>a</sup>	1.07	0.56	2.45
325	- <sup>a</sup>	- <sup>a</sup>	- <sup>a</sup>	0.82	0.63	2.49
	SUPELCOWAX 10			DB-WAX		
100	0.86	0.50	3.46	0.73	0.41	3.57
250	0.82	0.53	3.34	0.64	0.42	3.60
275	0.76	0.50	3.44	0.67	0.29	3.45
300	0.87	0.44	3.21	0.55	0.34	3.23
325	0.87	0.33	2.70	0.56	0.22	2.66
	HP-INNOWax			CP-Wax 52 CB		
100	0.63	0.33	3.63	0.80	0.49	3.09
250	0.56	0.32	3.43	0.73	0.44	3.08
275	0.50	0.31	3.55	0.67	0.45	3.02
300	0.54	0.25	3.39	0.74	0.50	3.01
325	0.50	0.21	2.80	0.76	0.43	2.54

<sup>a</sup>: Due to the poor separation, the resolution of selected analytes could not be measured.

and 4). In order to evaluate the selectivity of the crosslinked PIL-based stationary after high temperature conditioning, column 7 and the four commercial PEG-based columns were subsequently conditioned at 275 °C, 300 °C, and 325 °C. As shown in Table 2, the resolution for all PEG stationary phases were slightly decreased when the column was conditioned from 275 to 325 °C, which is a higher temperature than the suggested MAOT of these columns. Column 7 exhibited higher resolution compared to all PEG phases and its performance was not significantly affected after conditioning at 325 °C.

### 3.3.7 GC×GC separation of diesel fuel using selected crosslinked PIL-based stationary phase

In order to further examine the resolving power of the crosslinked PIL-based stationary phase towards aliphatic hydrocarbons, it is necessary to test the column using a more complex sample possessing high boiling constituents. Diesel fuel was selected as a model analyte in this study due to its high complexity and the fact that its group-type separation using GC×GC has been well described [32-35]. The GC×GC separation of diesel fuel employing the Rtx-5 × column 7 column set is shown in Figure 8A. Two distinct groups of analytes can be observed within the contour plot. Within the expanded chromatogram for this column set in Figure 8D, saturated hydrocarbons elute in a long and wide band at the bottom of the contour plot, occupying approximately 40% of the second-dimension separation window. The aromatic compounds exhibit a wider range of retention times on the second-dimension column and occupy nearly the remainder of the separation window. Two of the most widely used stationary phases in petroleum analysis, namely, SUPELCOWAX 10 and DB-17 (containing 50% phenyl) were evaluated for comparison purposes. The distribution of the analytes within the GC×GC contour plots are in good agreement with previously reported results employing similar stationary phases as the

second-dimension column [32,33]. It can be observed in Figure 8B and 8E that the SUPELCOWAX 10 column exhibits similar resolving power for aromatic compounds compared to column 7, as the aromatic compounds also occupy the top half of the GC×GC chromatogram. However, the aliphatic hydrocarbons elute in a much narrower band (approximately 25% of the second-dimension separation window). A very similar separation of saturated hydrocarbons was observed for the DB-17 column compared to SUPELCOWAX 10 (see Figure 8C and 8F). However, as shown in Figure 8F, only 60% of the separation space was utilized by the Rtx-5 × DB-17 column set. Moreover, a slight merge of the saturated hydrocarbon and aromatic regions in the GC×GC contour plot was observed. The crosslinked PIL-based stationary phase exhibited unique selectivity in the separation of individual aliphatic hydrocarbons from other aliphatic hydrocarbons within diesel fuel compared to the SUPELCOWAX 10 and DB-17 columns.

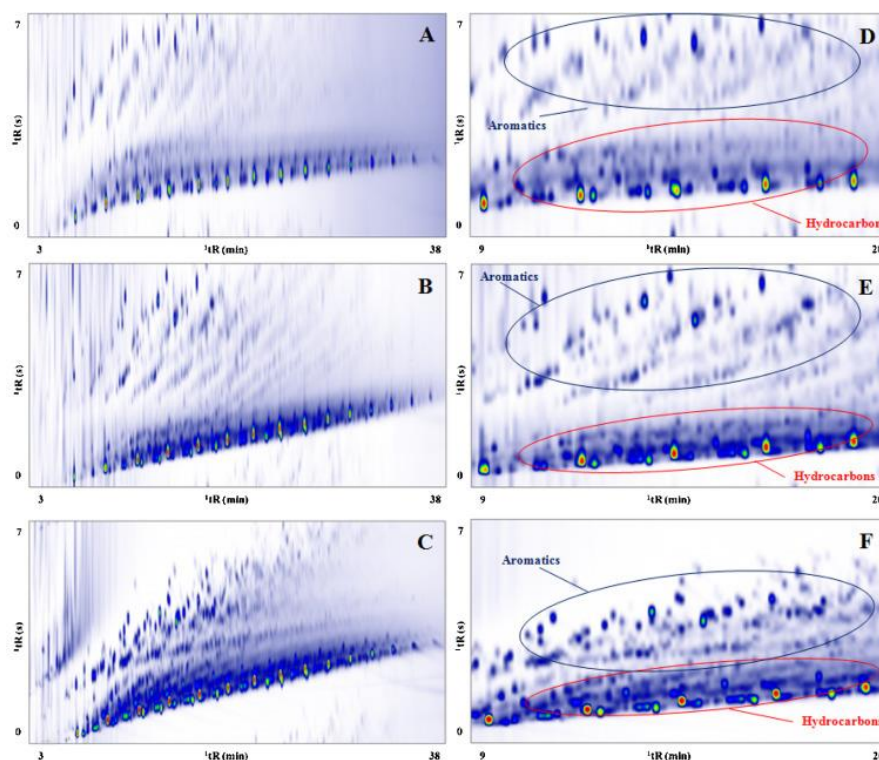


**Figure 8.** GC×GC contour plots showing the separation of diesel fuel employing commercial and crosslinked PIL-based stationary phases as second-dimension columns: (A) Rtx-5 × column 7, (B) Rtx-5 × SUPELCOWAX 10, and (C) Rtx-5 × DB-17. Expanded GC×GC contour plots showing the separation of hydrocarbons in diesel fuel: (D) Rtx-5 × column 7, (E) Rtx-5 × SUPELCOWAX 10, and (F) Rtx-5 × DB-17.

### 3.4 Conclusions

A total of fifteen PIL-based stationary phases were examined as second-dimension columns in this study for the separation of aliphatic hydrocarbons within kerosene using GC×GC. The IL monomers were functionalized with long alkyl chain substituents to provide the selectivity required for the resolution of different groups of aliphatic hydrocarbons. The thermal stability of the PIL-based stationary phase was further enhanced by employing IL -based crosslinkers. The PIL-based stationary phase containing 50% (w/w) of crosslinker with a dodecyl linkage chain exhibited the highest resolving power in the separation of aliphatic hydrocarbons. This best performing crosslinked PIL-based stationary phase was compared with four commercial PEG-based columns for the separation of aliphatic hydrocarbons after high temperature conditioning. The crosslinked PIL-based stationary phase exhibited higher resolution for selected analytes and better thermal stability compared to PEG phases. Finally, the crosslinked PIL-based stationary phase was compared with SUPELCOWAX 10 and DB-17 columns for the resolution of aliphatic hydrocarbons in diesel fuel. Better separation of hydrocarbon compounds was obtained when using crosslinked PIL-based stationary phase as the second-dimension column. This result proved that the solvation properties and thermal stability of PIL-based stationary phases can be tuned by varying the structure and composition of the IL monomer and crosslinker. This study demonstrates for the first time that structurally tuned IL monomers and crosslinkers can be designed and incorporated into crosslinked PIL-based stationary phases that exhibit high thermal stability and that the unique selectivity of the stationary phase is preserved.

## Acknowledgements

The authors acknowledge funding from Chemical Measurement and Imaging Program at the National Science Foundation (Grant number CHE-1413199).

## References

- [1] F. Santos, M. Galceran, Trends Anal. Chem. 21 (2002) 672
- [2] J. Dallüge, J. Beens, U.A.T. Brinkman, J. Chromatogr. A 1000 (2003) 69
- [3] P.J. Marriott, R. Shellie, Principles and applications of comprehensive two-dimensional gas chromatography, Trends Anal. Chem. 21 (2002) 573
- [4] M. Adahchour, J. Beens, R.J.J. Vreuls, U.A.T. Brinkman, Trends Anal. Chem. 25 (2006) 438
- [5] J.V. Seeley, S.K. Seeley, Anal. Chem. 85 (2013) 557
- [6] M. Adahchour, J. Beens, U.A.T. Brinkman, J. Chromatogr. A 1186 (2008) 67
- [7] P.J. Marriott, S.-T. Chin, B. Maikhunthod, H.-G. Schmarr, S. Bieri, Trends Anal. Chem. 34 (2012) 1
- [8] L. Mondello, P.Q. Tranchida, P. Dugo, G. Dugo, Mass Spectrom. Rev. 27 (2008) 101
- [9] C. Vendeuvre, F. Bertoncini, L. Duval, J.-L. Duplan, D. Thiébaut, M.-C. Hennion, J. Chromatogr. A 1056 (2004) 155
- [10] C.A. Bruckner, B.J. Prazen, R.E. Synovec, Anal. Chem. 70 (1998) 2796
- [11] L. Mondello, A. Casilli, P.Q. Tranchida, P. Dugo, G. Dugo, J. Chromatogr. A 1019 (2003) 187
- [12] H.-J. de Geus, I. Aidos, J. de Boer, J.B. Luten, A.T. Udo, J. Chromatogr. A 910 (2001) 95
- [13] L. Mondello, A. Casilli, P.Q. Tranchida, G. Dugo, P. Dugo, J. Chromatogr. A 1067 (2005) 235
- [14] R. Shellie, P.J. Marriott, A. Chaintreau, Flavour Frag. J 19 (2004) 91
- [15] C.F. Poole, S.K. Poole, J. Sep. Sci. 34 (2011) 888
- [16] C. Yao, J.L. Anderson, J. Chromatogr. A 1216 (2009) 1658
- [17] T.D. Ho, C. Zhang, L.W. Hantao, J.L. Anderson, Anal. Chem. 86 (2013) 262



- [18] C.F. Poole, N. Lenca, *J. Chromatogr. A* 1357 (2014) 87
- [19] P. Antle, C. Zeigler, A. Robbat Jr, *J. Chromatogr. A* 1361 (2014) 255
- [20] L. Mahé, T. Dutriez, M. Courtiade, D. Thiébaut, H. Dulot, F. Bertoncini, *J. Chromatogr. A* 1218 (2011) 534
- [21] T. Dutriez, J. Borrás, M. Courtiade, D. Thiébaut, H. Dulot, F. Bertoncini, M.-C. Hennion, *J. Chromatogr. A* 1218 (2011) 3190
- [22] L.W. Hantao, A. Najafi, C. Zhang, F. Augusto, J.L. Anderson, *Anal. Chem.* 86 (2014) 3717
- [23] C. Zhang, I.C. Ingram, L.W. Hantao, J.L. Anderson, *J. Chromatogr. A* 1386 (2015) 89
- [24] J.L. Anderson, D.W. Armstrong, *Anal. Chem.* 77 (2005) 6453
- [25] Y. Meng, J.L. Anderson, *J. Chromatogr. A* 1217 (2010) 6143
- [26] C. Zhang, J.L. Anderson, Polymeric ionic liquid bucky gels as sorbent coatings for solid-phase microextraction, *J. Chromatogr. A* 1344 (2014) 15
- [27] T.D. Ho, H. Yu, W.T.S. Cole, J.L. Anderson, *Anal. Chem.* 84 (2012) 9520
- [28] T. Browne, M. Chaimberg, Y. Cohen, *J. Appl. Polym. Sci.* 44 (1992) 671
- [29] P.V. Der Voort, E. Vansant, *J. Liq. Chromatogr. Related Technol.* 19 (1996) 2723
- [30] V. Nguyen, W. Yoshida, J.D. Jou, Y. Cohen, *J. Polym. Sci., Part A: Polym. Chem.* 40 (2002) 26
- [31] D.G. Kurth, T. Bein, *J. Phys. Chem.* 96 (1992) 6707
- [32] F. Adam, F. Bertoncini, V. Coupard, N. Charon, D. Thiébaut, D. Espinat, M.-C. Hennion, *J. Chromatogr. A* 1186 (2008) 236
- [33] J.V. Seeley, S.K. Seeley, E.K. Libby, J.D. McCurry, *J. Chromatogr. Sci.* 45 (2007) 650
- [34] P.A. Bueno, J.V. Seeley, *J. Chromatogr. A* 1027 (2004) 3
- [35] J.V. Seeley, S.K. Seeley, E.K. Libby, Z.S. Breitbach, D.W. Armstrong, *Anal. Bioanal. Chem.* 390 (2008) 323

## CHAPTER 4

### POLYMERIC IONIC LIQUID BUCKY GELS AS SORBENT COATINGS FOR SOLID-PHASE MICROEXTRACTION

Reprinted with permission from *Journal of Chromatography A* **2014**, 1344, 15-22.

Copyright © 2014, Elsevier

Cheng Zhang, Jared L. Anderson

#### Abstract

Novel cross-linked polymeric ionic liquid (PIL) bucky gels were formed by free-radical polymerization of polymerizable ionic liquids gelled with multi-walled carbon nanotubes (MWCNT) and used as sorbent coatings for solid-phase microextraction (SPME). The incorporation of PIL with MWCNTs significantly enhanced the  $\pi$ - $\pi$  interaction between the sorbent coatings and the aromatic analytes. Compared with the neat PIL-based sorbent coating, The PIL bucky gel sorbent coatings demonstrated higher extraction efficiency for the extraction of polycyclic aromatic hydrocarbons (PAHs). A partitioning extraction mechanism was observed for PIL/MWCNT-based sorbent coating, which indicates the addition of MWCNTs did not seem to affect the extraction mechanism of the sorbent coating. After the determination of the film thickness of all studied sorbent coatings. The analyte-to-coating partition coefficients ( $\log K_{fs}$ ) were estimated and the limits of detection (LOD) for selected PIL bucky gel sorbent coating were determined to be in the range of 1-2.5 ng L<sup>-1</sup>. Recovery studies were also performed for PAHs in river and tap water to validate the applicability of the developed method.

#### 4.1 Introduction

Solid-phase microextraction (SPME) has become a popular sampling and pre-concentration technique since its introduction by Pawliszyn and co-workers in the early 1990s [1]. This technique is based on the adsorption or partitioning of analytes to a thin sorbent coating film, which is physically coated or chemically immobilized on a support. The simple design of SPME fibers allow for quick and cost effective extractions in which analytes can be easily delivered to various chromatographic systems. Currently, there are a number of commercial sorbent coatings available including polydimethylsyloxane (PDMS), polyacrylate (PA), PDMS-divinylbenzene (PDMS-DVB) and Carboxen-PDMS. Based on their respective polarities, these coatings are applicable for a broad spectrum of analytes [2-5]. However, these coatings still lack the selectivity needed in the extraction of specific classes of analytes. As a result, there has been increasing interest in developing new coating materials to achieve better sensitivity and selectivity while expanding the lifetime of the SPME fiber.

Carbon nanotubes (CNTs) have fascinated the scientific community since their discovery by Iijima in 1991 [6]. Based on the number of layers of graphene sheets that are rolled up within their structures, these compounds can be classified as single-walled carbon nanotubes (SWCNTs) or multi-walled carbon nanotubes (MWCNTs). CNTs possess high surface areas, high mechanical strength, and high thermal stability. The characteristic structures of CNTs allow them to interact strongly with certain classes of organic molecules through  $\pi$ - $\pi$  interactions, electrostatic forces, and dispersion interactions [7]. Due to the aforementioned advantages of CNTs, they have been successfully applied in sample preparation as solid-phase extraction (SPE) sorbents and SPME sorbent coatings for the analysis of a variety of organic compounds, such as phenols, polycyclic aromatic

hydrocarbons (PAHs), polybrominated biphenyls, phthalate esters and organochlorine pesticides [8-14].

Various approaches have been previously employed to immobilize CNTs on a SPME support. These techniques include organic binders [12], physical deposition [13], electrochemical deposition [14], as well as the exploiting of sol-gel technology [15]. However, these methods of preparing SPME fibers can be time consuming or complicated. Additionally, the prepared coatings may exhibit low extraction efficiency and stability, which limits the applicability of the CNTs in SPME. Thus, it is necessary to find new materials to address these challenges.

In 2003, imidazolium-based ionic liquid (IL) monomers were used as a new class of dispersants for CNTs by Fukushima and co-workers [16]. After being mixed and ground with SWCNTs, the IL monomer forms a viscous gel. The gel can then be polymerized using 2,2'-azobis (2-methylpropionitrile) (AIBN) via thermal-initiated polymerization. This feature of the IL monomer/CNT-based composite provides potential advantages over previously reported approaches in the immobilization of CNTs onto the SPME support, which is due to the fact that the gel can be synthetically designed with appropriate IL monomers and then be polymerized on a SPME support.

Our group first utilized polymeric ionic liquids (PILs) as sorbent coatings for SPME and found that they can exhibit high thermal stability, good analytical performance, and often extended coating lifetimes [17-20]. More importantly, the PIL-based coating can be appropriately functionalized to provide the desired selectivity and sensitivity in the extraction of target analytes. Recently, a solvent-less on-fiber copolymerization approach for the preparation of PIL-based SPME sorbent coating was developed by our group [18]. The success of these approaches provides indications that with modification, the IL/CNT-based gel can be employed for the preparation of PIL/CNT-based SPME sorbent coating.

For the first time, we report the development and application of cross-linked PIL bucky gel sorbent coatings for SPME analysis. These sorbent coatings were prepared by an on-fiber copolymerization of 1-vinyl-3-butylimidazolium bis[(trifluoromethyl)sulfonyl]imide ([VC<sub>4</sub>IM] [NTf<sub>2</sub>]) with a IL cross-linker, namely, 1,12-di (3-vinylimidazolium) dodecane bis[(trifluoromethyl)sulfonyl]imide ([VIM]<sub>2</sub>C<sub>12</sub>] 2[NTf<sub>2</sub>]) in the presence of AIBN. Various polycyclic aromatic hydrocarbons (PAHs) were selected as model analytes to validate the new method and evaluate the extraction efficiency, selectivity and analytical performance of the sorbent coatings. The effect of MWCNTs on extraction efficiencies were also compared between different sorbent coatings by varying the amount of MWCNTs in the PIL bucky gel sorbent coatings. Since the addition of MWCNTs into the PIL-based coating has the potential to alter the morphology and rigidity of the SPME sorbent coating, the extraction mechanism of the PIL bucky gel sorbent coating in direct immersion mode was studied. In order to better understand the selectivity and sorption behavior of the homemade SPME sorbent coatings, the analyte-to-coating partition coefficients were estimated. The LOD of all analytes were determined to demonstrate the applicability of the PIL bucky gel sorbent coatings for the extraction of PAHs in trace level. Additionally, method validation was performed via recovery studies in river and tap water. This is the first report to exploit PIL/MWCNT-based sorbent coatings for SPME analysis.

## 4.2 Experimental

### 4.2.1 Chemicals and reagents

PAH standards of naphthalene, acenaphthene, fluorene, phenanthrene, anthracene, fluoranthene, pyrene and chrysene were obtained from Supelco (Bellefonte, PA, USA). MWCNTs (>98 % carbon basis, O.D. × L 6-13 nm × 2.5-20 μm), 1-octanol, vinyltrimethoxysilane (VTMS), ammonium hydrogen difluoride, 1-vinylimidazole, 1-

bromobutane, and 2,2'-azobis (2-methylpropionitrile) (AIBN) were purchased from Sigma–Aldrich (Milwaukee, WI, USA). Lithium bis[(trifluoromethyl)sulfonyl]imide was purchased from SynQuest labs (Alachua, FL, USA). Chloroform, acetonitrile, isopropanol, ethyl acetate, and hexane (HPLC grade) were purchased from Fisher Scientific (Fair Lawn, NJ, USA). A 100  $\mu\text{m}$  PDMS fiber was obtained from Supelco. Ultrapure water was obtained from a Milli-Q water purification system (Millipore, Bedford, MA, USA) and was used in the preparation of aqueous solutions.

Sample solutions were prepared by dissolving the PAHs individually in acetonitrile to prepare standard solutions with concentrations of 500 or 2000  $\mu\text{g mL}^{-1}$ . Standard stock solutions containing all analytes at a concentration of 20  $\mu\text{g mL}^{-1}$  was prepared using the individual stock solutions. Working solutions were prepared by spiking a certain amount of the standard stock solution into 10 mL of deionized water within a 10 mL sampling vial.

#### 4.2.2 Instrumentation

Thermally initiated polymerization of the IL monomer/MWCNT-based gel was performed using an Agilent 5890 gas chromatograph. Helium was used as the carrier gas and maintained at a constant flow rate of 1  $\text{mL min}^{-1}$ . The GC inlet was maintained at 80  $^{\circ}\text{C}$  to enable the polymerization of IL monomer.

Evaluation of the extraction efficiency and analyte-to-fiber partition coefficients for all coatings was performed using an Agilent 6850N gas chromatograph employing flame ionization detection (FID). Helium was used as the carrier gas and maintained at a constant flow rate of 1  $\text{mL min}^{-1}$ . All separations were performed via splitless injection mode using a HP-5 capillary column (30 m  $\times$  250  $\mu\text{m}$   $\times$  0.25  $\mu\text{m}$ ) purchased from Agilent Technologies (Santa Clara, CA, USA). The following temperature program was used for the separation of PAHs: initial temperature was set to 80  $^{\circ}\text{C}$ , held for 2 min, followed by a ramp of 10  $^{\circ}\text{C}$

/min to 200 °C. The temperature was then held for 3 min and increased to 300 °C at a ramp of 25 °C /min and held for 10 min.

Evaluation of the extraction mechanism and analytical performance of the PIL bucky gel sorbent coating was performed using an Agilent 7890 gas chromatograph coupled to a 5975C inert XL MSD with a Triple Axis detector (GC/MS). Detection of all analytes via single ion monitoring (SIM) mode was accomplished by monitoring 3 relevant m/z fragment ions for each analyte. Helium was used as the carrier gas and maintained at a constant flow rate of 1 mL min<sup>-1</sup>. For the extraction mechanism studies, separation was performed using a CP-Wax 57-CB (50 m × 250 µm × 0.20 µm) column purchased from Agilent Technologies. The following temperature program was used for the separation of naphthalene and 1-octanol: initial temperature was set to 70 °C and held for 2 min, followed by a ramp of 20 °C /min to 150 °C. The temperature was then increased to 225 °C at a ramp of 10 °C /min and held for 10 min.

#### 4.2.3 Synthesis of IL monomer and cross-linker and preparation of SPME fibers

The [VC<sub>4</sub>IM] [NTf<sub>2</sub>] IL monomer and the [(VIM)<sub>2</sub>C<sub>12</sub>] 2[NTf<sub>2</sub>] IL cross-linker were synthesized following previously reported procedures [18, 23]. Detailed synthesis procedures, in addition to <sup>1</sup>H NMR spectra and electrospray ionization (ESI) mass spectra of the [VC<sub>4</sub>IM] [NTf<sub>2</sub>] IL monomer are presented in Figures C1-C2 (Appendix C).

Homemade SPME fibers were prepared according to previous procedures [18]. The bare fused silica support was etched and derivatized to enhance the overall mechanical stability of the SPME fiber. As shown in Figure 1, a mixture containing 200 mg of the [VC<sub>4</sub>IM] [NTf<sub>2</sub>] IL monomer, 30 mg of the [(VIM)<sub>2</sub>C<sub>12</sub>] 2[NTf<sub>2</sub>] IL cross-linker, and a specific weight percentage of MWCNTs (3%, 5%, or 8% w/w) was ground in an agate mortar for 30 min. Subsequently, 6.9 mg of AIBN (3% w/w) was added to the resulting gel.

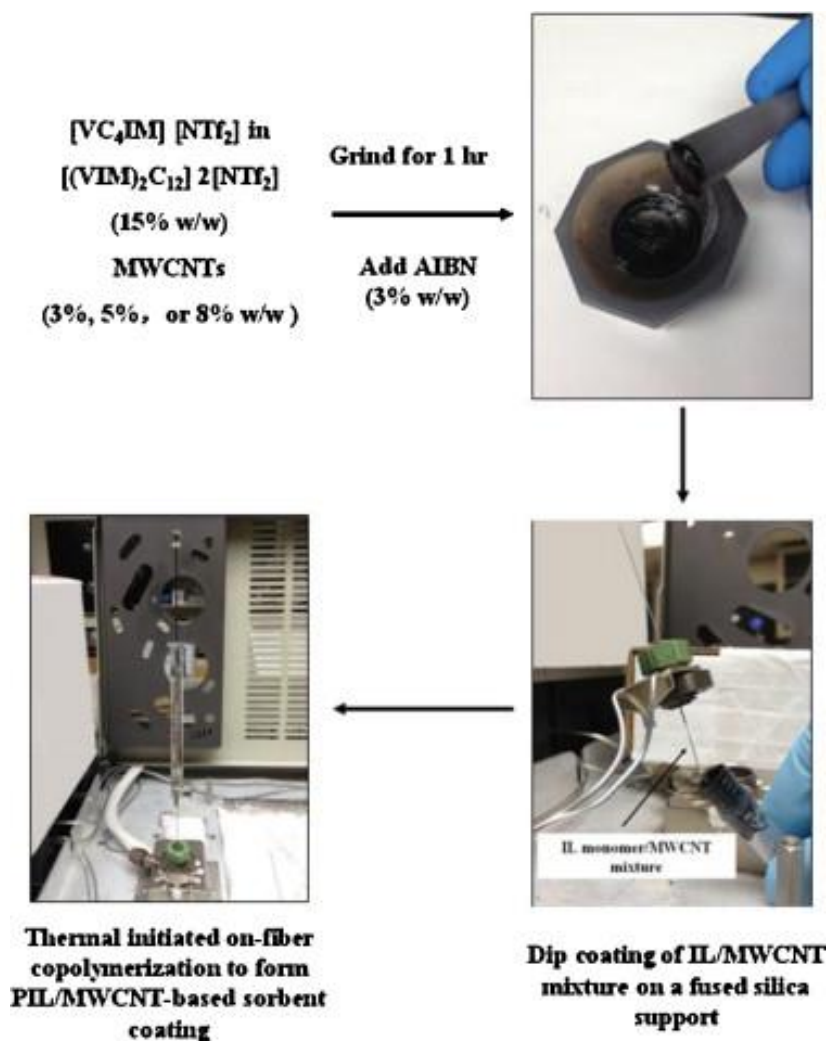


**Figure 1.** Schematic describing the approach used to prepare the PIL bucky gel sorbent coatings.

**Table 1.** IL monomers and cross-linkers used in the preparation of neat PIL-based and PIL/MWCNT-based SPME sorbent coatings.

Sorbent coatings	IL monomer	IL cross-linker <sup>a</sup>	Initiator <sub>b</sub>	MWCNTs <sub>b</sub>	Film thickness (μm)
Fiber 1				-	31
Fiber 2			AIBN 3% (w/w)	3% (w/w)	41
Fiber 3		15% (w/w)		5% (w/w)	36
Fiber 4				8% (w/w)	29

<sup>a</sup> Relative to the mass of the  $[VC_4IM] [NTf_2]$  IL monomer

<sup>b</sup> Relative to the mass of the IL monomer and cross-linker



The mixture was further ground for 1 min to ensure complete mixing of all components. The IL monomer/MWCNT-based gel was then evenly applied to the fused silica fiber via dip-coating. The coated fiber was carefully exposed to a GC injector at 80 °C under helium for 10 h. Finally, a black, solid-like sorbent coating was obtained. The composition of each prepared coating and their respective naming system are provided in Table 1. In order to confirm the polymerization of the IL monomer, the fibers were immersed in chloroform under high agitation for 5 min to observe loss of coating. No visible loss of the coating was observed by optical microscope. Following polymerization, each fiber was conditioned five times at 280 °C for 5 min.

#### 4.2.4 SPME procedure

For the extraction of PAHs, 10 mL of Milli-Q water and a specific amount of standard stock solution was placed in a 10 mL amber glass sampling vial containing a magnetic stir bar and agitated at 800 rpm. Extractions were performed by exposing the SPME fiber to the working solution for a specific amount of time. Desorption was performed by exposing the fiber to the GC inlet for 7 min at 280 °C. Carryover was examined following the desorption of a previous extraction by reinserting the SPME fiber in the injector for 7 min. The highest carryover for all samples was observed to be less than 5%.

Evaluation of the extraction mechanism was performed at room temperature by exposing the fiber coating to the headspace of a working solution (5 mL) containing a specific concentration of 1-octanol and naphthalene in a 10 mL vial. The extraction time was chosen based on the time required for both analytes to reach equilibrium with the sorbent coating. Desorption was performed by exposing the fiber to the GC inlet for 5 min at 175 °C. Carryover for both analytes was found to be less than 3%.

#### 4.2.5 Estimation of partition coefficient using SPME

The analyte-fiber partition coefficient ( $K_{fs}$ ) can be calculated according to Eq. (1)

$$K_{fs} = \frac{V_s}{V_f[(n_o/n_f)-1]} \quad (1)$$

where  $n_o$  is the initial amount of analyte in the sample. The amount of analyte partitioned to the fiber at equilibrium ( $n_f$ ) is calculated based on the response factors generated from external calibration curves. Calibration curves of the analyte peak areas versus the mass of the analyte injected onto the GC column were generated by injecting 1  $\mu$ L of standard mixtures ranging from 10  $\mu$ g mL<sup>-1</sup> to 500  $\mu$ g mL<sup>-1</sup> using identical inlet and column conditions as to those carried out for the SPME experiments.  $V_s$  is the volume of the matrix, which was maintained at 10 mL in this study.  $V_f$  is the volume of the sorbent coating which was estimated based on the filmthickness of the coating and the length of the sorbent immobilized on the SPME support.

#### 4.2.6 Real sample collection and recovery experiment

Recovery studies were performed using two matrixes. The tap water was collected in the lab and river water was collected from the Maumee River in Maumee, OH (USA). The river water was filtered through a 3 mL syringe with 0.45  $\mu$ m Nylon filter units (Fisher Scientific). The relative recoveries of all analytes were evaluated using direct immersion mode. Blank extractions of the sample matrixes were performed and no analytes was presented. Depending on the linear range of the calibration study, two concentration levels were chosen for each analyte. Relative recovery was determined by spiking a known concentration of the analyte to a sample solution and comparing the experimental concentration obtained with respect to the actual concentration. Carryover for all analytes was found to be less than 5%.

### 4.3 Results and Discussion

#### 4.3.1 Characterization of the PIL bucky gel sorbent coatings

As a new type of SPME sorbent coating, it is important to characterize the coating's morphology as well as to confirm the presence of the MWCNTs in the sorbent coating. After completing all extractions in this study, Fibers 1-4 containing 0-8% (w/w) of MWCNTs were sacrificed for analysis via scanning electron microscopy (SEM) to characterize the surface and cross section morphology as well as determine the approximate

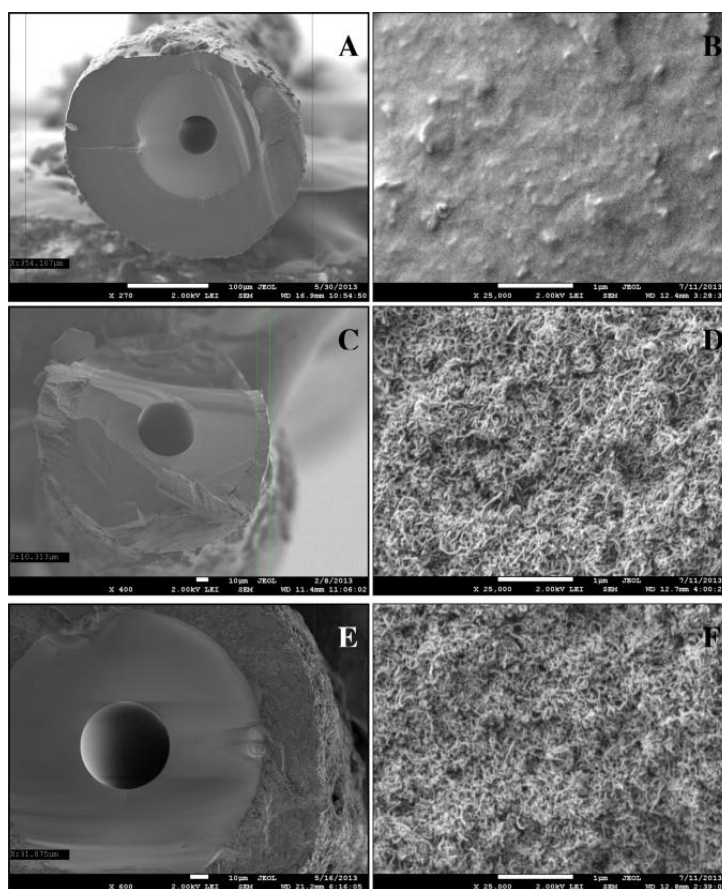


**Figure 2.** Scanning electron micrographs showing the cross-section and surface morphology of the PIL-based and PIL bucky gel sorbent coatings after 60 direct immersion extractions. (A, B) Neat PIL-based sorbent coating, (C, D) PIL bucky gel sorbent coating containing 3% (w/w) of MWCNTs, (E, F) PIL bucky gel sorbent coating containing 8% (w/w) of MWCNTs.

film thickness of the sorbent coating. Figure C3 (Appendix C) shows the surface morphology of the different sorbent coatings prepared in this study. After approximately 60 direct immersion extractions, a rough surface morphology was observed for all coatings.

The cross section of Fibers 1, 2, and 4 under different magnifications are shown in Figure 2. At higher magnification ( $\times 25000$ ), a relatively smooth surface can be observed for the neat PIL-based sorbent coating (Fiber 1) as shown in Figure 2B. However, a rougher surface morphology was observed for Fibers 2 and 4, as shown in Figures 2D and 2F. A large number of MWCNTs could be observed in the cross section view of the sorbent coatings, which demonstrates that the MWCNTs were homogenously distributed throughout the sorbent coating. As shown in Table 1, the film thicknesses for the neat PIL and PIL bucky gel sorbent coatings were in the range of 29-41  $\mu\text{m}$ .

#### 4.3.2 Optimization of extraction time

Extraction time is an important factor in achieving equilibration of the analyte between the sample and the sorbent coating. In this study, SPME extractions were carried out at various extraction times at 22 °C using a stir rate of 800 rpm. Figure 3 and Figure C4 (Appendix C) illustrate the sorption time profiles obtained using Fibers 1-4 and the 100  $\mu\text{m}$  commercial PDMS coating. As shown in Figure 3, naphthalene, acenaphthene, fluorine and

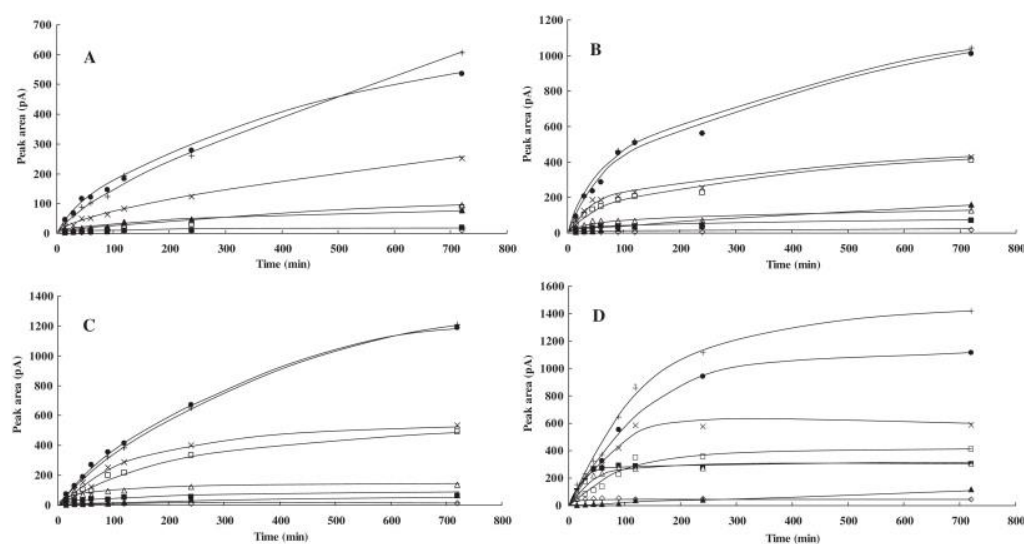


**Figure 3.** Sorption-time profiles of all selected coatings. (A) Fiber 1, (B) Fiber 2, (C) Fiber 4, (D) PDMS coating (100 $\mu\text{m}$ ). The stir rate was 800 rpm and the concentration of the analytes was 40  $\mu\text{g L}^{-1}$ . ( $\diamond$ ) Naphthalene, ( $\blacksquare$ ) Acenaphthene, ( $\Delta$ ) Fluorine, ( $\times$ ) Phenanthrene, ( $\square$ ) Anthracene, ( $\bullet$ ) Fluoranthene, ( $+$ ) Pyrene, ( $\blacktriangle$ ) Chrysene.

phenanthrene reached equilibrium in approximately 120 min using the PDMS coating. Equilibrium was not achieved even after 240 min extractions for all other PAHs. In the case of Fibers 1-4, all PAHs analytes did not reach equilibrium even after 240 min, which may be due to the lower mass transfer of the analytes within the sorbent coating containing MWCNTs. A similar observation was also reported by Jiang and co-workers. In their work, a 3  $\mu\text{m}$  sol-gel-CNT coating did not reach equilibrium in 120 min for the extraction of benzene, toluene, ethylbenzene, and o-xylene [15]. Since the PIL bucky gel sorbent coatings have much higher film thicknesses (29-41  $\mu\text{m}$ ), longer extraction time is required to reach equilibrium. In order to reach a compromise between throughput and extraction efficiency, an extraction of 45 min was chosen for all subsequent calibration studies.

#### 4.3.3 Comparison of extraction efficiency of the PIL-based and PIL bucky gel sorbent coatings with PDMS sorbent coating

In order to better understand the effect of the MWCNTs within the PIL sorbent coatings, the extraction efficiencies of the neat PIL-based sorbent coating and PIL bucky gel sorbent coatings were compared. A side by side comparison using the PDMS coating was also performed since this coating has previously been applied in the extraction of various non-polar aromatic compounds. Based on their sorption-time profiles, all fibers demonstrated the highest extraction efficiency at 720 min. As a result, 720 min was chosen as the optimum extraction time. The amount of analyte extracted using the five different sorbent coatings at a concentration of 40  $\mu\text{g L}^{-1}$  is shown in Figure 4. Compared to the PDMS coating, the neat PIL-based sorbent coating (Fiber 1) extracted a lower amount of all PAHs due to the low affinity of the coating for the PAHs. The mass of naphthalene, acenaphthene, and fluorene extracted by the PDMS coating ranged from two to thirty folds higher compared to the neat PIL-based sorbent coatings. The higher extraction efficiency

of the PDMS can be ascribed to its larger volume of sorbent phase, which is proportional to the film thickness (see Table 1).

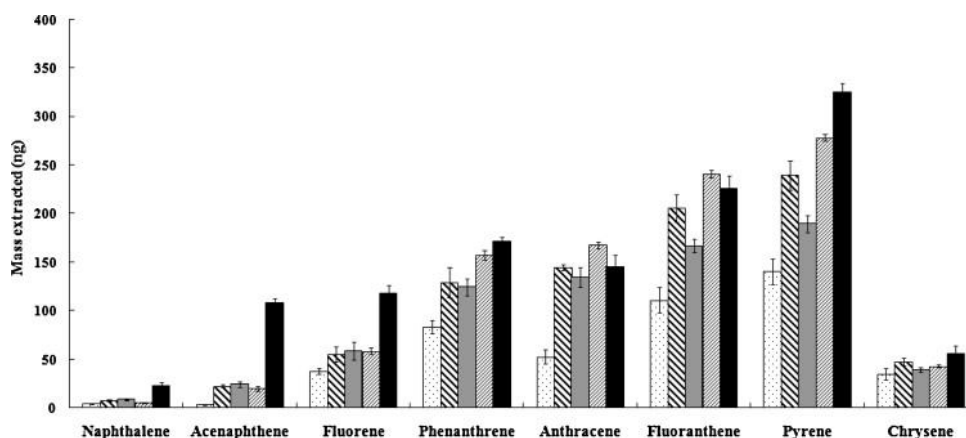


**Figure 4.** Mass of analytes extracted using selected sorbent coatings. (■) Fiber 1, (||) Fiber 2, (//) Fiber 3, (⊞) Fiber 4, (·) PDMS coating (100  $\mu$ m).

In the case of high molecular weight PAHs including phenanthrene, anthracene, fluoranthene, pyrene and chrysene, a similar or slightly higher amounts of analytes were extracted by the PIL-based and PIL bucky gel sorbent coatings compared to the PDMS coating. When comparing the neat PIL-based sorbent coating and PIL bucky gel sorbent coatings, similar amounts of naphthalene, fluorene, and chrysene were extracted using the four coatings. For all other analytes, the PIL bucky gel sorbent coatings exhibited noticeably higher extraction efficiency compared to the neat PIL-based sorbent coating. The addition of the MWCNTs to the PIL sorbent phase appears to increase the extraction efficiency of the sorbent coating, which is likely due to the enhanced  $\pi$ - $\pi$  interaction between the PAHs and MWCNT-enriched sorbent coatings. These observations are in good agreement with data published by Valcárcel and co-workers, who employed a soft material combined with IL and MWCNTs for the preconcentration of PAHs [21]. It is worth noting that Fiber 4 containing 8% MWCNTs outperformed all other PIL-based and PIL bucky gel sorbent coatings by exhibiting the highest extraction efficiencies for fluorene, phenanthrene,

anthracene, fluoranthene, and pyrene despite possessing the smallest film thickness (29  $\mu\text{m}$ ).

#### 4.3.4 Extraction mechanism of PIL bucky gel sorbent coatings

As a new type of SPME sorbent coating, it is important to evaluate the extraction mechanism of the PIL bucky gel sorbent coatings. The two most dominant mechanisms of extraction in SPME are adsorption and partition. If the PIL bucky gel sorbent coatings are adsorption-type coatings, the competition effects between the different analytes in a complex matrix can result in an erroneous quantitation [22]. Recently, the extraction mechanism of various PIL-based SPME sorbent coatings was studied by our group wherein a partitioning-type extraction mechanism was observed [23]. However, as shown in Figure 2, the incorporation of the MWCNTs within the PIL phase significantly alters the structure, morphology, and rigidity of the SPME sorbent coatings. Therefore, it is essential to determine whether these alterations may also affect the mechanism of extraction.

An investigation into the extraction mechanism was performed by following previously published procedures [23]. Fiber 3, which contained 3% (w/w) of MWCNTs within the PIL sorbent coating was chosen for evaluation in this study. A working solution containing 100  $\mu\text{g L}^{-1}$  of 1-octanol and 10  $\mu\text{g L}^{-1}$  of naphthalene was used in the optimization procedure. The extraction time was optimized to be slightly longer than the equilibration time of the analyte. As shown in Figure C5 (Appendix C), naphthalene and 1-octanol reached equilibrium at approximately 120 min, therefore this extraction time was employed for all subsequent mechanism studies.

As it has been previously demonstrated, SPME sorbent coatings that extract analytes through a partitioning mechanism exhibit no significant deviations in the linear range, sensitivity and the amount of the target analyte extracted in the presence of an interfering

compound. Calibration curves of 1-octanol with concentrations ranging from 1 to 1000  $\mu\text{g L}^{-1}$  were generated in the presence of naphthalene as an interfering compound to ascertain whether competition influences the extraction mechanism of the sorbent coating. As shown in Figure 5, there was no significant change in the linear range, sensitivity, or the amount of the analyte extracted when a significant amount of interfering compound was added to the same matrix (1:1 1-octanol: naphthalene). This observation indicates little-to-no competition between the target analyte and the interfering compound, which is a characteristic of a partitioning extraction mode. In other words, the addition of MWCNTs does not seem to affect the extraction mechanism typically observed with native PIL-based sorbent coatings prepared by analogous synthetic pathways.

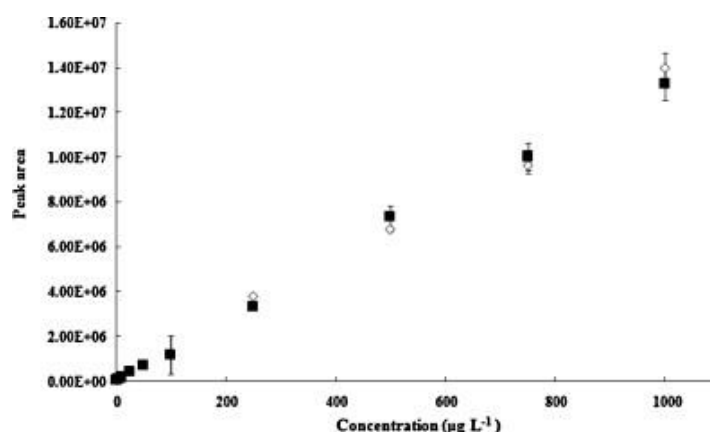


**Figure 5.** Calibration curves of 1-octanol at ( $\diamond$ ) 10:1 1-octanol: naphthalene, and ( $\blacksquare$ ) 1:1 1-octanol: naphthalene.

#### 4.3.5 Determination of analyte-to-sorbent coating partition coefficients

The analyte to coating partition coefficients were determined in an effort to correlate the chemical makeup of the sorbent coating and selectivity. As mentioned previously, most of the PAHs did not reach equilibrium with the PIL bucky gel sorbent coatings and PDMS coating even after 720 min. Therefore, the analyte to coating partition coefficients obtained in this study are only rough estimations. The amounts of analytes extracted by the sorbent coatings ( $n_f$ ) was calculated from the response factor generated by manual injection of



**Table 2.** Estimated partition coefficients ( $K_{fs}$ ) of PAHs to all studied sorbent coatings.

Analyte	Log $K_{fs} \pm \text{error}$					Log $K_{fs}$		
	Fiber 1	Fiber 2	Fiber 3	Fiber 4	PDMS (100 $\mu\text{m}$ )	PDMS (100 $\mu\text{m}$ , literature)		
Naphthalene	$2.74 \pm 0.07$	$2.77 \pm 0.03$	$2.87 \pm 0.05$	$2.77 \pm 0.08$	$3.27 \pm 0.03$	3.02 <sup>a</sup>	3.01 <sup>b</sup>	2.85 <sup>c</sup>
Acenaphthene	$2.65 \pm 0.08$	$3.24 \pm 0.04$	$3.34 \pm 0.04$	$3.36 \pm 0.1$	$4.07 \pm 0.06$	3.63 <sup>a</sup>		
Fluorene	$3.73 \pm 0.02$	$3.67 \pm 0.03$	$3.76 \pm 0.02$	$3.87 \pm 0.01$	$4.12 \pm 0.05$	3.71 <sup>a</sup>		
Phenanthrene	$4.13 \pm 0.02$	$4.11 \pm 0.05$	$4.16 \pm 0.05$	$4.41 \pm 0.02$	$4.38 \pm 0.02$	3.96 <sup>a</sup>	3.4 <sup>b</sup>	3.45 <sup>c</sup>
Anthracene	$3.89 \pm 0.02$	$4.18 \pm 0.01$	$4.20 \pm 0.03$	$4.45 \pm 0.04$	$4.26 \pm 0.01$	3.98 <sup>a</sup>	4.1 <sup>b</sup>	3.14 <sup>c</sup> 3.46 <sup>d</sup>
Fluoranthene	$4.29 \pm 0.03$	$4.41 \pm 0.08$	$4.34 \pm 0.04$	$4.71 \pm 0.08$	$4.62 \pm 0.01$	4.71 <sup>a</sup>	4.11 <sup>c</sup>	3.79 <sup>d</sup>
Pyrene	$4.44 \pm 0.11$	$4.53 \pm 0.02$	$4.42 \pm 0.02$	$4.84 \pm 0.08$	$4.92 \pm 0.06$	4.86 <sup>a</sup>	4.07 <sup>c</sup>	3.82 <sup>d</sup>
Chrysene	$3.69 \pm 0.02$	$3.70 \pm 0.02$	$3.57 \pm 0.01$	$3.72 \pm 0.02$	$3.71 \pm 0.02$	5.69 <sup>a</sup>	3.97 <sup>c</sup>	

<sup>a</sup> Ref. [24],

<sup>b</sup> Ref. [25],

<sup>c</sup> Ref. [26],

<sup>d</sup> Ref. [27]

1  $\mu\text{L}$  standard solution of analytes. The logarithmic values of the partition coefficients ( $\log K_{fs}$ ) obtained for all sorbent coatings are listed in Table 2. Literature values for the same PAHs using the 100  $\mu\text{m}$  PDMS coating are also included for comparison.

The partition coefficients of the PAHs to the PDMS coating are generally in good agreement with previously reported values from the literature. The large errors obtained for low-ring PAHs such as naphthalene, acenaphthene, fluorene, phenanthrene, and anthracene can be ascribed to the higher concentration of the working solutions used in this study compared to the literature. A similar observation was reported by Doong and co-workers. In their work, a small increase in the sample volume significantly decreased the amounts of PAHs analytes extracted by the fiber [24]. A side-by-side evaluation of the  $\log K_{fs}$  values showed that Fiber 4 possesses higher analyte-to-sorbent coating partition coefficients for phenanthrene, anthracene, fluoranthene, and chrysene compared to the PDMS coating. Similarly, this fiber exhibited higher  $\log K_{fs}$  values when compared to all other PIL-based and PIL bucky gel sorbent coatings. Thus, by gradually increasing the loading percentage of MWCNTs in the PIL-based sorbent coatings, a significant enhancement in the  $\log K_{fs}$  values can be obtained.

#### 4.3.6 Analytical performance of selected PIL bucky gel sorbent coating in the extraction of PAHs

Based on its higher extraction efficiencies (shown in Figure 4) and superior  $\log K_{fs}$  values, Fiber 4 was selected to evaluate its analytical performance in the extraction of PAHs. Calibration curves were generated by increasing the analyte concentration from 0.05 to 1000  $\mu\text{g L}^{-1}$  using a minimum of seven calibration points. Direct-immersion SPME was performed at 22  $^{\circ}\text{C}$  using an extraction time of 45 min.

**Table 3.** Analytical performance of Fiber 4 containing 8% (w/w) MWCNTs and compared with other reported coatings for the extraction of PAHs

Analytes	Fiber 4 (32 $\mu\text{m}$ )				PDMS (100 $\mu\text{m}$ )				Carbon nanoparticle-based sorbent coating (2.5 $\mu\text{m}$ ) <sup>e</sup>	
	Linear Range ( $\mu\text{g L}^{-1}$ )	R	LOD <sup>a</sup> ( $\text{ng L}^{-1}$ )	% RSD <sup>b</sup>	Linear Range ( $\mu\text{g L}^{-1}$ )	LOD ( $\text{ng L}^{-1}$ )			Linear Range ( $\mu\text{g L}^{-1}$ )	LOD ( $\text{ng L}^{-1}$ )
Naphthalene	0.005-1000	0.999	2.5	2.3	0.1-10 <sup>c</sup>	0.01-10 <sup>d</sup>	180 <sup>c</sup>	3 <sup>d</sup>	—	—
Acenaphthene	0.005-1000	0.990	2.5	9.8	0.1-10 <sup>c</sup>	0.01-10 <sup>d</sup>	100 <sup>c</sup>	6 <sup>d</sup>	—	—
Fluorene	0.005-250	0.985	1	11.1	0.1-10 <sup>c</sup>	0.01-10 <sup>d</sup>	70 <sup>c</sup>	2 <sup>d</sup>	0.01-200 <sup>e</sup>	3 <sup>e</sup>
Phenanthrene	0.005-100	0.988	1	17.4	0.1-10 <sup>c</sup>	0.02-10 <sup>d</sup>	80 <sup>c</sup>	17 <sup>d</sup>	—	—
Anthracene	0.005-50	0.998	2.5	12.1	0.1-10 <sup>c</sup>	0.03-10 <sup>d</sup>	100 <sup>c</sup>	20 <sup>d</sup>	0.01-150 <sup>e</sup>	2 <sup>e</sup>
Fluoranthene	0.005-50	0.988	1	6.3	0.1-10 <sup>c</sup>	0.01-10 <sup>d</sup>	100 <sup>c</sup>	1 <sup>d</sup>	0.01-150 <sup>e</sup>	1 <sup>e</sup>
Pyrene	0.005-100	0.991	1	0.7	0.1-10 <sup>c</sup>	0.01-10 <sup>d</sup>	110 <sup>c</sup>	1 <sup>d</sup>	—	—
Chrysene	0.05-5	0.980	1	12.8	0.1-10 <sup>c</sup>	0.01-10 <sup>d</sup>	30 <sup>c</sup>	5 <sup>d</sup>	—	—

<sup>a</sup> Determined by decreasing the analyte concentration until a 3:1 S:N ratio was achieved.

<sup>b</sup> Determined by performing repeated extractions at 0.1  $\mu\text{g L}^{-1}$  (n=4).

<sup>c</sup> Ref. [28],

<sup>d</sup> Ref. [29],

<sup>e</sup> Ref. [30].

**Table 4.** Recovery and reproducibility results of Fiber 4 for the extraction of PAHs from river and tap water

Analyte	River water				Tap water			
	1 $\mu\text{g L}^{-1}$	% RSD <sup>a</sup>	10 $\mu\text{g L}^{-1}$	% RSD <sup>a</sup>	1 $\mu\text{g L}^{-1}$	% RSD <sup>a</sup>	10 $\mu\text{g L}^{-1}$	% RSD <sup>a</sup>
Naphthalene	80.93	5.6	107.7	5.0	67.5	8.5	96.8	7.8
Acenaphthene	64.8	5.4	102.7	14.6	67.2	12.3	83.3	10.5
Fluorene	60	11.8	90.9	6.0	66.6	15.6	91.7	14.8
Phenanthrene	76.9	11.2	86.6	8.5	73.7	10.6	122.3	11.1
Anthracene	94.4	8.3	80.1	8.6	78.1	9.9	112.8	8.6
Fluoranthene	96.3	15.3	84.2	13.0	83.5	6.3	117.9	7.8
Pyrene	103.7	15.8	78	12.6	77.4	5.3	109.1	9.2
	0.25 $\mu\text{g L}^{-1}$	% RSD	2.5 $\mu\text{g L}^{-1}$	% RSD	0.25 $\mu\text{g L}^{-1}$	% RSD	2.5 $\mu\text{g L}^{-1}$	% RSD
Chrysene	72.8	10.3	114	14.6	112	2.6	107	6.3

<sup>a</sup> Determined by performing repeated extractions (n=3).

The figures of merit, including linear ranges, correlation coefficients, precision, and LODs are listed in Table 3. Wide linear ranges were achieved for all PAHs. The correlation coefficients varied between 0.980-0.999. The precision of the method for four consecutive extractions at a concentration of  $0.1 \mu\text{g L}^{-1}$  ranged from 0.7% to 17.4%. The limits of detection (LODs) were determined by decreasing the concentration of the analytes until a signal-to-noise ratio of 3 ( $S/N=3$ ) was achieved. The LODs for all PAHs were in the range of  $1\text{-}2.5 \text{ ng L}^{-1}$ . For comparison purposes, Table 3 also lists previously published linear ranges and LOD values obtained for the extraction of PAHs using the commercial PDMS coating and a carbon nanoparticle-based sorbent coating coupled to GC-MS. Compared with the  $100 \mu\text{m}$  PDMS fiber, Fiber 4 shows better linear range and LODs for the extraction of PAHs despite possessing a much smaller film thickness ( $32 \mu\text{m}$ ) [28, 29]. When compared with a  $2.5 \mu\text{m}$  carbon nanoparticle-based sorbent coating, Fiber 4 shows comparable linear range and LODs for the extraction of fluorene, anthracene, and fluoranthene [30]. Overall, the results indicate that the incorporation of MWCNTs to a PIL phase can provide a reproducible and sensitive SPME sorbent coating for the extraction of PAHs from water samples.

#### 4.3.7 Method validation and accuracy

In order to evaluate the accuracy and applicability of the PIL bucky gel sorbent coating, recovery studies were performed using river and tap water for the extraction of PAHs. Figure 6 shows the typical chromatograms of the river water samples with and without spiked eight PAHs obtained by SPME/GC-MS. As shown in Table 4, the relative recoveries obtained were from 60 to 114% for river water and 66.6 to 122.3% for tap water. The precision of the recovery tests was lower than 15.8%. Considering the low spiked

concentration level and the complexity of the sample matrix, the obtained recoveries and precision values are very good for direct-immersion SPME.

#### **4.4 Conclusions**

A novel PIL bucky gel SPME sorbent coating was prepared via thermal initiated on-fiber copolymerization for the selective extraction of PAHs from water. The new approach allows MWCNTs been finely dispersed within the PIL phase, which can significantly increases the contact surface areas between the MWCNTs and the PAHs. The PIL bucky gel sorbent coating containing 8% (w/w) of MWCNTs exhibited higher extraction efficiencies for the extraction of most PAHs compared with other PIL bucky gel sorbent coatings and commercial PDMS coating. A non-competitive extraction mechanism was observed for PIL bucky gel sorbent coating containing 3% (w/w) of MWCNTs, which indicates that small amount of MWCNTs did not affect the extraction mechanism of the PIL bucky gel sorbent coating. The analytical performance of the PIL bucky gel sorbent coating obtained in this study shows the incorporation of MWCNTs to PIL phase can provide a reproducible and sensitive SPME sorbent coating for the extraction of PAHs. Recovery studies in both river and tap water were in acceptable range. Future investigation will involve tuning the selectivity of the IL to design a PIL bucky gel sorbent coating which possesses higher extraction efficiency toward aromatic compounds.

## Acknowledgements

The authors wish to thank Dr. Pannee Burckel for her assistance in using the SEM. J.L.A acknowledges funding from the Analytical and Surface Chemistry Program in the Division of Chemistry and the Separation and Purification Processes Program in the Chemical, Environmental, Bioengineering, and Transport Systems Division from the National Science Foundation for a CAREER grant (CHE-0748612).

## Reference

- [1] C.L. Arthur, J. Pawliszyn, *Anal. Chem.* 62 (1990) 2145
- [2] H. Prosen, L. Zupančič-Kralj, *TrAC, Trends Anal. Chem.* 18 (1999) 272
- [3] G.F. Ouyang, J. Pawliszyn, *TrAC, Trends Anal. Chem.* 25 (2006) 692
- [4] A. Spietelun, A. Kloskowski, W. Chrzanowski, J. Namieśnik, *Chem. Rev.* 113 (2013) 1667
- [5] H.L. Yu, T.D. Ho, J.L. Anderson, *TrAC, Trends Anal. Chem.* 45 (2013) 219
- [6] S. Iijima, *Nature* 354 (1991) 56
- [7] B.T. Zhang, X. Zheng, H.F. Li, J.M. Lin, *Anal. Chim. Acta* 784 (2013) 1
- [8] L.M. Ravelo-Pérez, J. Hernández-Borges, M.A. Rodríguez-Delgado, *J. Chromatogr. A* 1211 (2008) 33
- [9] H. Zhao, L. Wang, Y. Qiu, Z. Zhou, W. Zhong, X. Li, *Anal. Chim. Acta* 586 (2007) 399
- [10] J.X. Lü, J.F. Liu, Y. Wei, K.L. Jiang, S.S. Fan, J.Y. Liu, G.B. Jiang, *J. Sep. Sci.* 30 (2007) 2138
- [11] Q. Zhou, J. Xiao, W. Wang, *J. Chromatogr. A* 1125 (2006) 152
- [12] J.X. Wang, D.Q. Jiang, Z.Y. Gu, X.P. Yan, *J. Chromatogr. A* 1137 (2006) 8
- [13] H.M. Liu, J.B. Li, X. Liu, S.X. Jiang, *Talanta* 78 (2009) 929
- [14] H. Asadollahzadeh, E. Noroozian, Sh. Maghsoudi, *Anal. Chim. Acta* 669 (2010) 32
- [15] R.F. Jiang, F. Zhu, T.G. Luan, Y.X. Tong, H. Liu, G.F. Ouyang, J. Pawliszyn, *J. Chromatogr. A* 1216 (2009) 4641

- [16] T. Fukushima, A. Kosaka, Y. Ishimura, T. Yamamoto, T. Takigawa, N. Ishii, T. Aida, *Science* 300 (2003) 2072
- [17] F. Zhao, Y.J. Meng, J.L. Anderson, *J. Chromatogr. A* 1208 (2008) 1
- [18] T.D. Ho, H.L. Yu, W.T. Cole, J.L. Anderson, *Anal. Chem.* 84 (2012) 9520
- [19] Y.J. Meng, J.L. Anderson, *J. Chromatogr. A* 1217 (2010) 6143
- [20] T.D. Ho, M.D. Joshi, M.A. Silver, J.L. Anderson, *J. Chromatogr. A* 1240 (2012) 29
- [21] M.L. Polo-Luque, B.M. Simonet, M. Valcárcel, *Talanta* 104 (2013) 169
- [22] T. Górecki, X.M. Yu, J. Pawliszyn, *Analyst* 124: (1999) 643
- [23] T.D. Ho, W.T. Cole, F. Augusto, J.L. Anderson, *J. Chromatogr. A* 1298 (2013) 146
- [24] R.A. Doong, S.M. Chang, *Anal. Chem.* 72 (2000) 3647
- [25] D.W. Potter, J. Pawliszyn *Environ. Sci. Technol.* 28 (1994) 298
- [26] J.J. Langenfeld, S.B. Hawthorne, D.J. Miller, *Anal. Chem.* 68 (1996) 144
- [27] A. Paschke, P. Popp, *J. Chromatogr. A* 999 (2003) 35
- [28] R.A. Doong, S.M. Chang, Y.C. Sun, *J. Chromatogr. A* 879 (2000) 177
- [29] A.J. King, J.W. Readman, J.L. Zhou, *Anal. Chim. Acta* 523 (2004) 259
- [30] M. Sun, J.J. Feng, H.M. Qiu, L.L. Fan, L.L. Li, C.N. Luo, *J. Chromatogr. A* 1300 (2013) 173



## CHAPTER 5

### **RAPID AND SENSITIVE ANALYSIS OF POLYCHLORINATED BIPHENYLS AND ACRYLAMIDE IN FOOD SAMPLES USING IONIC LIQUID-BASED IN SITU DISPERSIVE LIQUID-LIQUID MICROEXTRACTION COUPLED TO HEADSPACE GAS CHROMATOGRAPHY**

Cheng Zhang, Cecilia Cagliero, Stephen A Pierson, Jared L. Anderson

#### **Abstract**

A simple and rapid ionic liquid (IL)-based *in situ* dispersive liquid-liquid microextraction (DLLME) method was developed and coupled to headspace gas chromatography (HS-GC) employing electron capture (ECD) and mass spectrometry (MS) detection for the analysis of polychlorinated biphenyls (PCBs) and acrylamide at trace levels from milk and coffee samples. The chemical structures of the halide-based ILs were tailored by introducing various functional groups to the cations to evaluate the effect of different structural features on the extraction efficiency of the target analytes. Extraction parameters including the molar ratio of IL to metathesis reagent and IL mass were optimized. The effects of HS oven temperature and the HS sample vial volume on the analyte response were also evaluated. The optimized *in situ* DLLME method exhibited good analytical precision, good linearity, and provided detection limits down to the low ppt level for PCBs and the low ppb level for acrylamide in aqueous samples. The matrix-compatibility of the developed method was also established by quantifying acrylamide in brewed coffee samples. This method is much simpler and faster compared to previously reported GC-MS methods using solid-phase microextraction (SPME) for the extraction/preconcentration of PCBs and acrylamide from complex food samples.

## 5.1 Introduction

The monitoring of contaminants in foods is very important for human health risk assessment [1, 2]. The accumulation of toxic compounds such as PCBs from the environment [3] and the unintentional formation of toxic substances during the manufacturing process (e.g., generation of acrylamide during roasting of coffee beans [4]) are two major sources of food contamination. It is well known that continuous exposure to these toxic compounds can cause several chronic diseases, including cancer and serious endocrine disorders [5]. However, the identification and quantification of contaminants from food samples is a significant analytical challenge. Although GC and high-performance liquid chromatography (HPLC) coupled to MS have been widely adopted for food analysis, the direct analysis of food samples is often very challenging due to the high complexity of the sample matrices. To address this issue, highly selective, sensitive, and cost-effective sample preparation techniques must be selected and employed prior to downstream chromatographic, electrophoretic, or mass spectroscopic analysis [1, 6-10].

SPME is a solvent free, simple, and convenient technique which combines sampling and preconcentration into one step [11]. By applying various commercially available SPME coatings in the headspace or direct-immersion mode, a wide variety of compounds have been successfully extracted from food samples [1, 2]. Structurally-tuned polymeric ionic liquids (PILs) were recently employed by our group as sorbent coatings for the extraction of PCBs and acrylamide from milk and coffee samples, respectively [12-14]. The PIL-based sorbent coatings exhibited superior selectivity and sensitivity in the extraction of these compounds compared to commercially available SPME coatings. However, it was also observed that long extraction times (from 30 min to a couple hours) were required to extract detectable amounts of analytes from the sample matrices. Furthermore, the development of matrix-compatible SPME sorbent coatings remains a significant challenge.

When analyzing very complex sample matrices, irreversible fouling of the sorbent coating can dramatically decrease the lifetime of the SPME fiber [15]. In our previous work, matrix-compatible PIL-based sorbent coatings were applied for the in-solution extraction of acrylamide from brewed coffee samples. However, the developed method required a washing and reconditioning step after each extraction, which can significantly decrease the sample throughput [13, 14]. Therefore, alternative extraction techniques that are rapid, robust, selective, and sensitive need to be explored.

Dispersive liquid-liquid microextraction (DLLME) was first introduced by Rezaee and co-workers in 2006 [16]. Analyte preconcentration in this technique is achieved by dispersing a water-immiscible extraction solvent into fine droplets with the assistance of a water-miscible disperser solvent. Subsequently, the hydrophobic extraction solvent can be recovered by centrifugation [17-20] or by decreasing the temperature of the solution [21-23] followed by chromatographic analysis. Due to the significantly increased surface area of the extraction solvent, very short extraction times (often less than a minute) are required resulting in high extraction efficiencies for target analytes.

Ionic liquids (ILs) were first applied as extraction solvents for DLLME in 2008 [21, 24]. Compared to conventional extraction solvents employed for DLLME (i.e., chlorobenzene, chloroform, and carbon tetrachloride), ILs exhibit many unique physical properties including negligible vapor pressures and tunable viscosities [25, 26]. Moreover, the chemical structures of ILs can be custom designed to enhance extraction efficiencies toward different classes of analytes. In 2009, another modified DLLME approach termed *in situ* DLLME or *in situ* solvent formation microextraction based on ILs was introduced [27, 28]. In this approach, a hydrophilic IL-based extraction solvent is dissolved in an aqueous sample solution. An anion exchange reagent such as lithium bis[(trifluoromethyl)sulfonyl]imide ( $\text{LiNTf}_2$ ), is then added to the solution to form fine

droplets of the hydrophobic IL solvent that can be easily separated from the aqueous solution. This technique has been applied towards the analysis of many analytes from a variety of samples and has been recently reviewed [29]. Most analyses have been carried out using HPLC due to the fact that direct GC analysis can cause accumulation of the nonvolatile IL in the GC inlet. This has limited the use of IL-based *in situ* DLLME in the analysis of volatile and semi-volatile compounds.

Headspace sampling is an ideal technique for analyzing volatile and semi-volatile analytes from a non-volatile sample matrix [30-32]. This approach minimizes the amount of non-volatile matrix components introduced in the GC and results in lower background interference and better sensitivity. ILs have been employed as a new class of diluents in headspace gas chromatography (HS-GC) analysis [33-36]. Due to their high thermal stability and low volatility, the HS oven can be operated at high temperatures, thereby broadening the application of HS-GC.

In order to address the aforementioned limitations of the conventional DLLME method and develop a method that is fast and can be readily automated, ILs were studied as extraction solvents in *in situ* DLLME to provide preconcentration of PCBs and acrylamide from complex food samples followed by analysis of the IL-based extraction solvent by HS-GC. Five halide-based ILs containing varied cation moieties (i.e., long alkyl side chains, aromatic and hydroxyl groups) were prepared to evaluate the effect of different structural features on the extraction efficiency of the target analytes. Extraction parameters including the molar ratio of IL to metathesis reagent and mass of IL employed in the extraction were optimized. The effects of HS oven temperature and the HS sample vial volume on the analyte response were also evaluated. The matrix-compatibility of the developed method was also studied by quantifying acrylamide in brewed coffee samples. This method is much simpler and faster compared to the previously reported SPME GC-MS method [14] and has

tremendous potential to be applied for the routine analysis of contaminants present in complex food samples.

## 5.2 Experimental

### 5.2.1 Materials

The reagents 1-methylimidazole (99%), 1-benzylimidazole (99%), 1-bromobutane (99%), 2-bromoethanol (95%), 1-bromooctane (99%), 6-chlorohexanol (96%), acrylamide (99.9%), ninhydrin, ethanol (99.9%), and centrifuge tubes (natural polypropylene conical, 5 mL) were purchased from Sigma Aldrich (St. Louis, MO, USA). Acetone (99.5%), isopropanol (99.5%), ethyl acetate (99.9%), and glass beads (Walter Stern economical solid glass beads, 3 mm diameter) were purchased from Fisher Scientific (Fair Lawn, NJ, USA). Lithium bis[(trifluoromethyl)sulfonyl]imide ( $\text{LiNTf}_2$ ) was purchased from SynQuest Labs, Inc. (Alachua, FL, USA). The PCB mixture containing  $100 \mu\text{g mL}^{-1}$  of 21 different congeners in acetone was purchased from Accustandard (New Haven, CT, USA). The names and structures for each of the PCBs are listed in Table S1 (Supplementary information). Ultrapure water ( $18.2 \text{ M}\Omega \text{ cm}$ ) was obtained from a Milli-Q water purification system (Bedford, MA, USA). Headspace vials (10 mL) were purchased from Agilent (Santa Clara, CA, USA). Fat free, low fat, and reduced fat milk samples and a commercial blend of dark roasted coffee beans were purchased from a local market (Ames, IA, USA). The coffee beans were ground with a commercial coffee grinder before being subjected to brewing.

### 5.2.2 Synthesis of ILs

Chemical structures of the ILs employed in this study are shown in Figure 1. All ILs were synthesized according to previously published methods [18, 28, 37] and were fully

characterized by  $^1\text{H}$  NMR (see Figure S1-S5 supplementary information).  $^1\text{H}$  NMR spectra were collected in deuterated dimethyl sulfoxide or chloroform using a Bruker DRX 500 MHz nuclear magnetic resonance (NMR) spectrometer (Billerica, MA, USA).

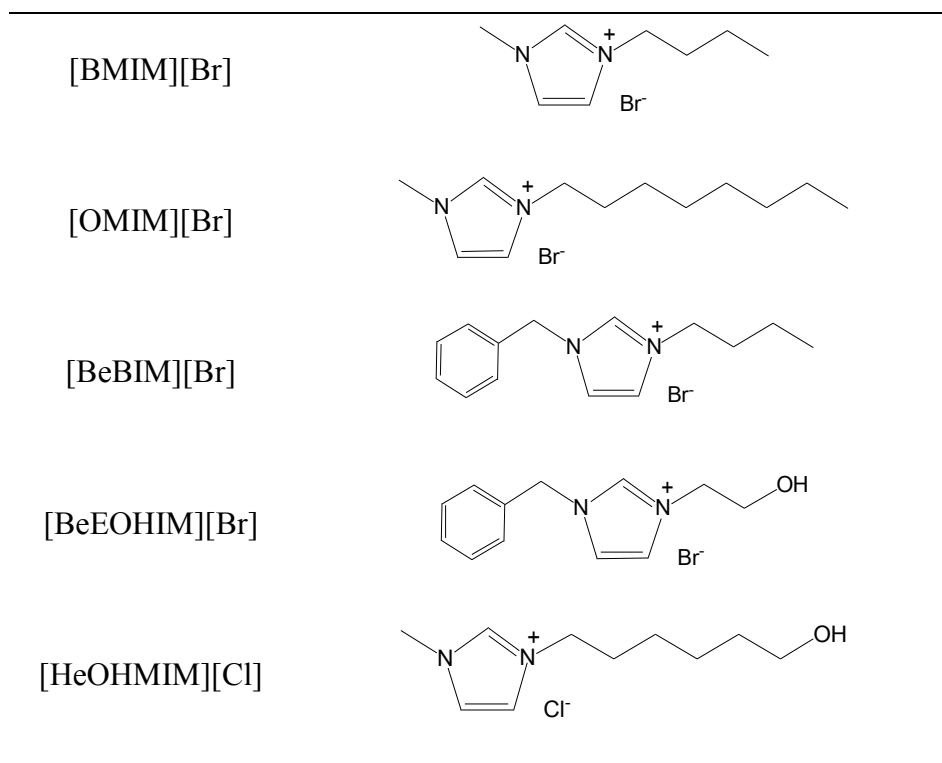


**Figure 1.** Chemical structures and abbreviations of the ILs employed in this study.

### 5.2.3 Instrumentation

An Agilent 7890B gas chromatograph (Santa Clara, CA, USA) equipped with an Agilent 7697A headspace sampler, electron capture detector as well as a 5977A mass spectrometer (MS) was employed in this study. For the analysis of 21 PCB congeners, the HS oven was operated at an optimal sampling temperature of 250 °C, which was determined through optimization. The sample loop and transfer line was operated at 10 °C and 20 °C higher, respectively, than the HS oven temperature. The equilibration time was 10 min. The GC injector was maintained at 280 °C with a 5:1 split ratio. The separation of 21 PCB congeners was achieved using a HP-5MS UI capillary column (30 m × 250 μm I.D.,  $d_f$  = 0.25 μm) obtained from Agilent Technologies (Santa Clara, CA, USA). Helium was used

as the carrier gas at constant flow of 1 mL min<sup>-1</sup>. The temperature program used for GC-ECD was as follows: initial temperature was set at 130 °C and held for 2 min, followed by a ramp from 130 °C to 240 °C at 5 °C min<sup>-1</sup> and held for 5 min. The temperature was then increased to 320 °C at 20 °C min<sup>-1</sup> and held for 5 min. The temperature for the ECD was set at 300 °C and the argon/methane make-up flow was maintained at 30 mL min<sup>-1</sup>.

For the analysis of aqueous acrylamide solution and brewed coffee spiked with acrylamide, the HS oven was operated at 205 °C. The sample loop and transfer line was operated at 215 °C and 225 °C, respectively. The equilibration time was 10 min. The GC injector was maintained at 250 °C with a 5:1 split ratio. The separation and quantification of acrylamide by GC-MS was achieved using a Mega-FFAP-EXT column (50 m × 200 µm I.D., d<sub>f</sub> = 0.20 µm) (Legnano, MI, Italy). Helium was used as the carrier gas at constant flow of 1 mL min<sup>-1</sup>. The temperature program used was as follows: initial temperature was set at 50 °C and held for 1 min, followed by a ramp of 2 °C min<sup>-1</sup> to 165 °C and then increased to 250 °C at 7.5 °C min<sup>-1</sup> and held for 2 min. The MS was operated in electron ionization mode (EI) at 70 eV. Data were initially acquired in SCAN mode to determine the retention time of acrylamide. Subsequently, single ion monitoring (SIM) acquisition mode was used for the detection/quantitation of acrylamide (target ion: 71 *m/z*, qualifier ion: 55 *m/z*).

#### 5.2.4 DLLME procedure for aqueous samples and food samples

To compare different incubation temperatures on the response of PCBs, 4.5 mL of ultrapure water containing 10 µg L<sup>-1</sup> of each PCB congener was added to a 5 mL conical centrifuge tube. After gentle shaking, an aqueous solution containing 120 mg of [BMIM][Br] was added into the solution. The IL was completely dissolved into the sample solution by vortexing for 30 s. An aqueous solution of LiNTf<sub>2</sub> (0.2 g mL<sup>-1</sup>) was then added

to achieve an IL to LiNTf<sub>2</sub> molar ratio of 1:1. The sample solution immediately became cloudy due to the metathesis reaction and the formation of hydrophobic [BMIM][NTf<sub>2</sub>] IL. The tube was then vortexed for 30 s and centrifuged for 5 min at 4500 rpm. Approximately 100  $\mu$ L of the hydrophobic IL containing preconcentrated PCBs was formed at the bottom of the centrifuge tube. A 20  $\mu$ L aliquot of [BMIM][NTf<sub>2</sub>] IL was then withdrawn via micropipette and evenly transferred to four 10 mL headspace vials for HS-GC analysis at different incubation temperatures (i.e., 220 °C, 240 °C, 250 °C, and 260 °C).

For the comparison of extraction efficiencies using different ILs, a 5 mL conical centrifuge tube was filled with 4.5 mL of the PCB working solution at a concentration of 10  $\mu$ g L<sup>-1</sup>. After gentle shaking, an aqueous solution containing a specific amount of halide-based IL was added into the solution (see Table D2, Appendix D). To ensure a fair comparison, the amount of each IL was calculated to yield 80 mg of the NTf<sub>2</sub><sup>-</sup>-based IL after the metathesis reaction. The IL was completely dissolved into the sample solution by vortexing for 30 s. An aqueous solution of LiNTf<sub>2</sub> (0.2 g mL<sup>-1</sup>) was then added to achieve an IL to LiNTf<sub>2</sub> molar ratio of 1:1 or 1:1.5. The centrifuge tube was then vortexed for 30 s and centrifuged for 5 min at 4500 rpm. A 20  $\mu$ L (12  $\mu$ L for [BeEOHIM][NTf<sub>2</sub>] IL) aliquot of the hydrophobic IL solvent was then withdrawn via micropipette and transferred to a 10 mL headspace vial for HS-GC analysis.

To prepare milk samples for analysis, the bovine milk sample was diluted with ultrapure water at a 1:1 v/v ratio. The *in situ* DLLME procedure shown in Figure 2 was applied to extract PCBs from the milk samples. After centrifugation, a very viscous sedimented IL solvent containing a white precipitate from the milk sample was formed on the bottom of the centrifuge tube. A 20  $\mu$ L aliquot of the hydrophobic IL solvent was then withdrawn via micropipette and transferred to a 10 mL headspace vial for HS-GC analysis.



An improved *in situ* DLLME approach employing a washing step was also designed for the extraction of PCBs from milk samples. As shown in Figure 2, after centrifugation and removal of the upper aqueous layer, 0.4 mL of ultrapure water was added to the sedimented IL layer. The mixture was then vortexed for 30 s and centrifuged for 5 min at 4500 rpm. A phase separation between the white precipitate and hydrophobic IL was immediately observed. All of the IL solvent was then withdrawn via micropipette and transferred to a 10 mL headspace vial for HS-GC analysis.

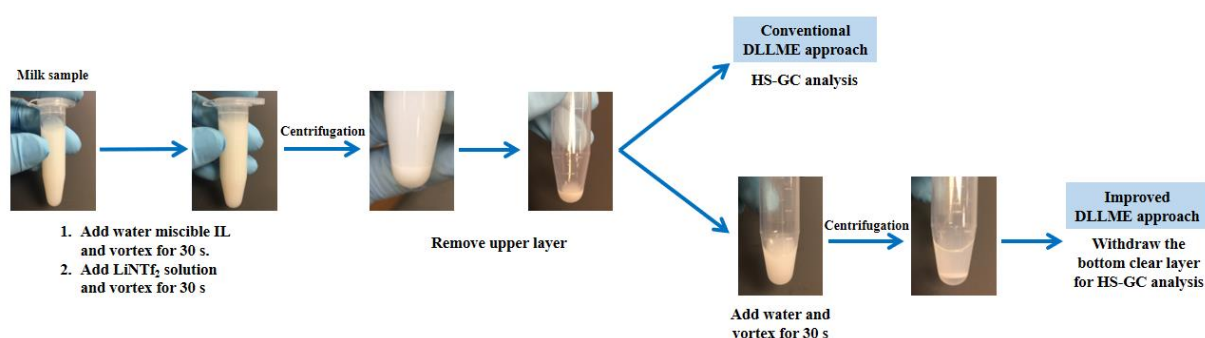


**Figure 2.** Schematic diagram demonstrating the IL-based *in situ* DLLME applied in this study for the extraction of PCBs from milk.

The *in situ* DLLME approach was also applied to extract acrylamide from ultrapure water and brewed coffee. A 2 mL solution containing 1 mg L<sup>-1</sup> of acrylamide was sampled using the previously employed conventional *in situ* DLLME method. The amounts of halide-based IL and LiNTf<sub>2</sub> used are listed in Table D3 (Appendix D). Brewed coffee samples were prepared using a household American coffee maker from 35 g of ground coffee extracted with 600 mL of tap water. As mentioned previously, interfering acrylamide can be produced at high temperature (220 °C) from free asparagine and glucose extracted from the brewed coffee [13, 14]. A quenching reaction using ninhydrin was therefore applied to inhibit this reaction. Before analysis, a 19 mL aliquot of the brewed coffee was mixed with 1 mL of 2% (w/v) ethanolic ninhydrin solution and heated on a hot plate at 80 °C (with constant agitation at 1500 rpm) for 10 min [13, 14]. *In situ* DLLME sampling was

performed immediately after the reaction. A sample volume of 2 mL was selected for brewed coffee and the amount of IL-based extraction solvent and ion-exchange reagent used in this approach is listed in Table D3 (Appendix D).

### 5.3 Results and Discussion

#### 5.3.1 Structural design of ILs as solvents for *in situ* DLLME coupled to HS-GC analysis

Five imidazolium-based ILs with varied functional groups were prepared in this study to examine their selectivity towards PCBs and acrylamide. The [BMIM][Br] IL has been previously reported as an extraction solvent in *in situ* DLLME and was employed as a reference IL in this study [28, 37]. In an effort to further increase the hydrophobicity of the sedimented IL, an IL containing an octyl side chain was prepared ([OMIM][Br]). It has been previously reported that incorporation of aromatic moieties to the imidazolium-based polymeric ionic liquids (PILs) can enhance the extraction efficiency of PCBs [12]. In order to further study this effect, the [BeBIM][Br] and [BeEOHIM][Br] ILs were synthesized. The [BeEOHIM][Br] and [HeOHMIM][Cl] ILs were also synthesized to examine the effect of aromatic and hydroxyl groups on the extraction efficiency of acrylamide.

#### 5.3.2 Applying ILs as solvent for HS-GC analysis after *in situ* DLLME sampling

The main aim of this work is to utilize ILs as the extraction solvent in *in situ* DLLME to provide preconcentration of the analytes and exploit the non-volatile nature of the ILs in direct HS-GC analysis. In order to promote the partitioning of the analytes to the headspace, the ILs must be exposed to high HS oven temperatures without significantly increasing the chromatographic background. After the *in situ* metathesis reaction, the thermal stability of the four ILs (i.e., [BMIM][NTf<sub>2</sub>], [OMIM][NTf<sub>2</sub>], [BeBIM][NTf<sub>2</sub>], and [BeEOHIM][NTf<sub>2</sub>]) employed for PCB analysis was screened. Figure 3 shows the HS-GC-ECD chromatograms

generated for all four ILs at an incubation temperature of 250 °C. The [BMIM][NTf<sub>2</sub>] IL exhibited significantly lower background compared to the other ILs containing varied cationic moieties. Even though the other three ILs exhibited some impurity peaks in their background, no significant overlay of these peaks with the PCB peaks was observed (see Figure 3).

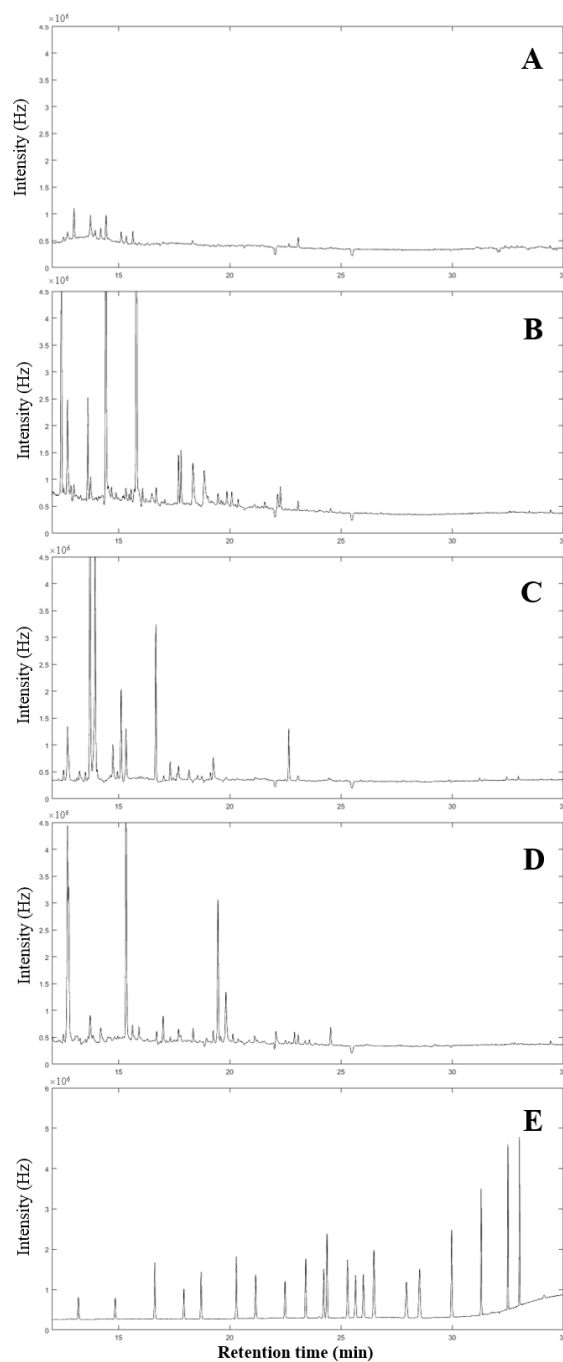


**Figure 3.** HS-GC-ECD chromatograms for ILs incubated at 250 °C for 10 min. (A) [BMIM][NTf<sub>2</sub>], (B) [OMIM][NTf<sub>2</sub>], (C) [BeBIM][NTf<sub>2</sub>], (D) [BeEOHIM][NTf<sub>2</sub>], and (E) direct injection of 21 PCBs

The thermal stability of the [HeOHMIM][NTf<sub>2</sub>] IL employed for acrylamide analysis was also examined. Due to the physico-chemical properties of acrylamide, an incubation temperature of 205 °C was applied. Enlarged HS-GC-MS chromatograms of [HeOHMIM][NTf<sub>2</sub>] are shown in Figure D6 (Appendix D). By comparing the chromatograms of the [HeOHMIM][NTf<sub>2</sub>] IL with and without sampling of acrylamide, no background interference with the acrylamide peak was observed. The aforementioned results confirm that the high thermal stability and low vapor pressure of the NTf<sub>2</sub><sup>-</sup>-based ILs make them appropriate solvents for the HS-GC analysis of PCBs and acrylamide after *in situ* DLLME sampling.

### 5.3.3 Effect of incubation temperature on the response of the analytes

In HS-GC analysis, the incubation temperature of the HS oven plays a vital role in the response of the analytes. Theoretically, decreasing the incubation temperature can decrease the chromatographic background and potentially increase the response for highly volatile analytes. However, lowering the incubation temperature can also vary the partition coefficient of the analytes and decrease the concentration of volatile analytes in the headspace. The effect of incubation temperature with respect to the response of 21 PCBs was evaluated by incubating 20 µL of [BMIM][NTf<sub>2</sub>] IL after the extraction of PCBs at varied HS oven temperatures for 10 min. As shown in Figure 4, all PCBs show relatively low response at 220 °C. This is especially noticeable for the late eluting PCBs (i.e., PCB 170, 195, 206, and 209), which possess higher boiling points. When the HS oven temperature was increased to 240 °C, the response of all PCBs was dramatically increased. Interestingly, an analyte dependent variation in response was observed when the HS oven was increased from 240 °C to 260 °C. For early eluting PCBs (i.e., PCB 8, 18, 28, and 52), a slight decrease in response was observed when the HS oven temperature was increased

from 240 °C to 260 °C. However, for PCBs that possess higher boiling points, the highest response was observed at 250 °C. This observation is in good agreement with previously reported results and can be attributed to the shifting in the equilibrium concentrations of the analytes between the headspace and IL solvent at elevated temperatures [33]. Based on this result, 250 °C was selected as the optimized incubation temperature for all subsequent PCB analyses.

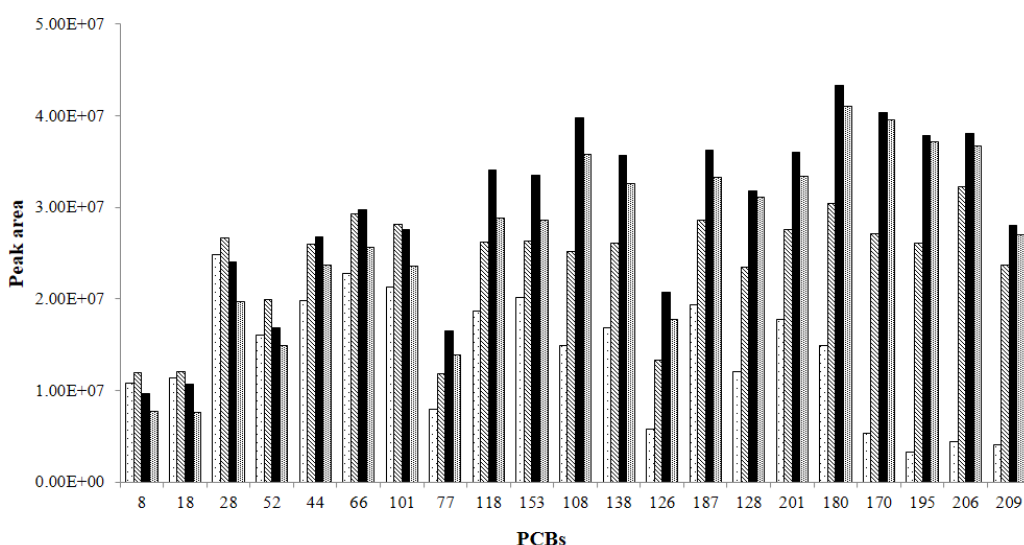


**Figure 4.** Incubation temperature effects on the response of PCBs in the [BMIM][NTf<sub>2</sub>] IL. (·) 220 °C, (▨) 240 °C, (■) 250 °C, (▩) 260 °C. See Table D1, Appendix D for list of all PCB structures and corresponding numbers of PCBs. The equilibration time was 10 min.

The effect of incubation temperature on the response of acrylamide was also evaluated at 185 °C, 205 °C, and 225 °C. As shown in Figure D7 (Appendix D), a HS oven temperature of 205 °C exhibited slightly higher response compared to 185 °C and 225 °C. Based on this result, an optimized incubation temperature of 205 °C was selected for subsequent acrylamide analyses.

#### 5.3.4 Comparison of extraction efficiencies using different ILs

The extraction efficiency of PCBs in ultrapure water using the [BMIM][Br], [OMIM][Br], [BeEOHIM][Br], and [BeBIM][Br] ILs was compared. To ensure a fair comparison, the

amounts of each IL applied was calculated to yield 80 mg of the  $\text{NTf}_2^-$ -based IL after the metathesis reaction. After centrifugation, a 20  $\mu\text{L}$  aliquot of the hydrophobic IL was withdrawn for HS-GC analysis. However, due to the high solubility of the  $[\text{BeEOHIM}][\text{NTf}_2]$  IL in water, only 12  $\mu\text{L}$  of the sedimented IL could be collected. As shown in Figure 5, even though a lower amount of the sedimented IL could be recovered

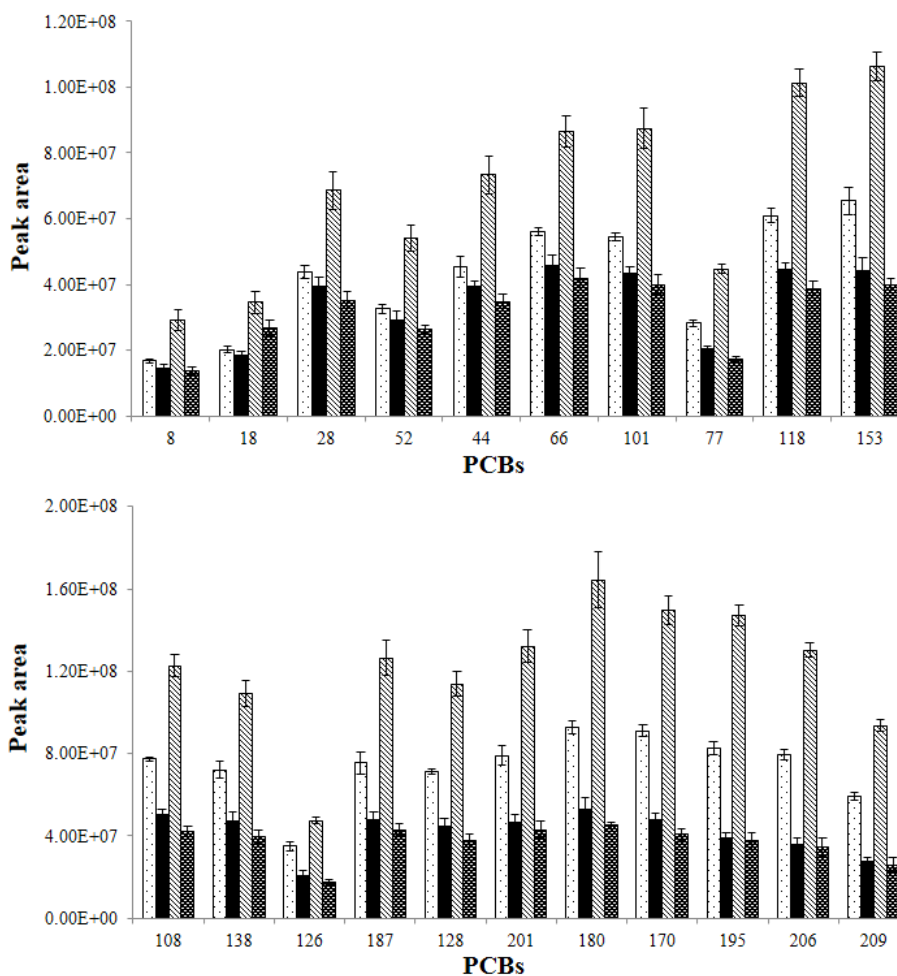


**Figure 5.** Extraction comparison for 21 PCBs extracted from ultrapure water using different ILs: (○)  $[\text{BMIM}][\text{Br}]$ , (■)  $[\text{OMIM}][\text{Br}]$ , (▨)  $[\text{BeEOHIM}][\text{Br}]$ , (▤)  $[\text{BeBIM}][\text{Br}]$ . See Table S1 for list of all PCB structures and corresponding numbers of PCBs. IL: $\text{LiNTf}_2$  = 1:1. Concentration of analytes: 10  $\mu\text{g L}^{-1}$ . HS oven was operated at 250  $^{\circ}\text{C}$  and the equilibration time was 10 min.

when applying the  $[\text{BeEOHIM}][\text{Br}]$  IL as extraction solvent, it still exhibited higher extraction efficiencies for all PCBs compared to the other ILs. The  $[\text{BMIM}][\text{Br}]$  IL also exhibited good extraction efficiencies for most PCBs, especially for the less volatile ones. The  $[\text{OMIM}][\text{Br}]$  and  $[\text{BeBIM}][\text{Br}]$  ILs were observed to produce lower extraction

efficiencies for all PCBs. Based on these results, [BeEOHIM][Br] was selected as the optimal IL for all subsequent studies.

Three ILs containing aromatic and/or hydroxyl moieties (i.e., [BeBIM][Br], [BeEOHIM][Br], and [HeOHMIM][Cl]) were employed for the extraction of acrylamide from ultrapure water. As shown in Figure 6, the [HeOHMIM][Cl] IL exhibited significantly higher extraction efficiency compared to the [BeBIM][Br] and [BeEOHIM][Br] ILs. Based on this result, [HeOHMIM][Cl] was selected as the optimal IL for all subsequent acrylamide analyses.

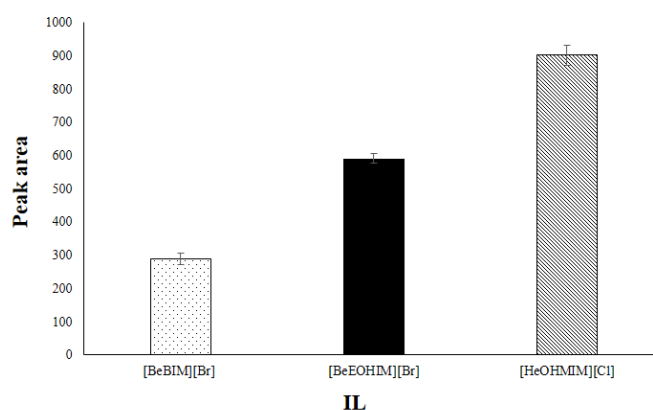


**Figure 6.** Comparison of extraction efficiency of acrylamide from ultrapure water using different ILs: (◻) [BeBIM][Br], (■) [BeEOHIM][Br], and (▨) [HeOHMIM][Cl]. IL:LiNTf<sub>2</sub> = 1:1. Concentration of analyte: 1 mg L<sup>-1</sup>. HS oven was operated at 205 °C and the equilibration time was 10 min.

### 5.3.5 Optimization of extraction parameters

The ILs that exhibited superior extraction efficiency for PCBs and acrylamide were applied for the optimization of extraction parameters. Several important extraction parameters for *in situ* DLLME including the amounts of ion-exchange reagent and IL mass were optimized. The effect of each extraction parameter on the extraction efficiency was evaluated based on the peak areas of the analytes obtained using the applied method. The conditions that generated the highest peak areas were adopted for subsequent experiments.

### 5.3.5.1 Effect of the molar ratio of IL to metathesis reagent on extraction efficiency of analytes

Two different molar ratios of IL to  $\text{LiNTf}_2$  metathesis reagent (i.e., 1:1 and 1:1.5) were examined to explore the effect of the amount of ion-exchange reagent on the extraction efficiency of the target analytes. As shown in Figure 7 for the extraction of PCBs from ultrapure water, a 1:1 molar ratio of  $[\text{BeEOHIM}][\text{Br}]:\text{LiNTf}_2$  exhibited significantly higher extraction efficiency compared to the extraction employing a molar ratio of 1:1.5. The same trend was also observed for the extraction of acrylamide using the  $[\text{HeOHMIM}][\text{Cl}]$  IL as extraction solvent (see Figure D8, Appendix D). This is in good agreement with previously reported results [28, 37]. A possible reason for this result could be that the additional ion-exchange reagent can increase the ionic strength of the sample matrix and affect the partitioning of the analytes into the IL solvent [28, 37]. Due to the better extraction performance that was obtained using a lower molar ratio of metathesis reagent, a IL: $\text{LiNTf}_2$  molar ratio of 1:1 was employed for all subsequent studies.

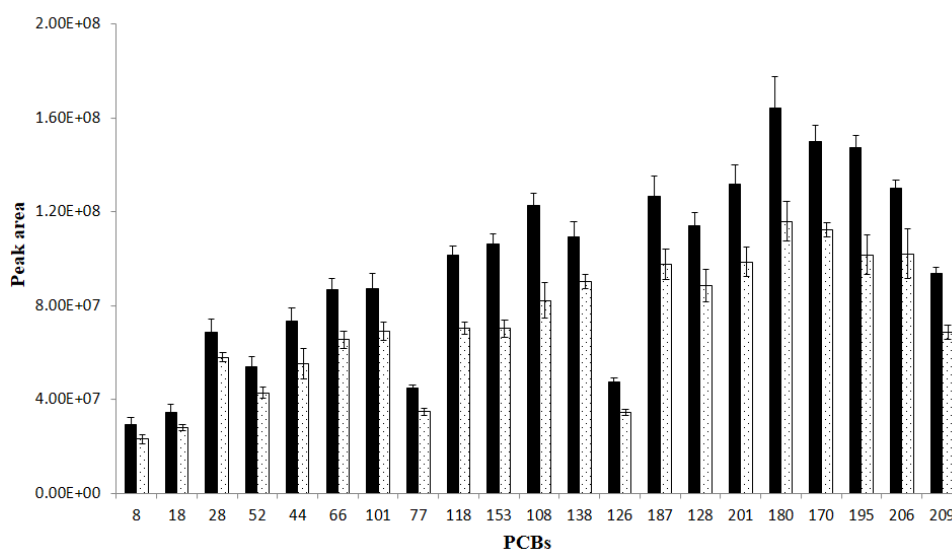


**Figure 7.** Effect of molar ratio of the  $[\text{BeEOHIM}][\text{Br}]$  IL and  $\text{LiNTf}_2$  on the extraction efficiency of PCBs. (■)  $[\text{BeEOHIM}][\text{Br}]:\text{LiNTf}_2=1:1$ , (◑)  $[\text{BeEOHIM}][\text{Br}]:\text{LiNTf}_2=1:1.5$ . See Table S1 for list of all PCB structures and corresponding numbers of PCBs. Concentration of analytes:  $10 \mu\text{g L}^{-1}$ . HS oven was operated at  $250^\circ\text{C}$  and the equilibration time was 10 min.



### 5.3.5.2 Effect of IL mass on extraction efficiency of analytes

The quantity of [BeEOHIM][Br] used as extraction solvent was varied to examine its effect on the extraction efficiency of PCBs. Three different quantities of [BeEOHIM][Br] IL, namely, 46 mg, 53 mg, and 60 mg, were tested to yield 12  $\mu\text{L}$ , 20  $\mu\text{L}$ , and 24  $\mu\text{L}$  of sedimented ILs, respectively. In order to maximize the sensitivity of the method, all sedimented ILs were collected after *in situ* DLLME sampling. As shown in Figure 5, higher peak areas for all PCBs were observed when the IL mass was increased from 46 mg to 53 mg. It was previously reported that higher enrichment factors for analytes could be obtained using a smaller volume of sedimented IL in *in situ* DLLME [37-39]. However, due to the significantly increased volume of sedimented IL (20  $\mu\text{L}$  versus 12  $\mu\text{L}$ ), higher amounts of PCBs could be extracted using 53 mg of [BeEOHIM][Br] IL. As shown in Figure 8, an interesting trend was observed when the amount of [BeEOHIM][Br] IL was increased from

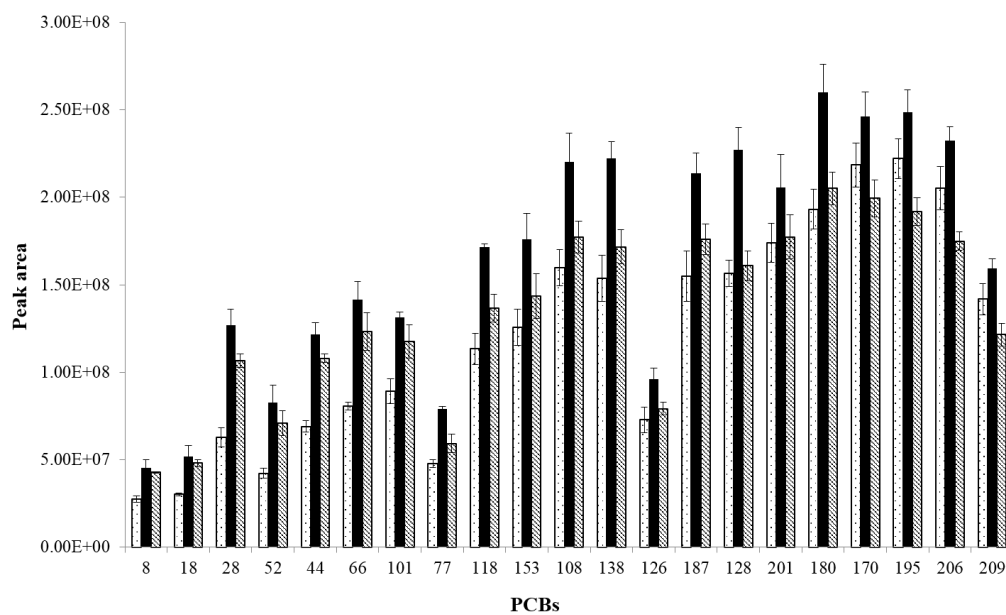


**Figure 8.** Effect of IL quantity on extraction efficiency of PCBs. (○) 46 mg, (■) 53 mg, (▨) 60 mg. Concentration of analytes:  $10 \mu\text{g L}^{-1}$ . All the sedimented ILs were collected for HS-GC analysis. Effect of IL mass on the extraction efficiency of PCBs. (○) 46 mg, (■) 53 mg, (▨) 60 mg. See Table S1 for list of all PCB structures and corresponding numbers of PCBs. Concentration of analytes:  $10 \mu\text{g L}^{-1}$ . All sedimented ILs were collected for HS-GC analysis. HS oven was operated at  $250^\circ\text{C}$  and the equilibration time was 10 min. interesting trend was observed when the amount of [BeEOHIM][Br] IL was increased from

53 mg to 60 mg. Peak areas were slightly decreased for all PCBs, indicating that the increased volume of sedimented IL (24  $\mu$ L versus 20  $\mu$ L) could not compensate for the loss of enrichment. Based on this result, an IL quantity of 53 mg was employed for subsequent PCB analyses.

The effect of [HeOHMIM][Cl] IL mass on the extraction efficiency of acrylamide was also examined. As shown in Figure D9 (Appendix D), the extraction efficiency of acrylamide increased when the mass of IL was increased from 38 mg to 57 mg. However, when the mass of IL was increased from 57 mg to 76 mg, a slight decrease in extraction efficiency of acrylamide was observed. Based on this result, an IL mass of 57 mg was employed as the optimum condition for subsequent acrylamide analyses.

#### 5.3.6 Effect of the headspace volume on the response of analytes

After *in situ* DLLME sampling, the IL containing the target analytes must be incubated at high HS oven temperature to permit the desorption of analytes to the headspace for subsequent GC separation and quantification. As discussed previously, the incubation temperature was optimized to increase the response of the analytes. Another important parameter that can determine the final concentration of the analytes in the HS is the phase ratio ( $\beta$ ) within the HS system (see Eq. 1). According to Eq. 1,  $V_g$  is the volume of gas

$$\beta = V_g/V_s \quad (1)$$

phase (headspace) and  $V_s$  is the volume of the sample phase (IL solvent). It has been reported previously that lower values of  $\beta$  will increase the concentration of volatile analytes in headspace and yield higher response [40]. In order to decrease  $\beta$ , two approaches can be applied, namely, an increase in sample volume and/or a decrease in headspace volume. An increase in the volume of the IL solvent ( $V_s$ ) did not yield a significant increase in the response of the PCBs (see Section 3.4.2). Moreover, this also increases the amount

of IL consumed and increases the cost of the analysis. Another approach is to decrease the headspace volume in the sample vial ( $V_g$ ). As shown in Figure 9, in order to make the HS vial compatible with the HS autosampler, 12.5 g of glass beads (3 mm diameter) and a glass vial with a flat bottom were transferred into a 10 mL HS vial (the smallest commercially available vials that are compatible with the Agilent HS sampler), resulting in a HS vial containing a headspace volume of 4.2 mL. As shown in Figure 10, a comparison of the PCB response from the HS vials with and without the addition of glass beads showed that for the early eluting PCBs (i.e., PCB 8, 18, 28, 52, 44, 66, and 101), approximately 20-40% higher responses were observed when using the vials with smaller HS volume. It should be noted that most of the background interference in the GC chromatogram appear before 20 min (see Figure 3). The increased response for early eluting PCBs could potentially increase the sensitivity of the HS-GC method. Only a few late eluting PCBs exhibited less than 10% loss in peak area, which could be due to adsorption of the analytes on the surface of the glass beads.

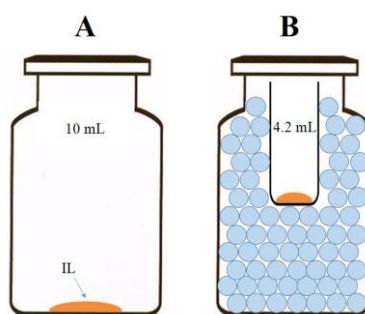


**Figure 9.** HS vials applied in this study with varied headspace volumes. (A) HS vial containing 10 mL of headspace volume. (B) After the addition of glass beads and glass vial, the headspace volume of the HS vial was decreased to 4.2 mL. Note: the 10 mL headspace vials are the smallest commercially available vials that are compatible with the Agilent 7697A headspace sampler.

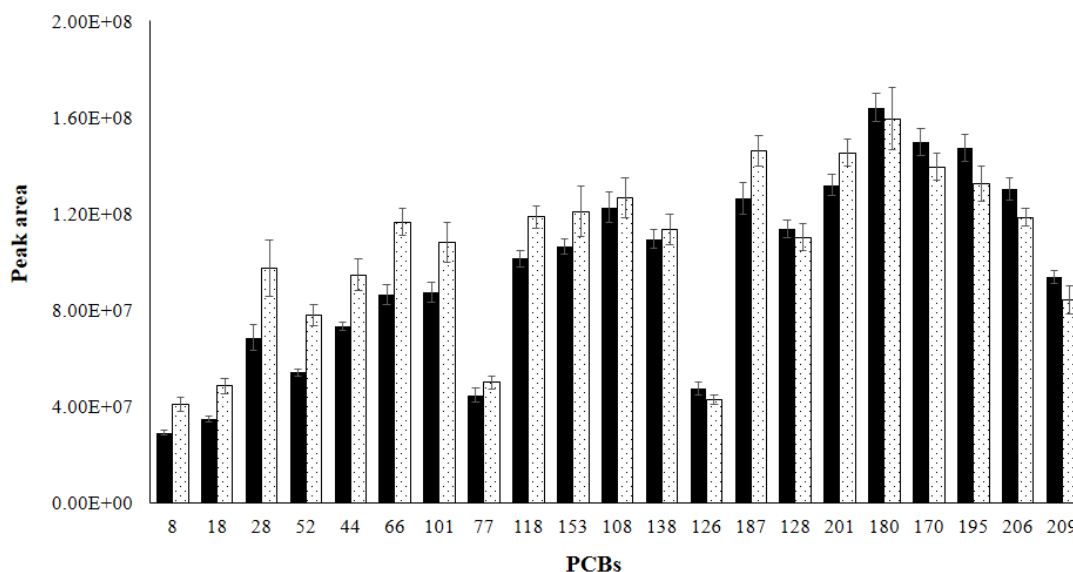


**Figure 10.** Effect of headspace volume on the response of PCBs. (■) headspace vial containing 10 mL of headspace volume. (▨) modified headspace vial possessing a headspace volume of 4.2 mL. See Table S1 for list of all PCB structures and corresponding numbers of PCBs. Concentration of analytes:  $10 \mu\text{g L}^{-1}$ . HS oven was operated at  $250^\circ\text{C}$  and the equilibration time was 10 min.

The same approach was also applied for the HS-GC analysis of acrylamide using the [HeOHMIM][NTf<sub>2</sub>] IL. As shown in Figure D10 (Appendix D), more than a 50 % increase in the peak area was observed when using the modified HS vials. Based on this result, a HS vial containing a headspace volume of 4.2 mL was employed for subsequent analyses.

### 5.3.7 Analytical performance of selected ILs for the extraction of PCBs and acrylamide from water and food samples

The analytical performance of the [BeEOHIM][Br] IL was evaluated by sampling aqueous solutions spiked with PCBs at different concentration levels. Table 1 shows the figures of merit based on a six-point calibration curve where the PCBs exhibited slightly different linear ranges. Good linearity with correlation coefficients ( $R^2$ ) varying from 0.995 to 0.999 was obtained. The LODs were determined by decreasing the analyte concentration until a 3:1 signal:noise (S/N) ratio was achieved. The LODs for the PCBs varied from

**Table 1** Figures of merit for *in situ* IL-based DLLME analysis of 21 PCBs in ultrapure water using the [BeEOHIM][Br] IL.

PCBs	Linear range (ng L <sup>-1</sup> )	Slope $\pm$ error	LOD (ng L <sup>-1</sup> )	Linearity (R <sup>2</sup> )	%RSD (n=3)	
					100 ng L <sup>-1</sup>	1000 ng L <sup>-1</sup>
8	25-5000	6067 $\pm$ 302	10	0.998	11.0	4.7
18	50-5000	7043 $\pm$ 333	10	0.999	4.4	8.4
28	25-5000	14847 $\pm$ 563	10	0.999	10.4	4.3
52	25-5000	10192 $\pm$ 509	10	0.998	9.6	5.4
44	25-5000	14382 $\pm$ 653	10	0.998	4.6	7.7
66	50-5000	13369 $\pm$ 584	10	0.998	4.4	6.7
101	25-5000	15035 $\pm$ 599	10	0.999	4.8	5.5
77	50-5000	6207 $\pm$ 352	10	0.996	5.6	8.1
118	50-5000	14183 $\pm$ 853	10	0.996	3.9	8.2
153	50-5000	15870 $\pm$ 847	10	0.997	10.2	8.2
108	25-5000	16502 $\pm$ 715	10	0.995	4.3	7.8
138	10-5000	16346 $\pm$ 617	2.5	0.997	10.1	8.4
126	50-5000	6068 $\pm$ 296	10	0.997	8.3	6.0
187	10-5000	19162 $\pm$ 327	2.5	0.999	8.1	5.9
128	10-5000	12867 $\pm$ 430	2.5	0.997	10.5	9.2
201	10-5000	19431 $\pm$ 820	5	0.998	9.6	15.0
180	10-5000	20157 $\pm$ 888	5	0.998	12.1	8.8
170	10-5000	17660 $\pm$ 765	5	0.998	5.3	10.1
195	10-5000	16163 $\pm$ 348	2.5	0.999	13.8	6.3
206	10-5000	14547 $\pm$ 329	2.5	0.999	10.8	4.4
209	10-5000	10644 $\pm$ 566	2.5	0.999	11.2	9.3

2.5 to 10 ng L<sup>-1</sup>. The precision of the developed method was studied at 100 ng L<sup>-1</sup> and 1000 ng L<sup>-1</sup>. The relative standard deviation (%RSD) values ranged from 3.9% to 13.8% at 100 ng L<sup>-1</sup> and from 4.3% to 15.0% at 1000 ng L<sup>-1</sup>.

To demonstrate the applicability of the proposed method, the IL-based *in situ* DLLME method was employed for the extraction of PCBs from milk samples. Milk is a very complex sample matrix containing proteins, carbohydrates, and lipids [41]. All of these components can severely interfere with the IL solvent and affect the extraction of PCBs. Following *in situ* DLLME sampling of fat free milk spiked with 10  $\mu$ g L<sup>-1</sup> of PCBs, a very

viscous mixture containing sedimented IL and precipitate from the milk sample was observed on the bottom of the centrifuge tube (see Figure 2). It has been reported previously that the [BMIM][Cl] IL exhibited good extraction efficiency for proteins from complex samples [42]. In the *in situ* DLLME sampling process, the proteins may preconcentrate in

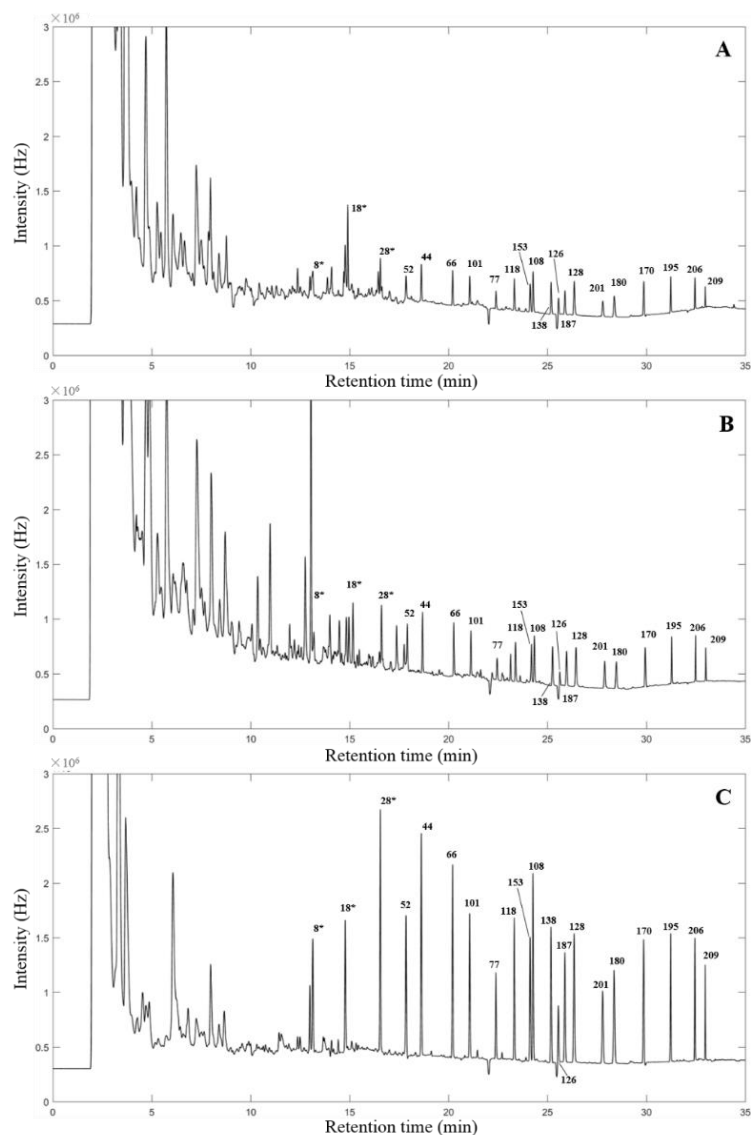


**Figure 11.** Chromatograms for HS-GC analysis of PCBs from milk. The conventional *in situ* DLLME approach was employed for the extraction of PCBs from milk. (A) The [BeEOHIM][Br] IL was employed as extraction solvent. (B) The [BMIM][Br] IL was employed as extraction solvent. (C) An improved approach using a washing step was applied to decrease the matrix effect with the [BMIM][Br] IL as extraction solvent. See Table S1 for list of all PCB structures and corresponding numbers of PCBs. Concentration of analytes:  $10 \mu\text{g L}^{-1}$ . HS oven was operated at  $250^\circ\text{C}$  and the equilibration time was 10 min.

the halide-based IL solvent and subsequently precipitate out after the *in situ* metathesis reaction. Due to its high viscosity, it was difficult to recover all of the sedimented IL solvent from the centrifuge tube. The collected sedimented IL solvent was subjected to HS-GC analysis and, as shown in Figure 11A, very low response of the PCBs was observed. Moreover, the background in the chromatogram was significantly higher compared to the pure [BeEOHIM][NTf<sub>2</sub>] IL (see Figure 3D, Appendix D), which makes peak identification and integration very challenging. The *in situ* DLLME analysis using other ILs was also tested and as shown in Figure 11B the [BMIM][Br] IL exhibited higher extraction efficiency for all PCBs compared to the [BeEOHIM][NTf<sub>2</sub>] IL. In an effort to decrease the matrix interference and increase the response of the PCBs, an improved approach was designed. As shown in Figure 2, a washing step was applied after the conventional DLLME approach to purify the sedimented IL solvent. After centrifugation, a clear layer of the sedimented IL could be collected. As depicted in Figure 11C, the improved approach resulted in a lower background and significantly enhanced the response for all PCBs compared to the DLLME approach without any purification.

Due to the varied water solubility of different ILs, the additional washing step can affect recovery of the sedimented IL. It was observed that when employing [BeEOHIM][Br] IL as the extraction solvent, only 5  $\mu$ L of the sedimented IL could be collected. This result indicates that the [BeEOHIM][Br] may not be the optimal IL for milk samples when employing the improved DLLME approach. The extraction of PCBs from milk samples using different ILs at varied IL:LiNTf<sub>2</sub> molar ratios is shown in Figure 12. Among all tested ILs, the [BMIM][Br] IL exhibited the highest extraction efficiency for all PCBs. A very strong matrix effect was also observed when comparing the extraction efficiency of PCBs for aqueous samples and milk samples. For the extraction of PCBs from ultrapure water, late eluting PCBs (i.e., PCB 180, 170, and 195) exhibited higher response compared to

early eluting PCBs (see Figure 5). However, for the sampling of milk samples, decreased analyte response was observed, especially for the late eluting PCBs.

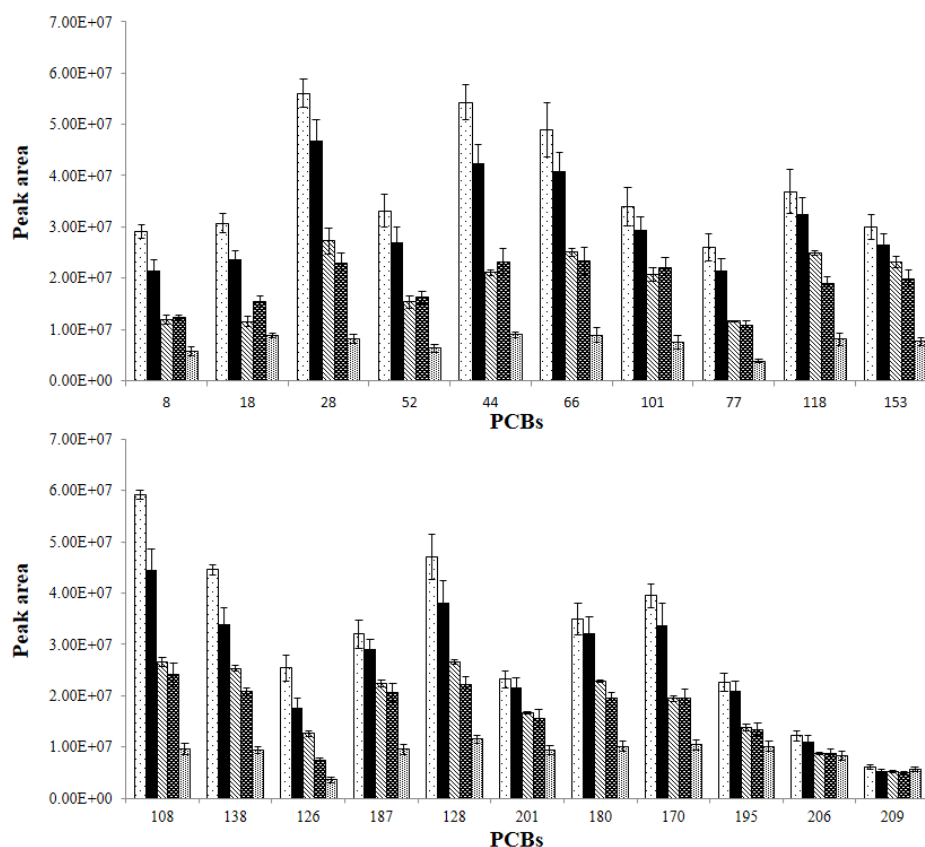


**Figure 12.** Comparison of extraction efficiencies of 21 PCBs from milk sample using different ILs: (□) [BMIM][Br], IL:LiNTf<sub>2</sub> = 1:1, (■) [BMIM][Br], IL:LiNTf<sub>2</sub> = 1:1.5, (▨) [OMIM][Br], IL:LiNTf<sub>2</sub> = 1:1, (▩) [BeOHIM][Br], IL:LiNTf<sub>2</sub> = 1:1. Result obtained by *in situ* DLLME sampling of fat free milk containing 10 µg L<sup>-1</sup> of PCBs. All sedimented ILs were collected for HS-GC analysis. HS oven was operated at 250 °C and the equilibration time was 10 min.

It is well known that due to their hydrophobic nature, PCBs will primarily partition into oil or fat rather than into water [43]. In order to study the effect of fat content on the extraction efficiency of the PCBs, the [BMIM][Br] IL was employed for the extraction of PCBs from milk samples containing varied amounts of fat. As shown in Figure D11 (Appendix D), good extraction efficiency for all PCBs could be obtained for fat free milk samples. However, when performing extractions on low fat and reduced fat milk, a significant decrease in extraction efficiency was observed. This may be due to the



competitive partitioning of the PCBs between the IL solvent and the fat from the milk samples. As a result, fat free milk was selected as the real-world sample to evaluate the analytical performance of [BMIM][Br] IL in the extraction of PCBs. Table 2 shows figures of merit based on a six-point calibration curve where the PCBs exhibited slightly different linear ranges. Good linearity with correlation coefficients ( $R^2$ ) varying from 0.996 to 0.999 was obtained. The LODs for the PCBs varied from 5 to 25 ng L<sup>-1</sup>. The precision of the

**Table 2** Figures of merit for IL-based *in situ* DLLME analysis of 21 PCBs in fat free milk using the [BMIM][Br] IL.

PCBs	Linear range (ng L <sup>-1</sup> )	Slope $\pm$ error	LOD (ng L <sup>-1</sup> )	Linearity ( $R^2$ )	%RSD (n=3)	
					100 ng L <sup>-1</sup>	1000 ng L <sup>-1</sup>
8	25-5000	5291 $\pm$ 252	10	0.998	8.5	7.6
18	100-5000	5418 $\pm$ 111	25	0.999	4.6	8.7
28	50-5000	11649 $\pm$ 626	25	0.996	3.2	9.2
52	100-5000	6801 $\pm$ 277	25	0.996	10.7	7.6
44	25-5000	10324 $\pm$ 240	10	0.998	11.6	7.0
66	50-5000	9851 $\pm$ 189	10	0.998	5.7	10.2
101	100-5000	6924 $\pm$ 74	25	0.999	12.9	6.7
77	50-5000	4448 $\pm$ 151	25	0.998	7.8	12.6
118	50-5000	7043 $\pm$ 112	10	0.998	4.7	7.6
153	100-5000	5735 $\pm$ 223	25	0.996	8.9	6.0
108	25-5000	8903 $\pm$ 260	10	0.997	9.3	5.3
138	25-5000	6470 $\pm$ 161	10	0.998	3.2	7.2
126	100-5000	3215 $\pm$ 106	25	0.997	3.9	6.5
187	25-5000	5365 $\pm$ 140	5	0.998	5.5	5.5
128	25-5000	5758 $\pm$ 47	5	0.999	13.3	9.5
201	50-5000	3662 $\pm$ 52	10	0.999	12.4	6.2
180	25-5000	5008 $\pm$ 145	10	0.998	8.4	6.1
170	25-5000	4810 $\pm$ 19	10	0.999	8.2	10.9
195	25-5000	2769 $\pm$ 18	5	0.999	8.2	6.6
206	25-5000	1298 $\pm$ 30	5	0.998	7.7	6.6
209	50-5000	588 $\pm$ 21	10	0.998	5.0	10.1

developed method was also studied at 100 ng L<sup>-1</sup> and 1000 ng L<sup>-1</sup> with relative standard deviation (%RSD) values ranging from 3.2% to 13.3% at 100 ng L<sup>-1</sup> and from 5.3% to 12.6% at 1000 ng L<sup>-1</sup>.

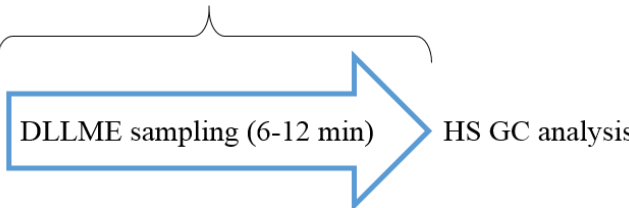
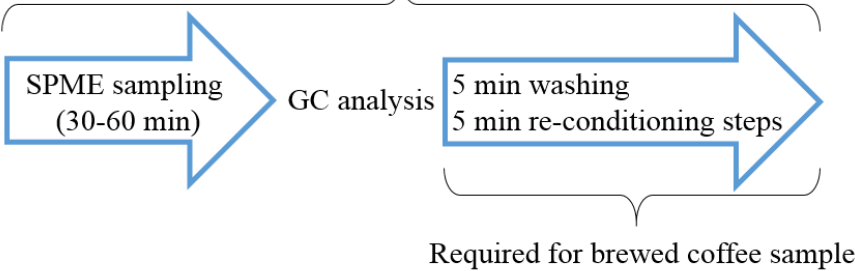
The analytical performance of [HeOHMIM][Cl] IL for the extraction of acrylamide was evaluated by sampling aqueous solutions containing different concentration levels of acrylamide. The results are summarized in Table 3. The precision of the developed method was studied at 100 µg L<sup>-1</sup> wherein a %RSD value of 3.6% was obtained. The linearity of the calibration curve was also studied based on a four-point calibration curve and excellent linearity with a correlation coefficient (R<sup>2</sup>) of 0.999 was obtained.

**Table 3.** Figures of merit for [HeOHMIM][Cl] IL examined in this study for the *in situ* DLLME analysis of acrylamide in ultrapure water and brewed coffee.

Sample matrix	Linear range (µg L <sup>-1</sup> )	Slope ± error	LOD (µg L <sup>-1</sup> )	Linearity (R <sup>2</sup> )	%RSD (n=3) 100 µg L <sup>-1</sup>	AA amount
Ultrapure water	50-1000	2.93 ± 0.08	25	0.998	3.6	-
Brewed coffee	100-1000	3.09 ± 0.15	-	0.999	2.9	91.2 µg L <sup>-1</sup>

The [HeOHMIM][Cl] IL was also applied for the quantification of acrylamide in brewed coffee. Quantitative analysis was carried out by the method of standard addition. A calibration curve was generated by sampling individual brewed coffee samples spiked with varying amounts of acrylamide. Table 3 reports the figures of merits of the calibration curves with the extrapolated concentration of acrylamide. The extrapolated concentration of acrylamide in the brewed coffee was determined to be 91.2 µg L<sup>-1</sup>, which is in good agreement with our previously reported result using SPME coupled to GC-MS (i.e., 77 µg L<sup>-1</sup>, 82 µg L<sup>-1</sup>, and 73 µg L<sup>-1</sup>, respectively, using different PIL-based SPME sorbent coatings) [14]. The precision of the developed method was studied at 100 µg L<sup>-1</sup> and a %RSD value of 3.6% was obtained.

**Figure 13** Features of IL-based *in situ* DLLME coupled to HS-GC and SPME couples to GC methods

Sampling technique	Analytes/Sample matrix	Time required for sampling 20 samples	Reusability	Carryover effect
IL-based <i>in situ</i> DLLME coupled to HS-GC	PCBs/Milk Acrylamide/Brewed coffee	<p>20 samples can be prepared at the same time</p>  <p>DLLME sampling (6-12 min) → HS GC analysis</p>	Consume ~50 mg of IL per extraction	No
SPME coupled to GC	PCBs/Milk [12] Acrylamide/Brewed coffee [13, 14]	<p>The same procedure needs to be repeated for 20 times</p>  <p>SPME sampling (30-60 min) → GC analysis → 5 min washing 5 min re-conditioning steps</p> <p>Required for brewed coffee sample</p>	~100 extractions	Needs to be considered for low volatility analyte

After performing the aforementioned experiments, the results demonstrated that the IL-based *in situ* DLLME approach developed in this study can be used for the detection and quantification of PCBs and acrylamide at trace levels in complex sample matrices. This technique also represents an alternative to the conventional SPME technique that often requires long sampling time and relative larger sample volumes. A comparison of the important features of the two techniques is shown in Figure 13. Compared to SPME, the IL-based *in situ* DLLME is more robust and can be applied for in-solution analysis of complex samples. The time required for sampling 20 samples further demonstrates that DLLME is a high-throughput and labor-saving technique compared to SPME. Moreover, even though the DLLME method consumes a small amount of IL in each extraction, it also eliminates the carryover effect and the need to consider the lifetime of the extraction device when performing large numbers of extractions in situations that demand high-throughput analysis.

#### 5.4 Conclusion

Structurally-tuned ILs were synthesized and utilized as extraction solvents in *in situ* DLLME coupled to HS-GC-ECD/or MS for the trace level analysis of PCBs and acrylamide in water, milk, and brewed coffee samples. The *in situ* DLLME approach showed good analytical precision, good linearity, and provided detection limits down to the low ppt level for PCBs and low ppb level for acrylamide in aqueous samples. The method also exhibited good matrix-compatibility with complex real-world samples. Good extraction efficiency was obtained using the [BMIM][Br] IL for the extraction of PCBs from milk samples. The quantification of acrylamide in brewed coffee was performed by the method of standard addition using the [HeOHMIM][Cl] IL as extraction solvent. Overall, *in situ* IL-based DLLME coupled to HS-GC exhibited fast sampling times, is

capable of achieving high sample throughput, and represents a significant advantage over the conventional SPME method. Further studies will focus on applying structurally-tuned ILs for the analysis of trace level analytes in matrices with higher complexity such as volatile and semi-volatile metabolites from biological samples. Moreover, a fully automated IL-based *in situ* DLLME procedure will be explored to further increase the speed of sample analysis.

### Acknowledgements

The authors acknowledge funding from Chemical Measurement and Imaging Program at the National Science Foundation (Grant number CHE-1413199).

### References

- [1] H. Kataoka, H.L. Lord, J. Pawliszyn, Applications of solid-phase microextraction in food analysis, *J. Chromatogr. A*, 880 (2000) 35-62.
- [2] W. Wardencki, M. Michulec, J. Curyło, A review of theoretical and practical aspects of solid-phase microextraction in food analysis, *Int. J. Food Sci. Tech.*, 39 (2004) 703-717.
- [3] S.H. Safe, Polychlorinated biphenyls (PCBs): Environmental impact, biochemical and toxic responses, and implications for risk assessment, *Crit. Rev. Toxicol.*, 24 (1994) 87-149.
- [4] D.S. Mottram, B.L. Wedzicha, A.T. Dodson, Food chemistry: Acrylamide is formed in the Maillard reaction, *Nature*, 419 (2002) 448-449.
- [5] R.M. Mann, R.V. Hyne, C.B. Choung, S.P. Wilson, Amphibians and agricultural chemicals: Review of the risks in a complex environment, *Environ. Pollut.*, 157 (2009) 2903-2927.
- [6] E. Baltussen, C. Cramers, P. Sandra, Sorptive sample preparation - a review, *Anal. Bioanal. Chem.*, 373 (2002) 3-22.
- [7] J. Lee, H.K. Lee, K.E. Rasmussen, S. Pedersen-Bjergaard, Environmental and bioanalytical applications of hollow fiber membrane liquid-phase microextraction: A review, *Anal. Chim. Acta*, 624 (2008) 253-268.
- [8] S. Dadfarnia, A.M. Haji Shabani, Recent development in liquid phase microextraction for determination of trace level concentration of metals-A review, *Anal. Chim. Acta*, 658 (2010) 107-119.

- [9] A. Jain, K.K. Verma, Recent advances in applications of single-drop microextraction: A review, *Anal. Chim. Acta*, 706 (2011) 37-65.
- [10] M. Rezaee, Y. Yamini, M. Faraji, Evolution of dispersive liquid-liquid microextraction method, *J. Chromatogr. A*, 1217 (2010) 2342-2357.
- [11] C.L. Arthur, J. Pawliszyn, Solid phase microextraction with thermal desorption using fused silica optical fibers, *Anal. Chem.*, 62 (1990) 2145-2148.
- [12] M.D. Joshi, T.D. Ho, W.T.S. Cole, J.L. Anderson, Determination of polychlorinated biphenyls in ocean water and bovine milk using crosslinked polymeric ionic liquid sorbent coatings by solid-phase microextraction, *Talanta*, 118 (2014) 172-179.
- [13] C. Cagliero, T.D. Ho, C. Zhang, C. Bicchi, J.L. Anderson, Determination of acrylamide in brewed coffee and coffee powder using polymeric ionic liquid-based sorbent coatings in solid-phase microextraction coupled to gas chromatography-mass spectrometry, *J. Chromatogr. A*, 1449 (2016) 2-7.
- [14] C. Cagliero, H. Nan, C. Bicchi, J.L. Anderson, Matrix-compatible sorbent coatings based on structurally-tuned polymeric ionic liquids for the determination of acrylamide in brewed coffee and coffee powder using solid-phase microextraction, *J. Chromatogr. A*, 1459 (2016) 17-23.
- [15] É.A. Souza Silva, J. Pawliszyn, Optimization of fiber coating structure enables direct immersion solid phase microextraction and high-throughput determination of complex samples, *Anal. Chem.*, 84 (2012) 6933-6938.
- [16] M. Rezaee, Y. Assadi, M.-R. Milani Hosseini, E. Aghaee, F. Ahmadi, S. Berijani, Determination of organic compounds in water using dispersive liquid-liquid microextraction, *J. Chromatogr. A*, 1116 (2006) 1-9.
- [17] C. Yao, T. Li, P. Twu, W.R. Pitner, J.L. Anderson, Selective extraction of emerging contaminants from water samples by dispersive liquid-liquid microextraction using functionalized ionic liquids, *J. Chromatogr. A*, 1218 (2011) 1556-1566.
- [18] T. Li, M.D. Joshi, D.R. Ronning, J.L. Anderson, Ionic liquids as solvents for in situ dispersive liquid-liquid microextraction of DNA, *J. Chromatogr. A*, 1272 (2013) 8-14.
- [19] E. Zeini Jahromi, A. Bidari, Y. Assadi, M.R. Milani Hosseini, M.R. Jamali, Dispersive liquid-liquid microextraction combined with graphite furnace atomic absorption spectrometry: Ultra trace determination of cadmium in water samples, *Anal. Chim. Acta*, 585 (2007) 305-311.
- [20] N. Fattahi, Y. Assadi, M.R.M. Hosseini, E.Z. Jahromi, Determination of chlorophenols in water samples using simultaneous dispersive liquid-liquid microextraction and derivatization followed by gas chromatography-electron-capture detection, *J. Chromatogr. A*, 1157 (2007) 23-29.
- [21] M. Baghdadi, F. Shemirani, Cold-induced aggregation microextraction: A novel sample preparation technique based on ionic liquids, *Anal. Chim. Acta*, 613 (2008) 56-63.

- [22] H. Bai, Q. Zhou, G. Xie, J. Xiao, Enrichment and sensitive determination of dichlorodiphenyltrichloroethane and its metabolites with temperature controlled ionic liquid dispersive liquid phase microextraction prior to high performance liquid phase chromatography, *Anal. Chim. Acta*, 651 (2009) 64-68.
- [23] H. Zhang, X. Chen, X. Jiang, Determination of phthalate esters in water samples by ionic liquid cold-induced aggregation dispersive liquid-liquid microextraction coupled with high-performance liquid chromatography, *Anal. Chim. Acta*, 689 (2011) 137-142.
- [24] Q. Zhou, H. Bai, G. Xie, J. Xiao, Trace determination of organophosphorus pesticides in environmental samples by temperature-controlled ionic liquid dispersive liquid-phase microextraction, *J. Chromatogr. A*, 1188 (2008) 148-153.
- [25] R. Liu, J.-f. Liu, Y.-g. Yin, X.-l. Hu, G.-b. Jiang, Ionic liquids in sample preparation, *Anal. Bioanal. Chem.*, 393 (2009) 871-883.
- [26] T.D. Ho, C. Zhang, L.W. Hantao, J.L. Anderson, Ionic liquids in analytical chemistry: fundamentals, advances, and perspectives, *Anal. Chem.*, 86 (2014) 262-285.
- [27] M. Baghdadi, F. Shemirani, In situ solvent formation microextraction based on ionic liquids: A novel sample preparation technique for determination of inorganic species in saline solutions, *Anal. Chim. Acta*, 634 (2009) 186-191.
- [28] C. Yao, J.L. Anderson, Dispersive liquid-liquid microextraction using an in situ metathesis reaction to form an ionic liquid extraction phase for the preconcentration of aromatic compounds from water, *Anal. Bioanal. Chem.*, 395 (2009) 1491-1502.
- [29] M.J. Trujillo-Rodríguez, P. Rocío-Bautista, V. Pino, A.M. Afonso, Ionic liquids in dispersive liquid-liquid microextraction, *TrAC, Trends Anal. Chem.*, 51 (2013) 87-106.
- [30] B. Kolb, Headspace sampling with capillary columns, *J. Chromatogr. A*, 842 (1999) 163-205.
- [31] N.H. Snow, G.C. Slack, Head-space analysis in modern gas chromatography, *TrAC, Trends Anal. Chem.*, 21 (2002) 608-617.
- [32] J.C. Flórez Menéndez, M.L. Fernández Sánchez, J.E. Sánchez Uría, E. Fernández Martínez, A. Sanz-Medel, Static headspace, solid-phase microextraction and headspace solid-phase microextraction for BTEX determination in aqueous samples by gas chromatography, *Anal. Chim. Acta*, 415 (2000) 9-20.
- [33] T.D. Ho, P.M. Yehl, N.P. Chetwyn, J. Wang, J.L. Anderson, Q. Zhong, Determination of trace level genotoxic impurities in small molecule drug substances using conventional headspace gas chromatography with contemporary ionic liquid diluents and electron capture detection, *J. Chromatogr. A*, 1361 (2014) 217-228.
- [34] M. Andre, J. Loidl, G. Laus, H. Schottenberger, G. Bentivoglio, K. Wurst, K.H. Ongania, Ionic liquids as advantageous solvents for headspace gas chromatography of compounds with low vapor pressure, *Anal. Chem.*, 77 (2005) 702-705.

- [35] F.-h. Liu, Y. Jiang, Room temperature ionic liquid as matrix medium for the determination of residual solvents in pharmaceuticals by static headspace gas chromatography, *J. Chromatogr. A*, 1167 (2007) 116-119.
- [36] G. Laus, M. Andre, G. Bentivoglio, H. Schottenberger, Ionic liquids as superior solvents for headspace gas chromatography of residual solvents with very low vapor pressure, relevant for pharmaceutical final dosage forms, *J. Chromatogr. A*, 1216 (2009) 6020-6023.
- [37] H. Yu, K.D. Clark, J.L. Anderson, Rapid and sensitive analysis of microcystins using ionic liquid-based in situ dispersive liquid-liquid microextraction, *J. Chromatogr. A*, 1406 (2015) 10-18.
- [38] S. Li, H. Gao, J. Zhang, Y. Li, B. Peng, Z. Zhou, Determination of insecticides in water using in situ halide exchange reaction-assisted ionic liquid dispersive liquid-liquid microextraction followed by high-performance liquid chromatography, *J. Sep. Sci.*, 34 (2011) 3178-3185.
- [39] Q. Zhong, P. Su, Y. Zhang, R. Wang, Y. Yang, In-situ ionic liquid-based microwave-assisted dispersive liquid-liquid microextraction of triazine herbicides, *Microchim. Acta*, 178 (2012) 341-347.
- [40] L.S. Ettre, C. Welter, B. Kolb, Determination of gas-liquid partition coefficients by automatic equilibrium headspace-gas chromatography utilizing the phase ratio variation method, *Chromatographia*, 35 (1993) 73-84.
- [41] G. Meurant, *Handbook of milk composition*, Academic press, 1995, pp. 5-50.
- [42] Z. Du, Y.-L. Yu, J.-H. Wang, Extraction of proteins from biological fluids by use of an ionic liquid/aqueous two-phase system, *Chem. Eur. J*, 13 (2007) 2130-2137.
- [43] E. Björklund, A. Müller, C. von Holst, Comparison of fat retainers in accelerated solvent extraction for the selective extraction of PCBs from fat-containing samples, *Anal. Chem.*, 73 (2001) 4050-4053.



## CHAPTER 6

### GENERAL CONCLUSIONS

The first part of this dissertation describes the applications of IL-based materials in gas chromatographic separations. Dicationic ILs containing various functional groups were employed as GC stationary phases for the separation of nonpolar aliphatic hydrocarbons using GC×GC. The structural tuning of dicationic ILs was guided by examining the solvation properties of ILs using the solvation parameter model as well as evaluating the separation results of kerosene sample using GC×GC. It was observed that ILs containing long side alkyl chain substituents (decyl chain) and long linker chains (decyl chain) between the cations offer the best selectivity for aliphatic hydrocarbons. This knowledge was subsequently applied for the design of high thermally stable PIL-based stationary phases that provide strong dispersive interactions for the separation of nonpolar analytes within complex samples. The PIL-based stationary phase containing IL monomer with long alkyl chain substituents (hexadecyl chain) and 50% (w/w) of crosslinker with a dodecyl linkage chain exhibited high resolving power for the separation of aliphatic hydrocarbons. This best performing crosslinked PIL-based stationary phase also exhibited higher resolution for selected analytes and better thermal stability compared to PEG phases. Finally, the crosslinked PIL-based stationary phase was employed for the separation of aliphatic hydrocarbons in diesel fuel and exhibited superior resolution power when compared with commercial SUPELCOWAX 10 and DB-17 columns.

The second part of this dissertation presents the application of PILs as sorbent coatings in SPME. PIL bucky gel SPME sorbent coatings were prepared via thermal initiated on-fiber copolymerization for the selective extraction of PAHs from water. The new approach allows MWCNTs to be finely dispersed within the PIL phase, which can significantly

increase the  $\pi$ - $\pi$  interactions between the target analytes (i.e., PAHs) and SPME sorbent coating. The PIL bucky gel sorbent coating exhibited higher extraction efficiencies for the extraction of most PAHs compared to commercial PDMS coating.

The PIL bucky gel fiber can also be applied for the sampling of complex environmental samples with excellent analytical performance and high fiber lifetime.

In the last part of the dissertation, structural-tuned ILs were employed as extraction solvents in *in situ* DLLME coupled to HS-GC-ECD/or MS for the analysis of PCBs and acrylamide from complex food samples at trace levels. Extraction parameters including molar ratio of IL to metathesis reagent and IL quantity were optimized. The effects of HS oven temperature and the HS volume of the sample vial on the analyte response were also evaluated. The matrix-compatibility of the developed method was also proven by quantifying acrylamide in brewed coffee samples. The developed procedure exhibited higher sample throughput compared to the previously reported SPME GC-MS method and can be applied for the routine analysis of contaminants present in complex food samples.

## SUPPLEMENTAL INFORMATION ACCOMPANYING CHAPTER 2

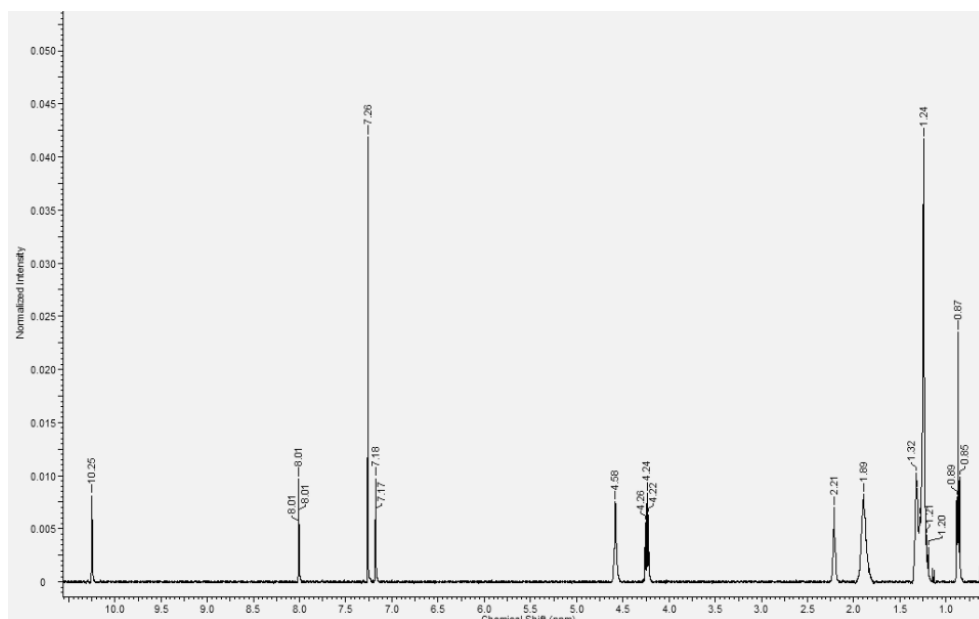


**Figure A3.**  $^1\text{H}$  NMR (600 MHz,  $\text{CDCl}_3$ ) spectrum of  $[(\text{C}_{10}\text{im})_2\text{C}_4]^{2+} 2[\text{Br}]^-$ : 10.25 (s, 2H), 8.01 (s, 2H), 7.18 (s, 2H), 4.68 (t, 4H), 4.24 (t, 4H), 2.21 (t, 4H), 1.89 (m, 12H), 1.24 (m, 20H), 0.87 (t, 6H).

ESI-MS:  $[(\text{C}_{10}\text{im})_2\text{C}_4]^{2+}[\text{Br}]^-$  at  $m/z$  553.4.

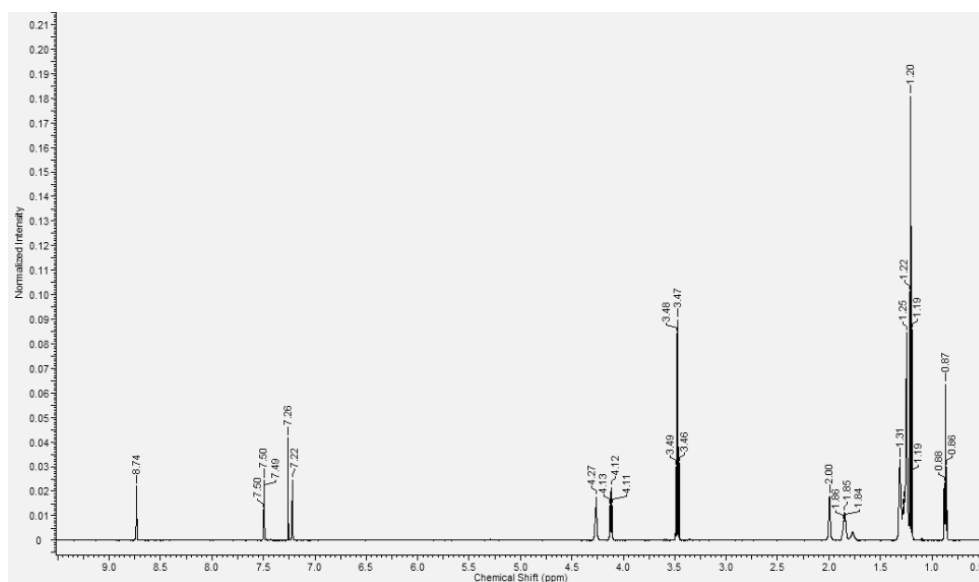


**Figure A4.**  $^1\text{H}$  NMR (600 MHz,  $\text{CDCl}_3$ ) spectrum of  $[(\text{C}_{10}\text{im})_2\text{C}_4]^{2+} 2[\text{NTf}_2]^-$ : 8.74 (s, 2H), 7.50 (s, 2H), 7.27 (s, 2H), 4.27 (t, 4H), 4.12 (t, 4H), 3.47 (m, 8H), 2.00 (t, 4H), 1.85 (t, 4H), 1.20 (m, 20H), 0.87 (t, 6H).

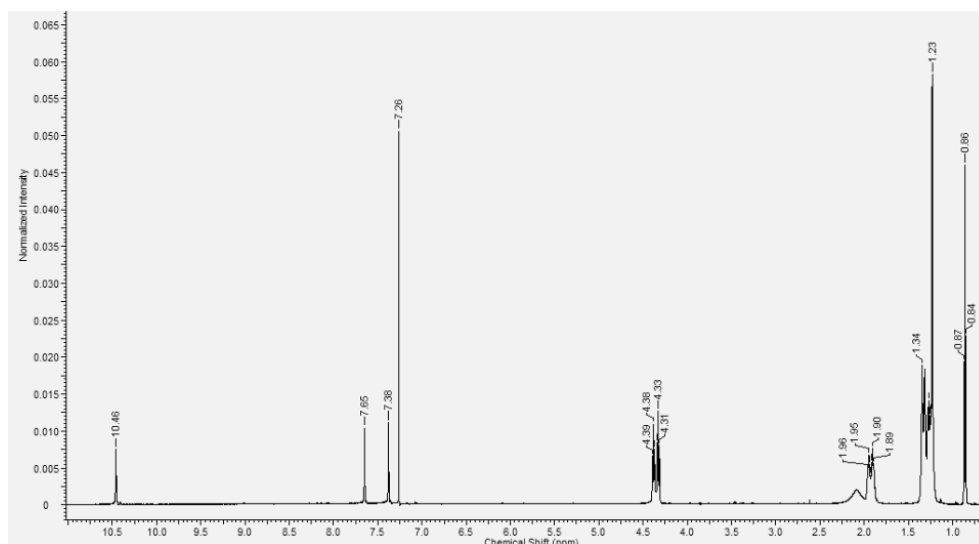


**Figure A5.**  $^1\text{H}$  NMR (600 MHz,  $\text{CDCl}_3$ ) spectrum of  $[(\text{C}_{10}\text{im})_2\text{C}_{10}]^{2+} 2[\text{Br}]^-$ : 10.46 (s, 2H), 7.65 (s, 2H), 7.38 (s, 2H), 4.39 (t, 4H), 4.33 (t, 4H), 1.90 (t, 12H), 1.23-1.34 (m, 36H), 0.86 (t, 6H).

ESI-MS:  $[(\text{C}_{10}\text{im})_2\text{C}_{10}]^{2+}$  at  $m/z$  278.6,  $[(\text{C}_{10}\text{im})_2\text{C}_{10}]^{2+}[\text{Br}]^-$  at  $m/z$  637.3.

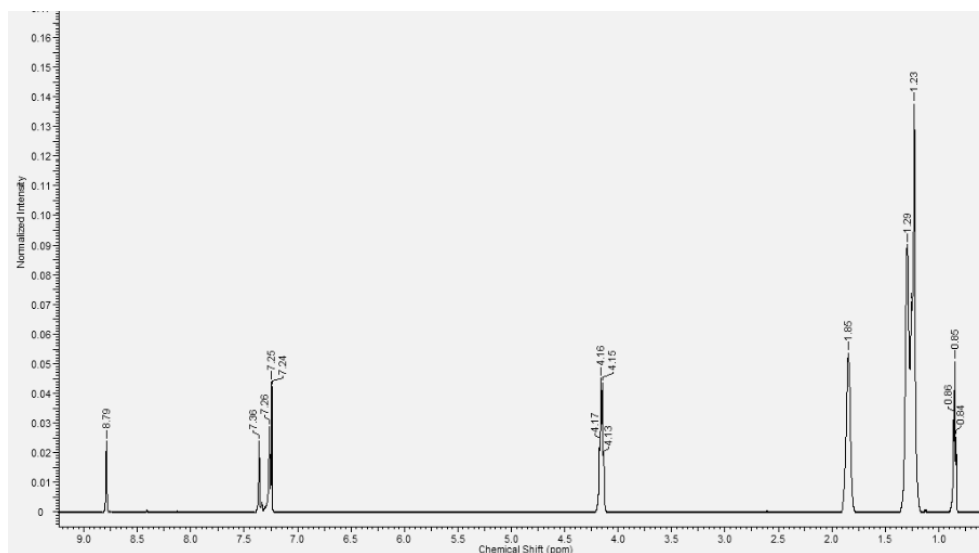


**Figure A6.**  $^1\text{H}$  NMR (600 MHz,  $\text{CDCl}_3$ ) spectrum of  $[(\text{C}_{10}\text{im})_2\text{C}_{10}]^{2+} 2[\text{NTf}_2]^-$ : 8.79 (s, 2H), 7.36 (s, 2H), 7.25 (s, 2H), 4.16 (t, 4H), 4.15 (t, 4H), 1.85 (t, 12H), 1.23-1.29 (m, 36H), 0.85 (t, 6H).

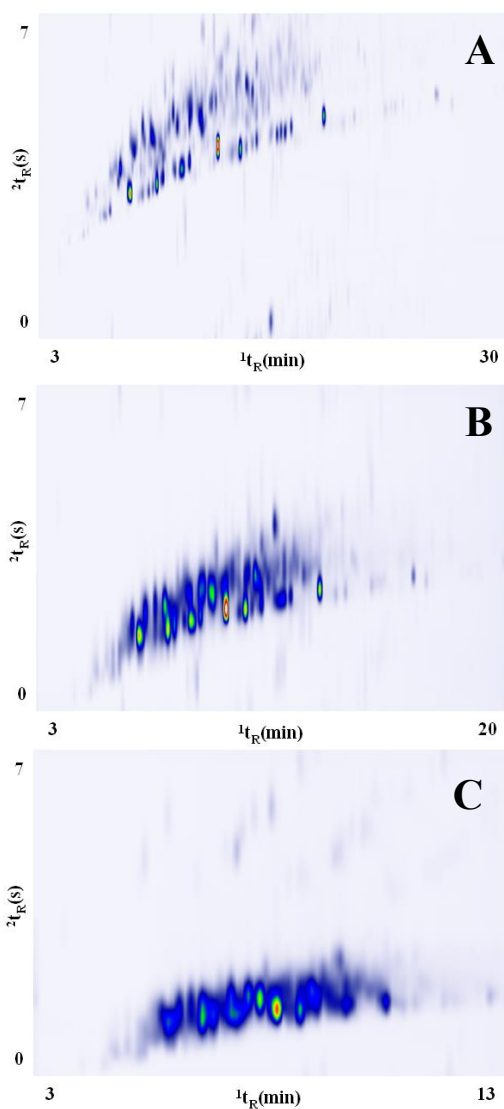


**Figure A7.** GC×GC chromatograms of kerosene using different temperature rates on Rtx-5 × IL 7 column set: (A) 2°C/min, (B) 4°C/min, (C) 6.4°C/min.

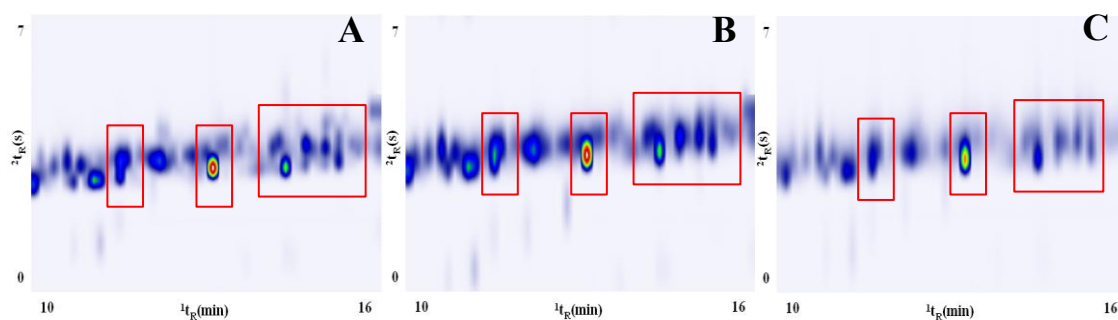


**Figure A8.** Expanded GC×GC chromatograms of kerosene employing (A) Rtx-5 × IL 4, (B) Rtx-5 × IL 5, and (C) Rtx-5 × IL 6.

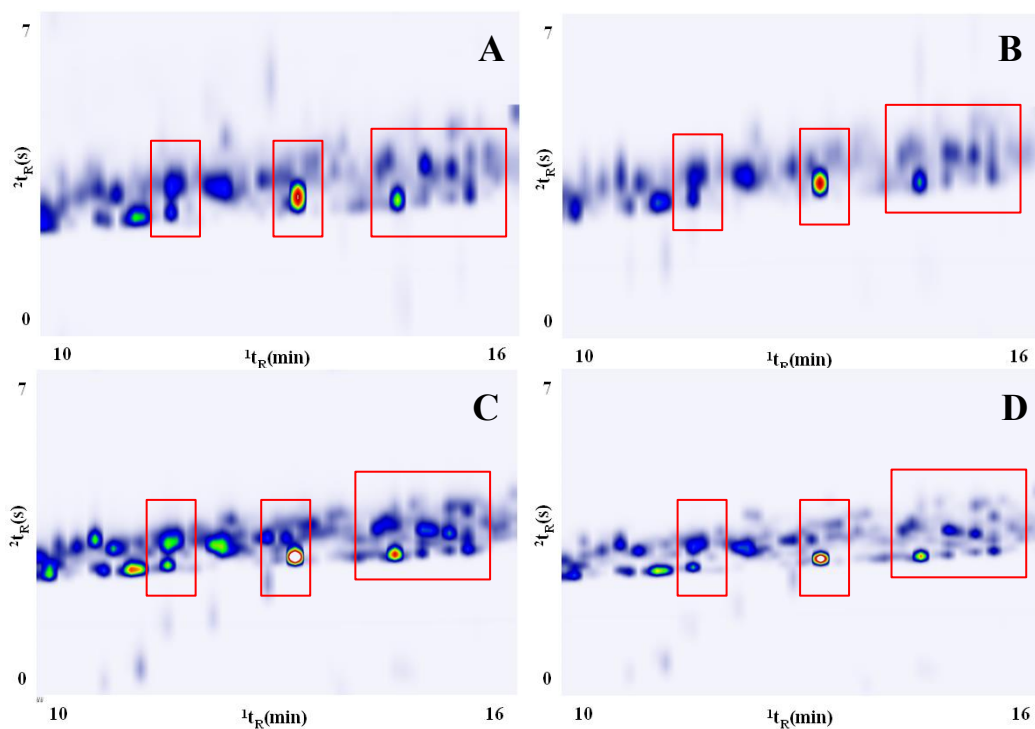


**Figure A9.** Expanded GC×GC chromatograms of kerosene employing (A) Rtx-5 × IL 7 (B) Rtx-5 × IL 9, (C) Rtx-5 × IL 8, and (D) Rtx-5 × IL 10.

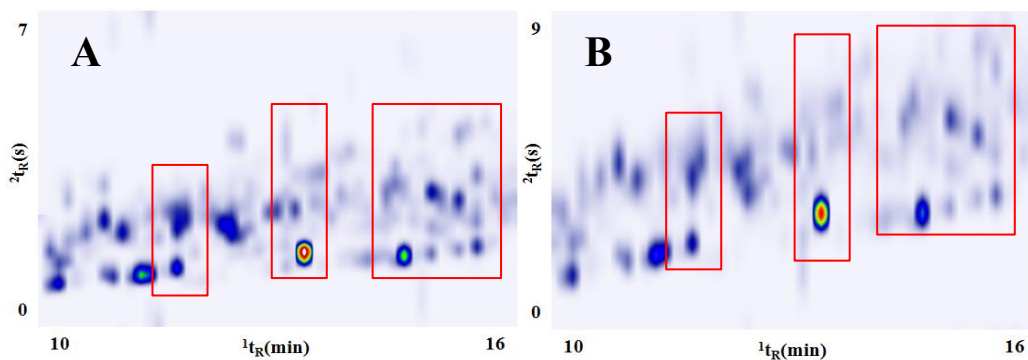


**Figure A10.** Expanded GC×GC chromatograms of kerosene employing select IL-based stationary phases with 0.28  $\mu\text{m}$  film thickness as  $^2\text{D}$  columns: (A) Rtx-5 × IL 7, and (B) Rtx-5 × IL 3.

**Table A1.** Complete list of all probe molecules and their corresponding solute descriptors used to characterize the IL-based stationary phases employing the solvation parameter model

Probe molecule	E	S	A	B	L
Acetic acid	0.265	0.65	0.61	0.44	1.75
Acetophenone	0.818	1.01	0	0.48	4.501
Aniline	0.955	0.96	0.26	0.41	3.934
Benzaldehyde	0.82	1	0	0.39	4.008
Benzene	0.61	0.52	0	0.14	2.786
Benzonitrile	0.742	1.11	0	0.33	4.039
Benzyl alcohol	0.803	0.87	0.33	0.56	4.221
Bromoethane	0.366	0.4	0	0.12	2.62
1-Bromooctane	0.339	0.4	0	0.12	5.09
1-Butanol	0.224	0.42	0.37	0.48	2.601
Butyraldehyde	0.187	0.65	0	0.45	2.27
2-Chloroaniline	1.033	0.92	0.25	0.31	4.674
1-Chlorobutane	0.21	0.4	0	0.1	2.722
1-Chlorohexane	0.201	0.4	0	0.1	3.777
1-Chlorooctane	0.191	0.4	0	0.1	4.772
<i>p</i> -Cresol	0.82	0.87	0.57	0.31	4.312
Cyclohexanol	0.46	0.54	0.32	0.57	3.758
Cyclohexanone	0.403	0.86	0	0.56	3.792
1,2-Dichlorobenzene	0.872	0.78	0	0.04	4.518
N,N-Dimethylformamide	0.367	1.31	0	0.74	3.173
1,4-Dioxane	0.329	0.75	0	0.64	2.892
Ethyl acetate	0.106	0.62	0	0.45	2.314
Ethyl benzene	0.613	0.51	0	0.15	3.778
1-Iodobutane	0.628	0.4	0	0.15	4.13
Methyl caproate	0.067	0.6	0	0.45	3.844
Naphthalene	1.34	0.92	0	0.2	5.161
Nitrobenzene	0.871	1.11	0	0.28	4.557
1-Nitropropane	0.242	0.95	0	0.31	2.894
1-Octanol	0.199	0.42	0.37	0.48	4.619
Octylaldehyde	0.16	0.65	0	0.45	4.361



**Table A1.** Continued

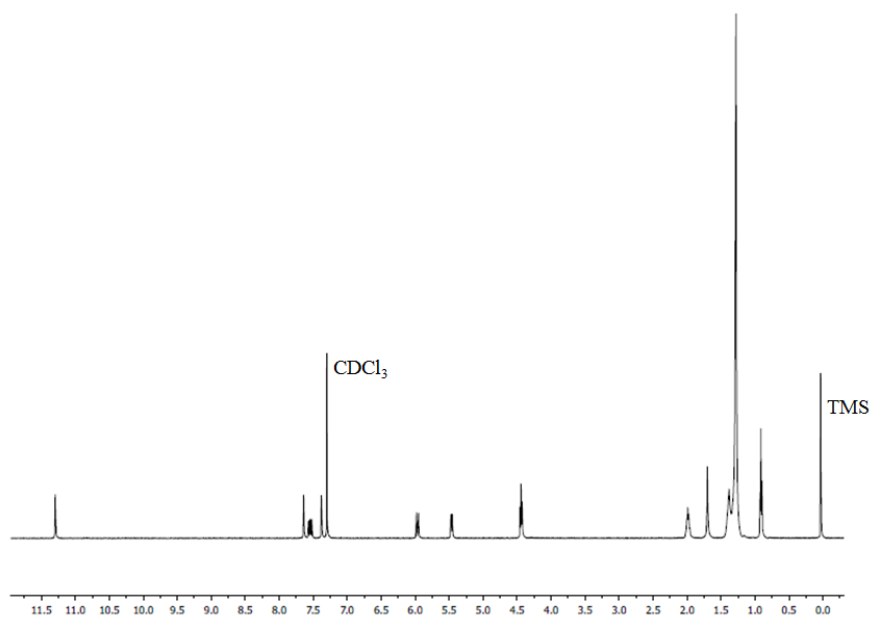
1-Pentanol	0.219	0.42	0.37	0.48	3.106
2-Pentanone	0.143	0.68	0	0.51	2.755
Ethyl phenyl ether	0.681	0.7	0	0.32	4.242
Phenol	0.805	0.89	0.6	0.3	3.766
Propionitrile	0.162	0.9	0.02	0.36	2.082
Pyridine	0.631	0.84	0	0.52	3.022
Pyrrole	0.613	0.73	0.41	0.29	2.865
Toluene	0.601	0.52	0	0.14	3.325
m-Xylene	0.623	0.52	0	0.16	3.839
o-Xylene	0.663	0.56	0	0.16	3.939
p-Xylene	0.613	0.52	0	0.16	3.839
2-Propanol	0.212	0.36	0.33	0.56	1.764
2-Nitrophenol	1.015	1.05	0.05	0.37	4.76
1-Bromohexane	0.349	0.4	0	0.12	4.13
Propionic acid	0.233	0.65	0.6	0.45	2.29
1-Decanol	0.191	0.42	0.37	0.48	5.628

Data obtained from [1].

## Reference

[1] M.H. Abraham, Chem. Soc. Rev. 22 (1993) 73

## APPENDIX B

SUPPLEMENTAL INFORMATION ACCOMPANYING  
CHAPTER 3

**Figure B1.** <sup>1</sup>H NMR (500 MHz, CDCl<sub>3</sub>) spectrum of [VHDIM] [Br]: 11.28 (s, 1H), 7.64 (s, 1H), 7.55 (m, 1H), 7.38 (s, 1H), 5.96 (d, 1H), 5.45 (d, 1H), 4.43 (t, 2H), 1.98 (m, 2H), 1.30 (m, 26H), 0.91 (t, 3H).

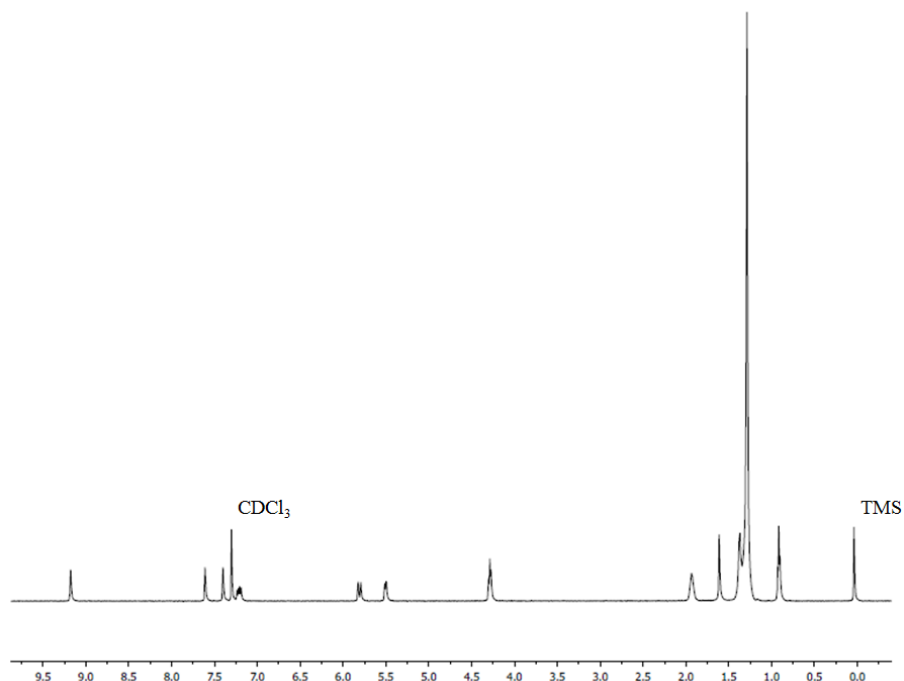


**Figure B2.** <sup>1</sup>H NMR (Bruker DRX-500 MHz, CDCl<sub>3</sub>) spectrum of [VHDIM] [NTf<sub>2</sub>]: 9.16 (s, 1H), 7.59 (s, 1H), 7.39 (s, 1H), 7.19 (m, 1H), 5.76 (d, 1H), 5.48 (d, 1H), 4.26 (t, 2H), 1.92 (m, 2H), 1.31 (m, 26H), 0.90 (t, 3H).

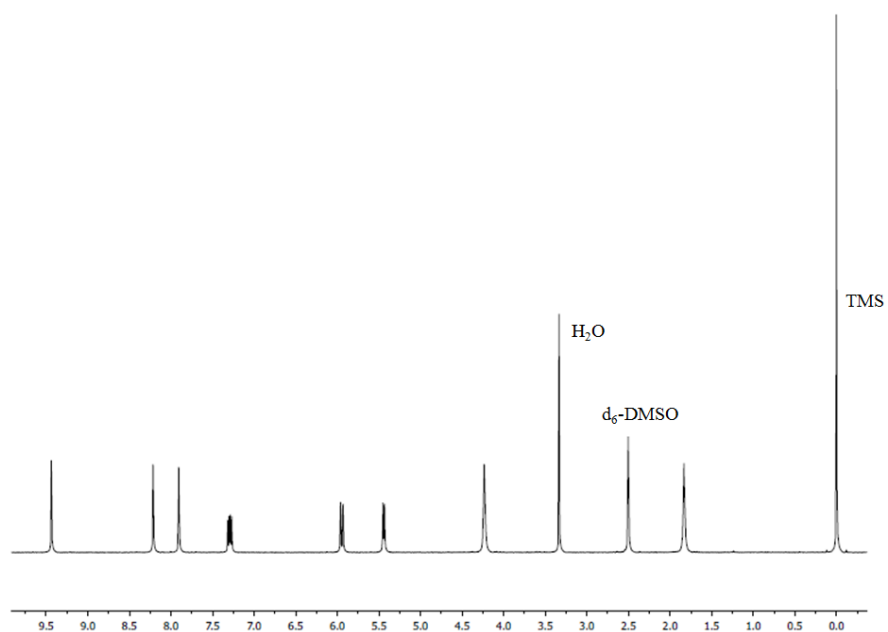


**Figure B3.**  $^1\text{H}$  NMR (Bruker DRX-500 MHz,  $\text{d}_6\text{-DMSO}$ ) spectrum of  $[(\text{VIM})_2\text{C}_4] 2[\text{NTf}_2]$ : 9.43 (s, 2H), 8.21 (s, 2H), 7.90 (s, 2H), 7.29 (m, 2H), 5.94 (d, 2H), 5.43 (d, 2H), 4.21 (t, 4H), 1.82 (t, 4H).

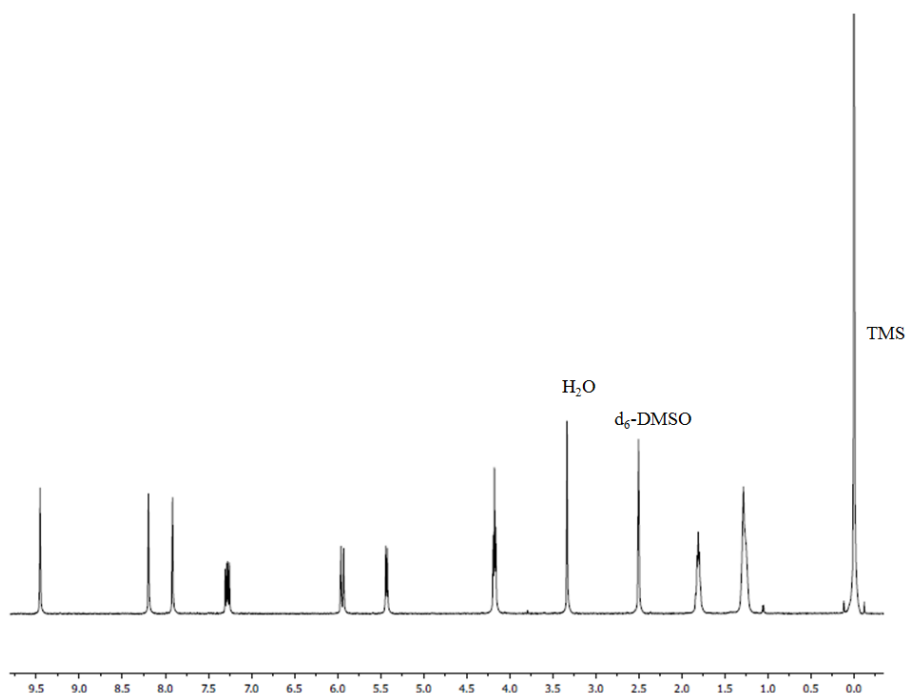


**Figure B4.**  $^1\text{H}$  NMR (Bruker DRX-500 MHz,  $\text{d}_6\text{-DMSO}$ ) spectrum of  $[(\text{VIM})_2\text{C}_8] 2[\text{NTf}_2]$ : 9.45 (s, 2H), 8.19 (s, 2H), 7.91 (s, 2H), 7.27 (m, 2H), 5.93 (d, 2H), 5.42 (d, 2H), 4.16 (t, 4H), 1.80 (t, 4H), 1.26 (m, 8H).

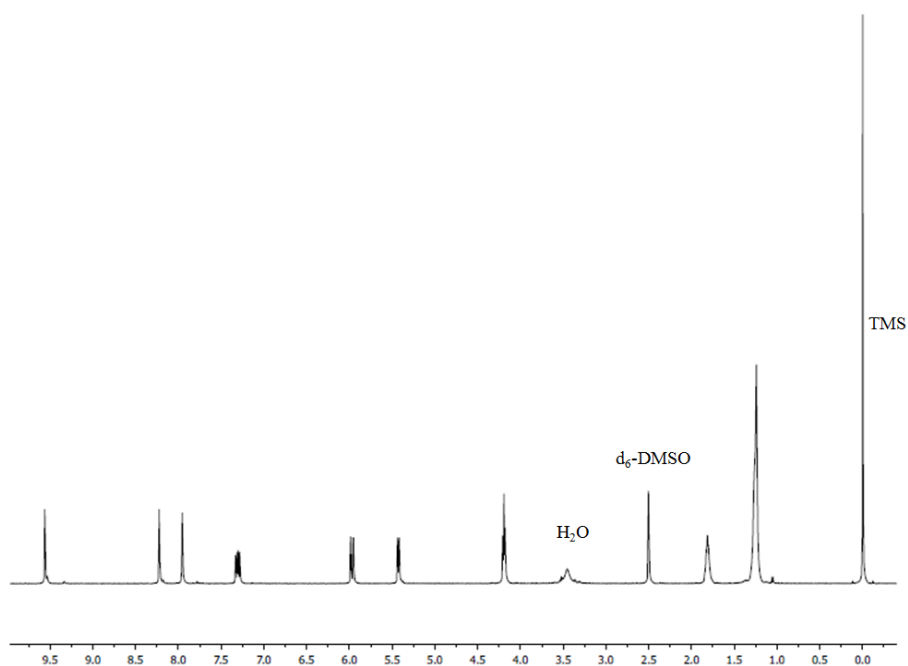


**Figure B5.**  $^1\text{H}$  NMR (Bruker DRX-500 MHz,  $\text{d}_6\text{-DMSO}$ ) spectrum of  $[(\text{VIM})_2\text{C}_{12}] 2[\text{Br}]$ : 9.55 (s, 2H), 8.22 (s, 2H), 7.95 (s, 2H), 7.30 (m, 2H), 5.97 (d, 2H), 5.42 (d, 2H), 4.18 (t, 4H), 1.80 (t, 4H), 1.24 (m, 16H).

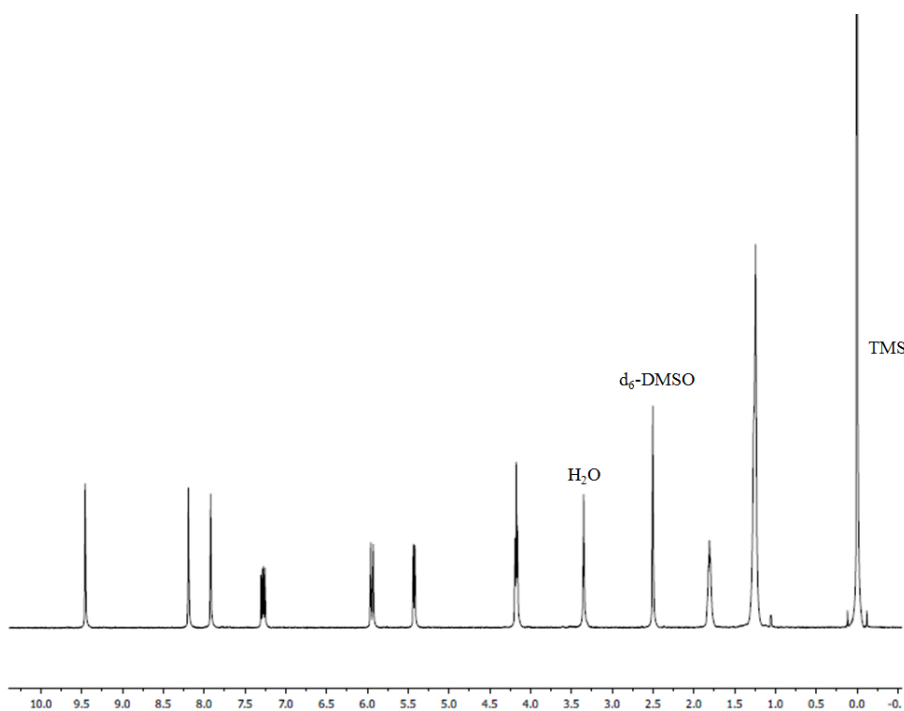


**Figure B6.**  $^1\text{H}$  NMR (Bruker DRX-500 MHz,  $\text{d}_6\text{-DMSO}$ ) spectrum of  $[(\text{VIM})_2\text{C}_{12}] 2[\text{NTf}_2]$ : 9.43 (s, 2H), 8.18 (s, 2H), 7.91 (s, 2H), 7.26 (m, 2H), 5.93 (d, 2H), 5.40 (d, 2H), 4.16 (t, 4H), 1.79 (t, 4H), 1.23 (m, 16H).

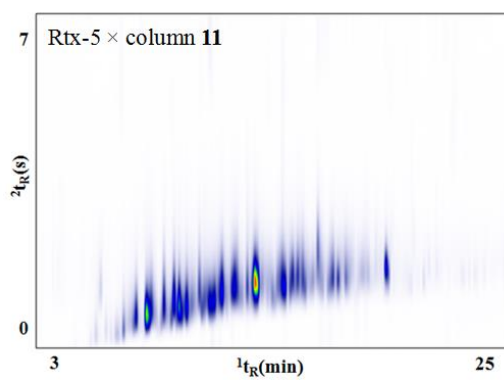


**Figure B7.** GC×GC chromatogram of kerosene employing column **11** as the second-dimension column.

## APPENDIX C

SUPPLEMENTAL INFORMATION ACCOMPANYING  
CHAPTER 4

Synthetic procedures used to prepare 1-vinyl-3-butylimidazolium bis[(trifluoromethyl)sulfonyl]imide [VC<sub>4</sub>IM] [NTf<sub>2</sub>]:

0.05 mol of 1-vinylimidazole and 0.075 mol of 1-bromobutane were mixed in 15 mL isopropanol and stirred vigorously at 70 °C for 48 h. The product was then purified by dissolving in 30 mL of water and extracted six times with 10 mL aliquots of ethyl acetate. The water layer containing the IL monomer was recovered and dried under vacuum at 80 °C for 24h. The halide counteranion was then exchanged to [NTf<sub>2</sub>] by metathesis reaction using one equivalent of lithium bis[(trifluoromethyl)sulfonyl]imide. The mixture solution was then stirred overnight at room temperature and washed with water to yield [VC<sub>4</sub>IM] [NTf<sub>2</sub>].

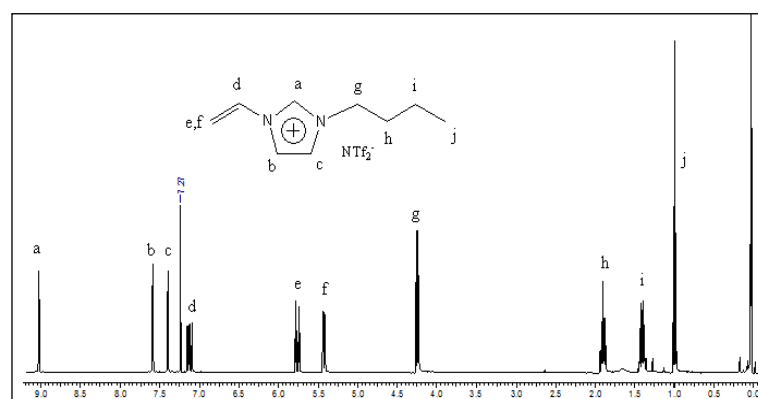


**Figure C1.** <sup>1</sup>H NMR of [VC<sub>4</sub>IM] [NTf<sub>2</sub>]

<sup>1</sup>H NMR (400MHz, CDCl<sub>3</sub>) of [VC<sub>4</sub>IM] [NTf<sub>2</sub>] 9.068 (s, 1H), 7.623 (s, 1H), 7.431 (s, 1H), 7.058 (m, 1H), 5.899 (d, 1H), 5.478 (d, 1H), 4.248 (t, 2H), 1.887 (m, 2H), 1.382 (m, 2H), 0.976 (m, 3H)

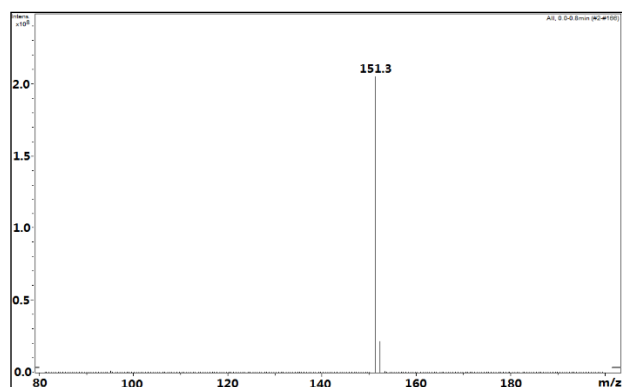


**Figure C2.** ESI-MS (Positive Ion Mode) for [VC<sub>4</sub>IM] [NTf<sub>2</sub>]

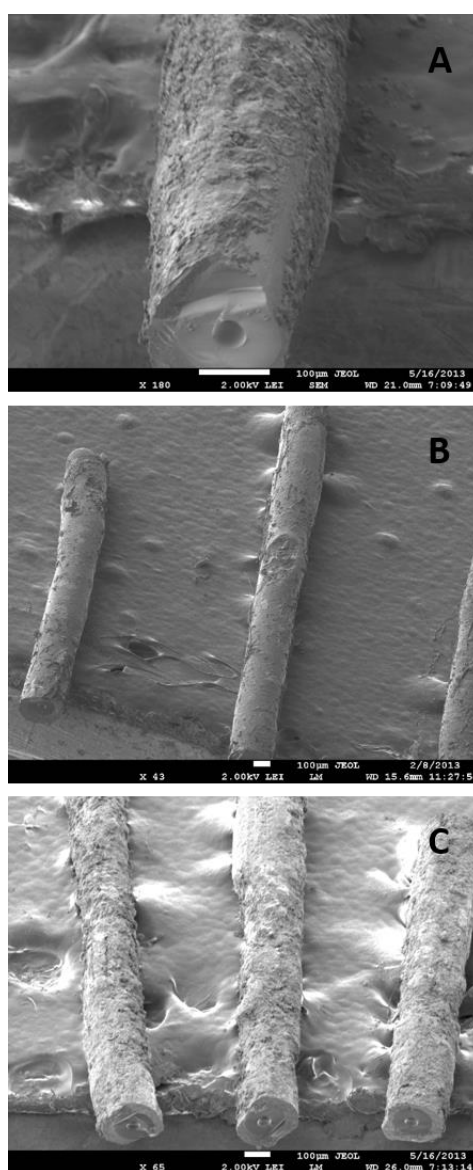


**Figure C3.** Scanning electron micrographs of the PIL-based and PIL bucky gel sorbent coatings after 60 direct immersion extractions. (A) Fiber 1, (B) Fiber 2, (C) Fiber 4.

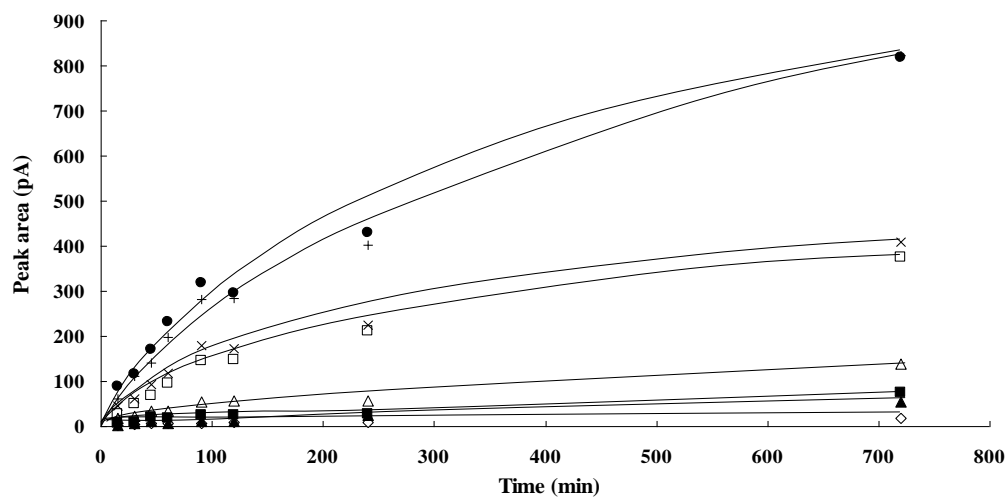


**Figure C4.** Sorption-time profile of the Fiber 3. The stir rate was 800 rpm and the concentration of the analytes was  $40 \mu\text{g L}^{-1}$  ( $\diamond$ ) Naphthalene, ( $\blacksquare$ ) Acenaphthene, ( $\Delta$ ) Fluorine, ( $\times$ ) Phenanthrene, ( $\square$ ) Anthracene, ( $\bullet$ ) Fluoranthene, ( $+$ ) Pyrene, ( $\blacktriangle$ ) Chrysene.

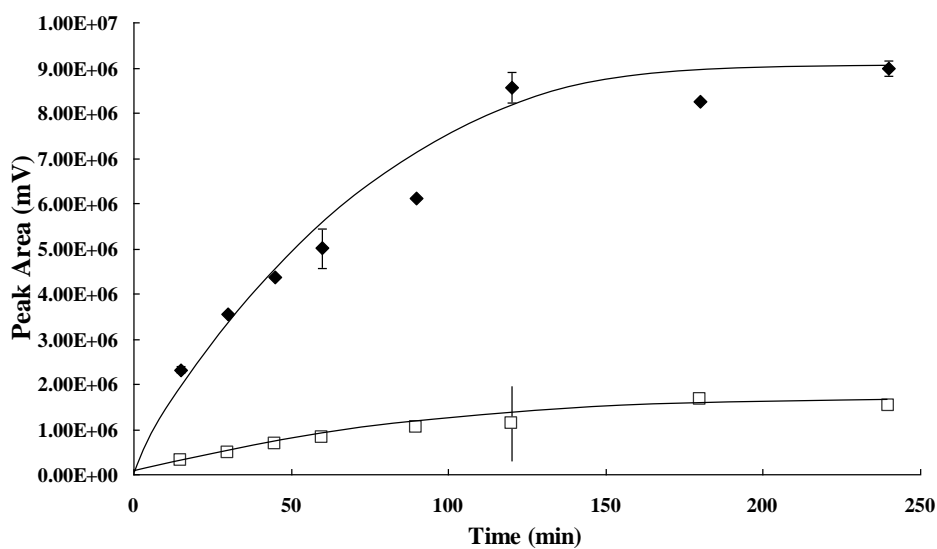


**Figure C5.** Sorption time profile using Fiber 3 for ( $\blacklozenge$ ) naphthalene and ( $\square$ ) 1-octanol at  $10 \mu\text{g L}^{-1}$  and  $100 \mu\text{g L}^{-1}$  respectively.



**APPENDIX D****SUPPLEMENTAL INFORMATION ACCOMPANYING  
CHAPTER 6****Synthesis of ILs**

Synthesis of the [BMIM][Br] and [OMIM][Br] were performed by mixing 0.05 mol of 1-methylimidazole and 0.06 mol of alkyl halides (i.e., 1-bromobutane or 1-bromooctane) in 10 mL isopropanol and heating at 70 °C for 12 hrs. After removal of the solvent under reduced pressure, the product was then dissolved in 10 mL of water and washed with three 10 mL aliquots of ethyl acetate. The water layer containing the IL was recovered and dried under vacuum at 80 °C for 24 h.

Synthesis of the [BeBIM][Br] IL was performed by mixing 0.05 mol of 1-benzylimidazole and 0.06 mol of 1-bromobutane in 10 mL isopropanol and heating at 70 °C for 12 hrs. After removal of the solvent under reduced pressure, the product was then dissolved in 10 mL of water and washed with three 10 mL aliquots of ethyl acetate. The water layer containing the IL was recovered and dried under vacuum at 80 °C for 24 h.

Synthesis of the [BeEOHIM][Br] IL was carried out by mixing 0.05 mol of 1-benzylimidazole and 0.06 mol of 2-bromoethanol in 10 mL isopropanol and heating at 70 °C for 3 days. The [BeEOHIM][Br] was purified by following the same procedure as the [BMIM][Br]. After being dried under vacuum at 80 °C for 24 h, a 3 g aliquot of [BeEOHIM][Br] was dissolved in 1 mL of isopropanol and stored in a vial at 4 °C for 2 days. Following this storage process, clear crystals were formed on the bottom of the vial. The crystal layer was washed with 2 mL of cold isopropanol and dried under vacuum at 80 °C for 12 h. The final product appeared as a viscous liquid with a faint yellow color.

Synthesis of the [HeOHMIM][Cl] IL was performed by mixing 0.05 mol of 1-methylimidazole and 0.06 mol of 6-chloro-1-hexanol in 10 mL isopropanol and heating at

70 °C for 3 days. After the removal of solvent under reduced pressure, the product was then dissolved in 10 mL of water and washed with three 10 mL aliquots of ethyl acetate. The water layer containing the IL was recovered and dried under vacuum at 80 °C for 24 h.

All final products were subsequently characterized by proton nuclear magnetic resonance spectroscopy ( $^1\text{H}$  NMR).

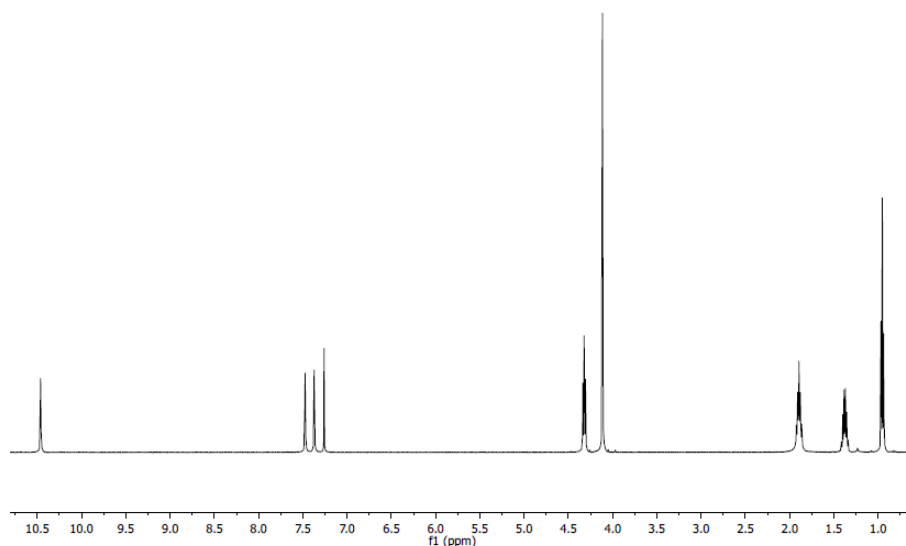


**Figure D1.**  $^1\text{H}$ -NMR (500 MHz, Chloroform-*d*) spectrum of [BMIM][Br]: 10.46 (s, 1H), 7.47 (t,  $J = 1.8$  Hz, 1H), 7.37 (t,  $J = 1.8$  Hz, 1H), 4.32 (t,  $J = 7.4$  Hz, 2H), 4.12 (s, 3H), 1.95-1.84 (m, 2H), 1.42-1.32 (m, 2H), 0.95 (t,  $J = 7.4$  Hz, 3H).

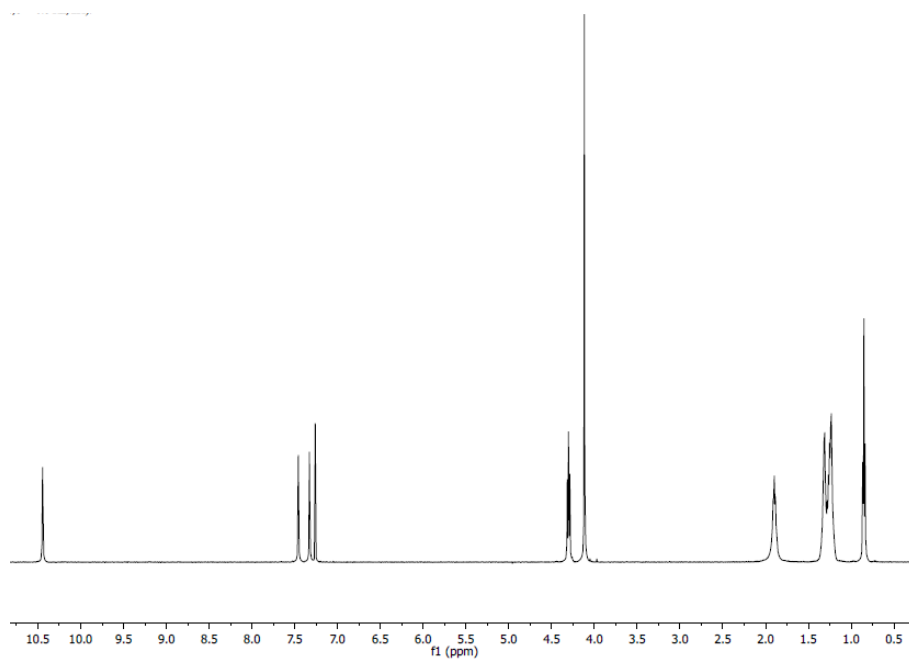


**Figure D2.**  $^1\text{H}$ -NMR (500 MHz, Chloroform- $d$ ) spectrum of [OMIM][Br]: 10.45 (s, 1H), 7.46 (t,  $J = 1.8$  Hz, 1H), 7.33 (t,  $J = 1.8$  Hz, 1H), 4.30 (t,  $J = 7.5$  Hz, 2H), 4.12 (s, 3H), 1.95-1.84 (m, 2H), 1.37 - 1.18 (m, 10H), 1.85 (t,  $J = 6.8$  Hz, 3H).

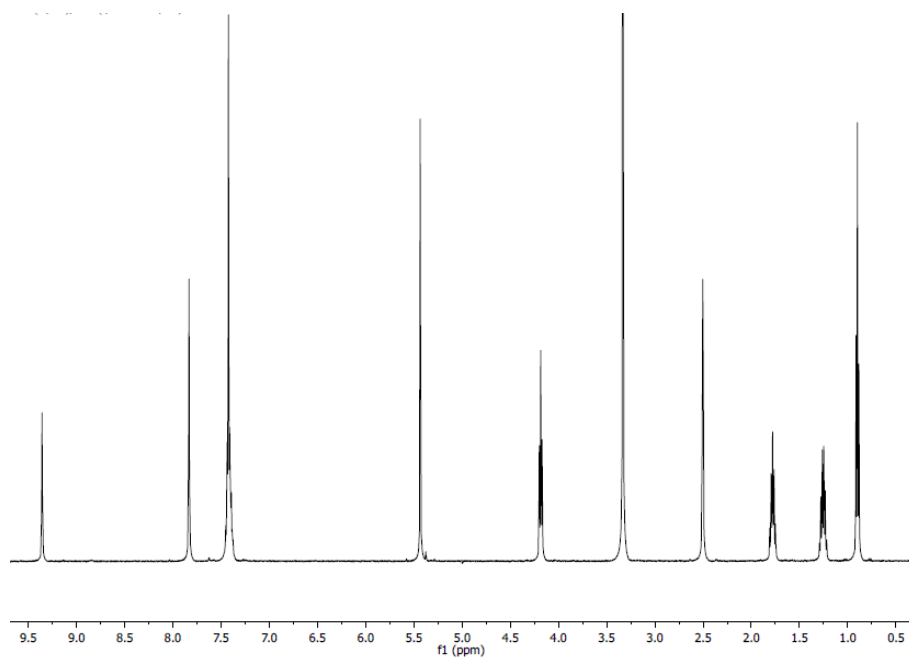


**Figure D3.**  $^1\text{H}$ -NMR (500 MHz, DMSO- $d_6$ ) spectrum of [BeBIM][Br]: 9.35 (s, 1H), 7.83 (d,  $J = 1.7$  Hz, 2H), 7.47-7.36 (m, 5H), 5.43 (s, 2H), 4.18 (t,  $J = 7.2$  Hz, 2H), 1.83-1.72 (m, 2H), 1.31-1.20 (m, 2H), 0.9 (t,  $J = 7.4$  Hz, 3H).

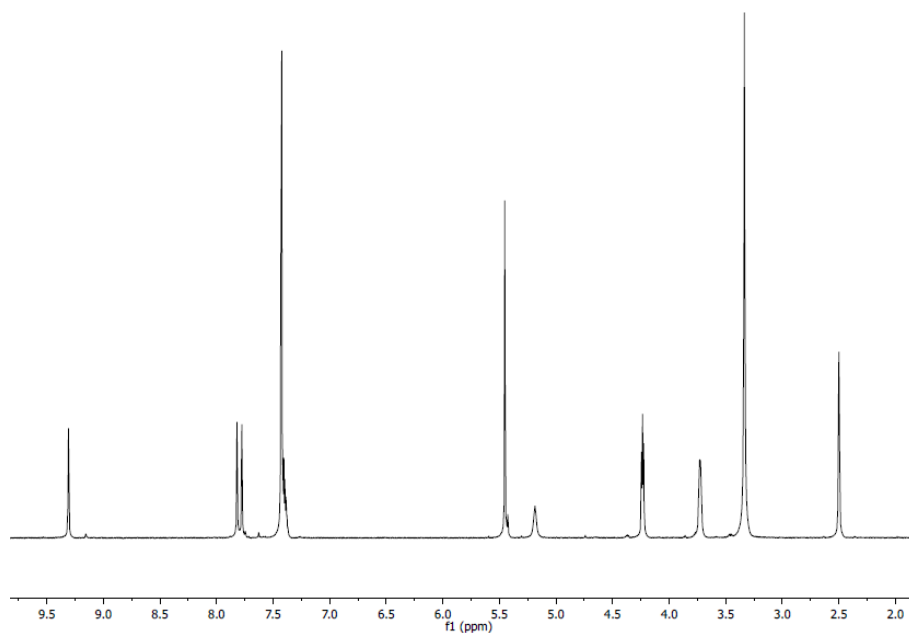


**Figure D4.**  $^1\text{H}$ -NMR (500 MHz,  $\text{DMSO-}d_6$ ) spectrum of  $[\text{BeEOHIM}][\text{Br}]$ : 9.31 (s, 1H), 7.82 (t,  $J = 1.8$  Hz, 1H), 7.78 (t,  $J = 1.8$  Hz, 1H), 7.46-7.37 (m, 5H), 5.45 (s, 2H), 5.20 (br. s., 1H), 4.24 (t,  $J = 5.0$  Hz, 2H), 3.73 (t,  $J = 4.0$  Hz, 2H).

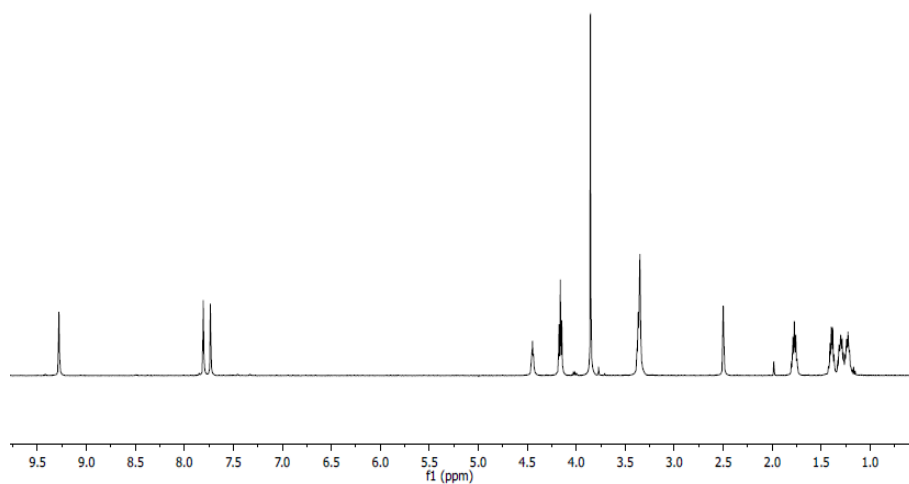


**Figure D5.**  $^1\text{H}$ -NMR (500 MHz,  $\text{DMSO-}d_6$ ) spectrum of  $[\text{HeOHMIM}][\text{Cl}]$ : 9.28 (s, 1H), 7.81 (t,  $J = 1.8$  Hz, 1H), 7.73 (t,  $J = 1.8$  Hz, 1H), 4.45 (br. s., 1H), 4.16 (t,  $J = 7.2$  Hz, 2H), 3.86 (s, 3H), 3.36 (t,  $J = 5.7$  Hz, 2H), 1.77 (td,  $J = 7.5, 14.8$  Hz, 2H), 1.44 - 1.35 (m, 2H), 1.33 - 1.25 (m, 2H), 1.25 - 1.17 (m, 2H).

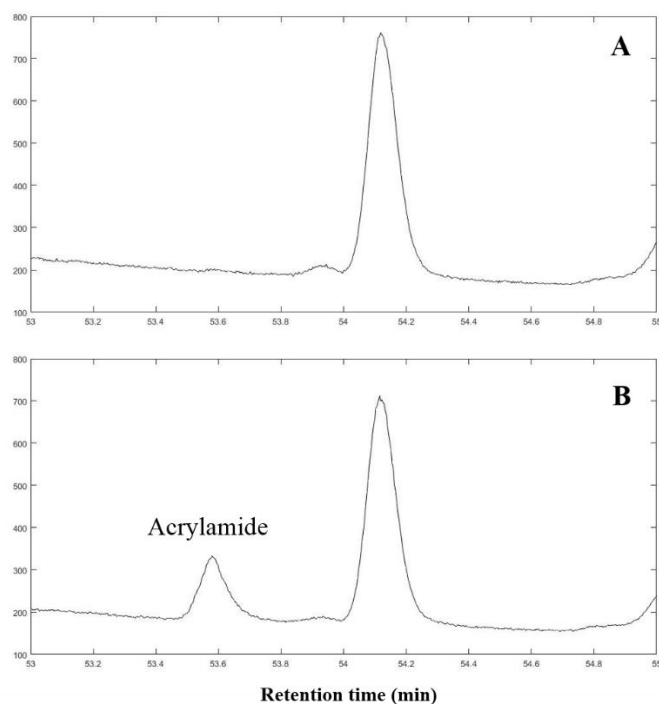


**Figure D6.** (A) HS-GC-MS chromatogram for the [HeOHMIM][NTf<sub>2</sub>] IL incubated at 205 °C for 10 min. (B) HS-GC chromatogram for the [HeOHMIM][NTf<sub>2</sub>] IL incubated at 205 °C for 10 min after in situ DLLME sampling of ultrapure water containing 1 mg L<sup>-1</sup> of acrylamide.

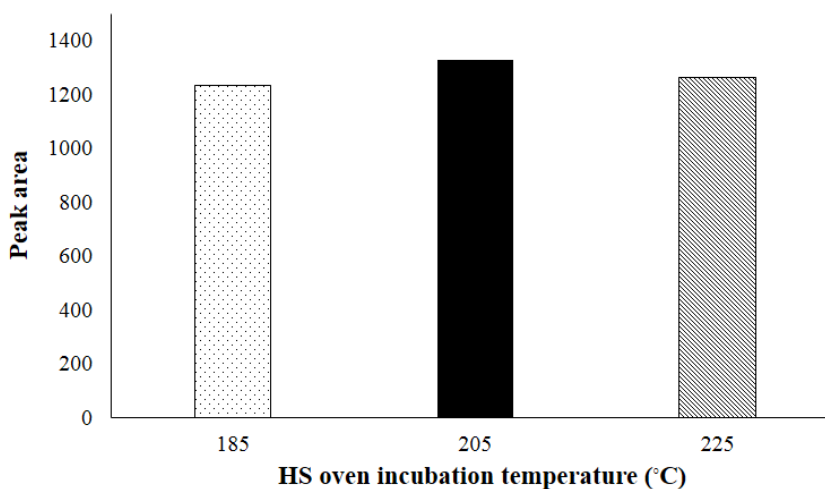


**Figure D7.** Effect of HS oven incubation temperature on the response of acrylamide. The [HeOHMIM][Cl] IL was employed as extraction solvent. (⋯) 185 °C, (■) 205 °C, and (▨) 225 °C. The equilibration time was 10 min.

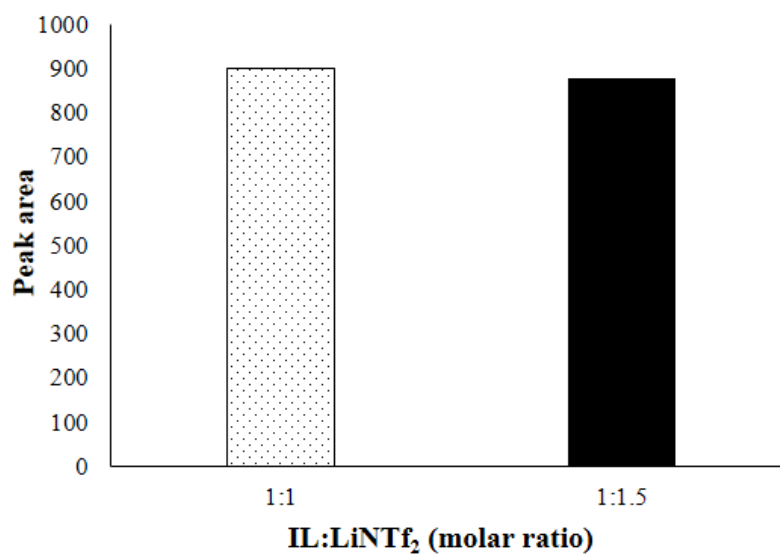


**Figure D8.** Effect of molar ratio of the [HeOHMIM][Cl] IL and LiNTf<sub>2</sub> on the extraction efficiency of acrylamide. ( ··· ) [HeOHMIM][Cl]:LiNTf<sub>2</sub>=1:1, ( ■ ) [HeOHMIM][Cl]:LiNTf<sub>2</sub>=1:1.5. Concentration of analyte: 1 mg L<sup>-1</sup>. HS oven was operated at 205 °C and the equilibration time was 10 min.

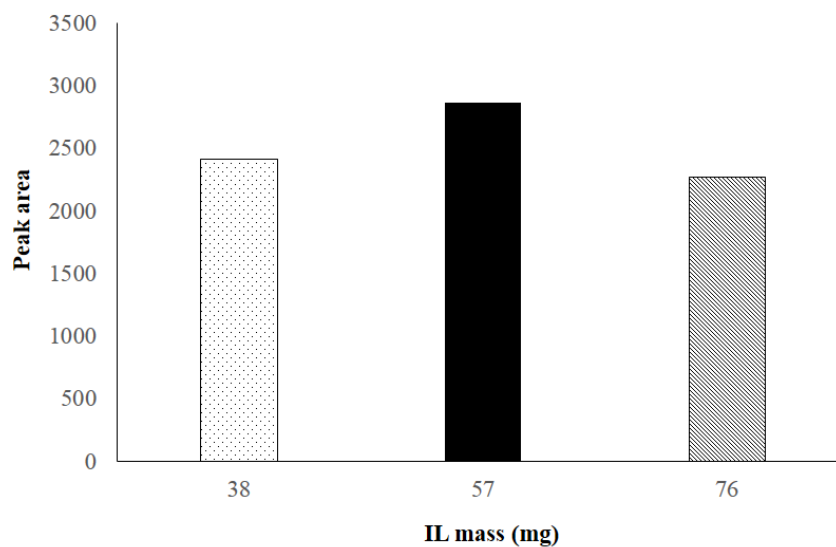


**Figure D9.** Effect of the mass of the [HeOHMIM][Cl] IL on extraction efficiency of acrylamide. ( ··· ) 38 mg, ( ■ ) 57 mg, ( ▨ ) 76 mg. Concentration of analyte: 1 mg L<sup>-1</sup>. HS oven was operated at 205 °C and the equilibration time was 10 min.

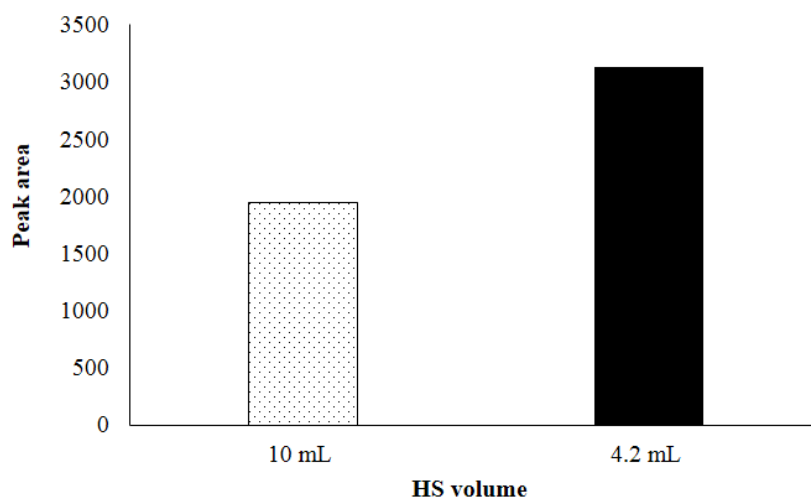


**Figure D10.** Effect of the headspace volume on the response of acrylamide. (◻) HS vial containing 10 mL headspace volume. (■) headspace vial containing 4.2 mL headspace volume. Concentration of analyte:  $1 \text{ mg L}^{-1}$ . HS oven was operated at  $205^\circ\text{C}$  and the equilibration time was 10 min.

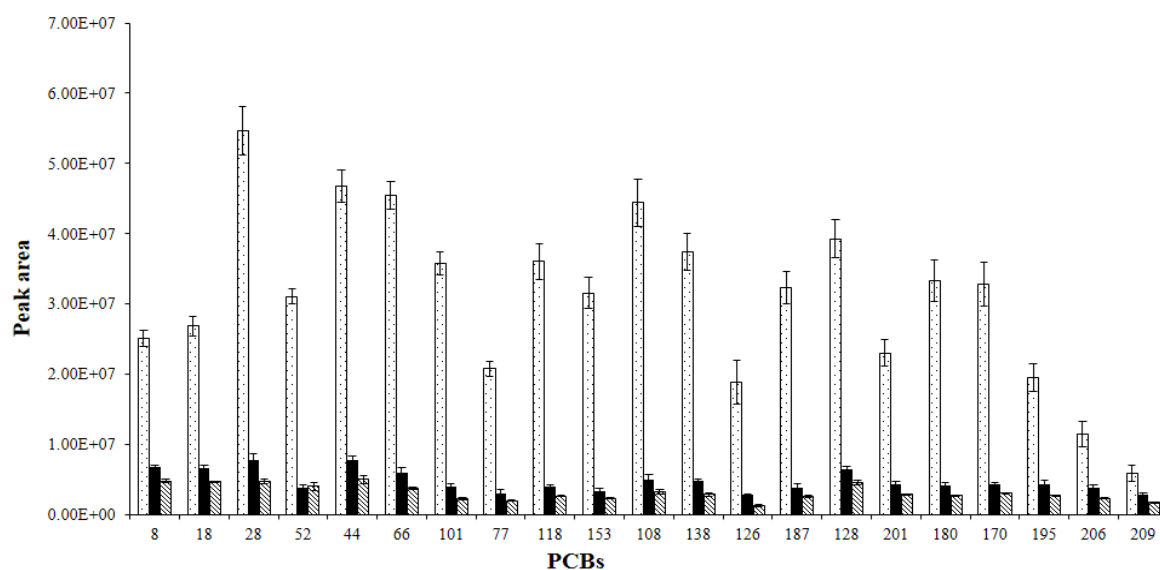


**Figure D11.** Comparison of extraction efficiencies of 21 PCBs from different milk samples using [BMIM][Br] IL: (◻) fat free milk (containing 0% of fat), (■) low fat milk (containing 1% of fat), (▨) reduced fat milk (containing 2% of fat). See Table S1 for list of all PCB structures and corresponding numbers of PCBs. Result obtained by *in situ* DLLME sampling of milk samples containing  $10 \mu\text{g L}^{-1}$  of PCBs. IL:LiNTf<sub>2</sub> = 1:1. All sedimented ILs were collected for HS-GC analysis. HS oven was operated at  $250^\circ\text{C}$  and the equilibration time was 10 min.

**Table D1.** Names and structures for all studied PCBs.

PCB	Name	Structure
8	2,4'-dichlorobiphenyl	
18	2,2',5-trichlorobiphenyl	
28	2,4,4'-trichlorobiphenyl	
52	2,2',5,5'-tetrachlorobiphenyl	
44	2,2',3,5'-tetrachlorobiphenyl	
66	2,3',4,4'-tetrachlorobiphenyl	
101	2,2',4,5,5'-pentachlorobiphenyl	
77	3,3',4,4'-tetrachlorobiphenyl	
118	2,3',4,4',5-pentachlorobiphenyl	
153	2,2',4,4',5,5'-hexachlorobiphenyl	
108	2,3,3',4,4'-pentachlorobiphenyl	
138	2,2',3,4,4',5'-hexachlorobiphenyl	
126	3,3',4,4',5-pentachlorobiphenyl	



**Table D1.** Continued

187	2,2',3,4',5,5',6-heptachlorobiphenyl	
128	2,2',3,3',4,4',-hexachlorobiphenyl	
201	2,2',3,3',4,5',6,6'-octachlorobiphenyl	
180	2,2',3,4,4',5,5'-heptachlorobiphenyl	
170	2,2',3,3',4,4',5-heptachlorobiphenyl	
195	2,2',3,3',4,4',5,6-octachlorobiphenyl	
206	2,2',3,3',4,4',5,5',6-nonachlorobiphenyl	
209	2,2',3,3',4,4',5,5',6,6'-decachlorobiphenyl	

**Table D2.** The volumes of IL and LiNTf<sub>2</sub> solution applied for *in situ* DLLME analysis of PCBs from ultrapure water.

IL applied for DLLME	Volume of the IL solution added <sup>a</sup>	Volume of the LiNTf <sub>2</sub> solution added <sup>b</sup>	Theoretical yield of the NTf <sub>2</sub> <sup>-</sup> -based IL
[BMIM][Br]	<sup>c</sup>	273	80 mg
	<sup>d</sup> 127	409	
[OMIM][Br]	<sup>c</sup>	240	
	<sup>d</sup> 139	360	
[BeBIM][Br]	<sup>c</sup>	230	
	<sup>d</sup> 140	345	
[BeEOHIM][Br]	<sup>c</sup>	238	
	<sup>d</sup> 139	357	

<sup>a</sup>: The IL solution was prepared by dissolving 1.66 g of IL in 5 mL of ultrapure water.

<sup>b</sup>: The LiNTf<sub>2</sub> solution was prepared by dissolving 2 g of LiNTf<sub>2</sub> in 10 mL of ultrapure water.

<sup>c</sup>: Molar ratio of IL:LiNTf<sub>2</sub>=1:1.

<sup>d</sup>: Molar ratio of IL:LiNTf<sub>2</sub>=1:1.5.

**Table D3.** The volumes of IL and LiNTf<sub>2</sub> solution applied for *in situ* DLLME analysis of acrylamide from ultrapure water and brewed coffee.

Sample matrix	IL applied for DLLME	Volume of the IL solution added <sup>a</sup>	Volume of the LiNTf <sub>2</sub> solution added <sup>b</sup>	Theoretical yield of the NTf <sub>2</sub> <sup>-</sup> -based IL
Ultrapure water	[BeBIM][Br]	140	230	80 mg
	[BeEOHIM][Br]	139	238	
	[HeOHMIM][Cl]	112	245	
Brewed coffee	[HeOHMIM][Cl]	168	368	120 mg

<sup>a</sup>: The IL solution was prepared by dissolving 1.66 g of IL in 5 mL of ultrapure water.

<sup>b</sup>: The LiNTf<sub>2</sub> solution was prepared by dissolving 2 g of LiNTf<sub>2</sub> in 10 mL of ultrapure water.